

50 YEARS OF CHANNEL CHANGE ON A REACH OF THE BIG BLUE RIVER,
NORTHEAST KANSAS

by

NICHOLAS E. GRAF

B.S., University of Wyoming, 2006

A THESIS

submitted in partial fulfillment of the requirements for the degree

MASTER OF ARTS

Department of Geography
College of Arts and Sciences

KANSAS STATE UNIVERSITY
Manhattan, Kansas

2008

Approved by:

Major Professor
Richard A. Marston

Abstract

River migration has resulted in a land owner losing 80% of his farmable land along the west bank of a reach h of the Big Blue River near Marysville, Kansas. Analysis of meander geometry and meander movement revealed that a single meander is moving downvalley, resulting in the loss of farmland. The rate and direction of river meander migration were measured using photogrammetric analysis of aerial photographs and topographic maps covering a period from 1956 to 2006. The greatest annual rates of channel migration and farmland erosion were closely associated with high flow events on the river between 1983 and 1986 and between 1986 and 1988. Analysis of recurrence interval, riparian vegetation, and bend curvature indicate that the rates of farmland lost and total meander migration are explained largely by the magnitude of floods. The direction in which the meander moved is largely explained by the bend curvature.

Table of Contents

List of Figures	v
List of Tables	vii
Acknowledgements	viii
CHAPTER 1 - Introduction	1
Problem Statement	1
Significance:	1
Purpose and Objectives	2
Study Area	2
The Study Reach	3
Watershed	10
CHAPTER 2 - Literature Review	12
Description of the Spatial and Temporal Patterns of Channel Shifting	12
Use of Maps and Historical Aerial Photography in Geomorphology	12
Measurement of Meander Geometry and Movement	13
Explanation of the Patterns and Process of Channel Shifting	20
Theories of River Meanders	20
Flow Characteristics of River Meanders	26
Processes and Rates of Meander Migration	34
Resistance to Meander Migration	38
CHAPTER 3 - Methods	41
Description of the Spatial and Temporal Patterns of Channel Shifting	41
Photographic Analysis	41
Measurement of Farmable Area	47
Measurement of Meander Geometry	49
Explanation of the Patterns and Process of Channel Shifting	50
CHAPTER 4 - Results and Discussion	56
Description of the Spatial and Temporal Patterns of Channel Shifting	56
Explanation of the Patterns and Process of Channel Shifting	60

Discussion.....	69
CHAPTER 5 - Conclusions	72
References.....	74
Appendix A - Gage and Recurrence Interval Data	81
Appendix B - Cross Section Data	83
Appendix C - Farmable Area Lost.....	85
Appendix D - Meander Movement.....	94

List of Figures

Figure 1.1 Measure of meander movement. Source: Modified from Knighton 1998.	2
Figure 1.2 2006 Aerial Photo of the Study Reach	4
Figure 1.3 Riverbanks along the Big Blue River looking downstream (Southeast). April 2008.....	5
Figure 1.4 Meander Bend on the Big Blue River looking downstream (South). April 2008.....	6
Figure 1.5 Geologic Cross Section Upstream of the Study Reach. Source: Walters 1954	7
Figure 1.6 Geologic Cross Section Downstream of the Study Reach. Source: Walters 1954.....	7
Figure 1.7 Map of Watershed Boundary and EPA Level IV Ecoregions	8
Figure 2.1 Meander Parameters. Source: Leopold and Wolman 1960	14
Figure 2.2 Simple Types of Meander Movement. Source: Hooke 1984.	17
Figure 2.3 Categories of Meander Change. Source: Hooke 1984.	17
Figure 2.4 Types of Meander Migration. Source: Knighton 1998.	18
Figure 2.5 Pools and Riffles on a Glass Plate. Source Gorycki 1973.....	22
Figure 2.6 Meander Development. Source: Thompson 1986.....	25
Figure 2.7 Helix Strength at Various Flow Rates. Source: Hooke 1975.	28
Figure 2.8 Map of Sediment Movement in Meander Bends. Source: Hooke 1975.....	29
Figure 2.9 Meander Bed Shear Stress. Source: Hooke 1975.....	30
Figure 2.10 Plan View of Meander Shear Stress. Source: Hooke 1975	31
Figure 2.11 Concave Bank Shear Stress in a Meander Bend. Source: Hooke 1975.....	31
Figure 2.12 Meandering Flow in Straight Channels. Source: Thompson 1986.....	32
Figure 2.13 Flow in a Meandering Channel. Source: Thompson 1986.....	33
Figure 2.14 Bend Curvature and Relative Migration Rates. Source: Hickin and Nanson 1984.....	36
Figure 3.1 Meander geometry.....	49
Figure 3.2 Regression between two Big Blue River gages.....	52
Figure 3.3 Annual Peak Flow at Marysville Gage.....	53
Figure 3.4 Departure from Average Precipitation at Beatrice, NE.....	53

Figure 4.1 Overlay Map of Channel Change	57
Figure 4.2 Cross sections Viewed Looking Upstream.....	60
Figure C.1 Farmable Area Change 1956-1969	85
Figure C.2 Farmable Area Change 1969-1977	86
Figure C.3 Farmable Area Change 1977-1983	87
Figure C.4 Farmable Area Change 1983-1986.....	88
Figure C.5 Farmable Area Change 1986-1988	89
Figure C.6 Farmable Area Change 1988-1991	90
Figure C.7 Farmable Area Change 1991-1997	91
Figure C.8 Farmable Area Change 1997-2002	92
Figure C.9 Farmable Area Change 2002-2006	93
Figure D.1 Meander Geometry 1956	94
Figure D.2 Meander Migration 1956 - 1969.....	95
Figure D.3 Meander Migration 1969 - 1977.....	96
Figure D.4 Meander Migration 1977 - 1983.....	97
Figure D.5 Meander Migration 1983 - 1986.....	98
Figure D.6 Meander Migration 1986 - 1988.....	99
Figure D.7 Meander Migration 1988 - 1991.....	100
Figure D.8 Meander Migration 1991 - 1997.....	101
Figure D.9 Meander Migration 1997 - 2002.....	102
Figure D.10 Meander Migration 2002 - 2006.....	103

List of Tables

Table 3.1 Summary of select attributes for time interval data and sources	42
Table 3.2 Aerial photograph interpretation.....	48
Table 4.1 Measured Variables	59
Table 4.2 Observed Changes	59
Table 4.3 Data Transformations	61
Table 4.4 Transformed Observed Changes.....	62
Table 4.5 Pearson Correlation Matrix.....	63
Table 4.6 Pearson Probability Matrix	64
Table 4.7 Annual Hectares Lost Explained	66
Table 4.8 Annual Total Migration Explained	67
Table 4.9 Translation/Extension Explained.....	68
Table 4.10 Relative Rates of Meander Migration.....	71

Acknowledgements

I would like to thank Dr. Richard A. Marston for his continued advice and insights throughout the process of the thesis work. He has provided invaluable guidance and support throughout my time here at Kansas State University. His belief in my abilities has been an inspiration for me to continue to push myself and to achieve more than I thought possible. With Dr. Marston's support and knowledge as a geographer, I have been allowed to utilize resources that have proved to be invaluable.

I would also like to thank my committee for their advice and contributions of knowledge in making my thesis more comprehensive. I would like to thank Dr. Charles W. Martin for his support throughout my academic career. I would also like to thank Dr. Martin for the use of his personal tools, which contributed greatly to the success of my fieldwork. I would like to thank Dr. J.M. Shawn Hutchinson for his knowledge and encouragement in the areas of photogrammetry, geographic information systems, and cartography. Dr. Hutchinson has been an inspiration for analysis and display of digital data.

I am grateful to be the recipient of the Rumsey B. Marston scholarship for fieldwork in geomorphology. This scholarship has made it financially feasible to accomplish my fieldwork.

I would also like to thank my fellow graduate students for their encouragement and willingness to share their knowledge of the many fields involved in my research. I am especially grateful for the assistance of Mark Gossard, Jeff Neel, and Ben Meade for help with field investigations.

I would also like to thank my wife for her contributions to my success in academics as well as in life.

CHAPTER 1 - Introduction

Problem Statement

An agricultural field adjacent to the Big Blue River, approximately five kilometers downstream of Marysville in Northeast Kansas, has been eroded significantly over the last 50 years. The magnitude, timing, and reason for the erosion are not known.

Significance:

The site selected for the study contains a river, its floodplain, and adjacent river terrace in which the migration of a meandering river has significantly decreased the amount of farmable area on the terrace. The site also includes a location in which a sand and gravel dredging operation began in September 2007 and is currently operating. This study will show the history of the geomorphological changes that have taken place over the last 50 years in the 1,000-meter long reach. Kansas law states that if a river moves by progressive erosion the property boundary moves with the river; however, if the river moves by an avulsions the property boundary stays at the previous location. With this understanding of the changes that have taken place before the dredging started, an opportunity exists for future examination into the effects of dredging in streams, although the impact of dredging will not be covered as part of this thesis.

Meander migration has been well studied and the rates of migration well documented. An area of meander research that has not been emphasized is the direction of movement. In this study meander movement is broken down in terms of translation, extension, and rotation (Figure 1.1). Translation occurs when the meander moves in a direction normal to that of a line connecting the centroid and the apex of the meander, extension occurs when meander moves parallel to the axis, and rotation occurs when the apex moves without corresponding changes to the radius of curvature of location of the centroid.

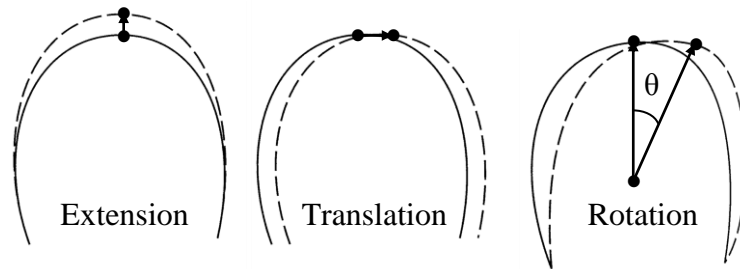


Figure 1.1 Measure of meander movement. Source: Modified from Knighton 1998.

Purpose and Objectives

The purpose of this study is to evaluate channel change and the associated loss of farmland along a short reach of the Big Blue River, downstream of Marysville, Kansas, between 1956 and 2006. The objectives of this study are to:

1. Describe the spatial and temporal patterns of channel shifting between 1956 and 2006, and the associated impact on farmland erosion along the west bank of the Big Blue River in Northeast Kansas.
2. Explain the patterns and process of channel shifting, farmland erosion, and direction of meander movement

Study Area

This chapter of the thesis provides information about the study reach of the Big Blue River, followed by background on the watershed upstream of the study site.

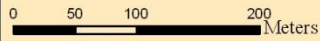
The Study Reach

The study reach is located in Marshall County, Northeast Kansas on a reach of the Big Blue River approximately five kilometers south of Marysville, Kansas, bounded by cross sections one and three on Figure 1.2. The farmland in this investigation is located on a river terrace along the west side of the Big Blue River, labeled as ‘endangered field’ (Figure 1.2). Riverbanks along the west side of the Big Blue River on this reach as 5-6 meter in height and are nearly vertical (Figure 1.3).

The loss of farmland has raised concern about the potential impacts of dredging on this particular reach of the Big Blue River. This area was chosen because of a sand and gravel dredging operation that began in September 2007 and continues to operate to the present-day. The dredging site, located on the E ½, SE ¼, Section 7, Township 3 south, Range 7 east, Sixth Principle Meridian, Marshall County, Kansas as indicated by the hatch pattern (Figure 1.2). The dredging operation removes sand and gravel from a point bar located on the east side of the river (Figure 1.2). The dredging company has specified that they will dredge to a depth of approximately 4.5 – 6 meters below the water surface level, removing the entire point bar up to the area of mature trees on the east side of that point bar, as indicated by the hatch pattern in Figure 1.2.

A second concern of the farmer on the west side of the river is the potential impact of a knickpoint created by the dredging pit, moving upstream undermining the pipe feeding his field sprinkler. The irrigation pipe, located near cross section number one, can be seen in the northeast portion of the map (Figure 1.2). The location and extent of the three cross sections surveyed on 11-12 August 2007 can be seen on the map.

Site Map: Big Blue River Quarry



Data Source: 2006 FSA NAIP Imagery second shipment
Projection: UTM Zone 14 North
Datum: NAD 1983



February 2008



Figure 1.2 2006 Aerial Photo of the Study Reach



Figure 1.3 Riverbanks along the Big Blue River looking downstream (Southeast). April 2008.

A meandering river is suspected to have caused erosion reported by a local farmer. The claimed erosion occurred between cross sections one and three from 1956 to 2006 and affected the west bank of the study reach. The local farmer has indicated that at one point he remembers farming where the river is today. Figure 1.4 is a photograph taken looking south along the river across what the local farmer claims to have been his field at one point. The portion of the field remaining is seen along the west bank.

Soils along the west bank are primarily of the Muir soils series with components of Kennebec, Nodaway and Wabash soils series. The terrace slopes range from 0% to 2%. Muir soils are most commonly located on river valley terrace forming in fine-silty alluvium parent material. The Muir soils series are established in well-drained areas and have moderately high water movement, even at the most restrictive layer. The Muir soils series makes up 80% of the soils on the west bank and are classified as a fine-silty, mixed, mesic Cumulic Haplustolls. The Muir soil contains the following horizons: A horizon from 0 – 41 cm below ground surface, Bw horizon from 41 – 114 cm, and C horizon from greater than 114 cm. The A horizon has 1 – 20% sand, 50 – 70% silt, 18 – 27% clay, and 2 – 4% Organic matter. The Bw horizon has 1 – 30% sand, 40 – 70% silt, 18 – 35% clay, and 1 – 3% organic matter. The C horizon has 1 – 30% sand, 40 – 70% silt, 18 – 35% clay, and 0.5% organic matter (U.S. Department of Agriculture 2006).

Underneath the thick layer of alluvium in the area are alternating layers of limestone and shale. An area of exposed bedrock is located along the western edge of the study reach and is visible in Figure 1.2 where it is bisected by cross section two. The exposure of bedrock is comprised of limestone and is nearly flat, so accurate measurements of strike and dip are difficult. The dip was measured on site at 2° roughly parallel to the river in a southwest direction. The Kansas Geological Survey has published cross sections (Figure 1.5 and Figure 1.6) of the bedrock in the area showing the alternating layers of limestone and shale. Figure 1.5 is located approximately 15 kilometers north of the study reach, and Figure 1.6 is located approximately four kilometers to the south. Both cross sections are orientated west to east. The dip appears to be to the west direction on the cross sections, but the offset in elevation in the layers shows that the dip could also have a northern component, which goes against field observation where the layers were clearly dipping to the southwest, parallel to the study reach.



Figure 1.4 Meander Bend on the Big Blue River looking downstream (South). April 2008.

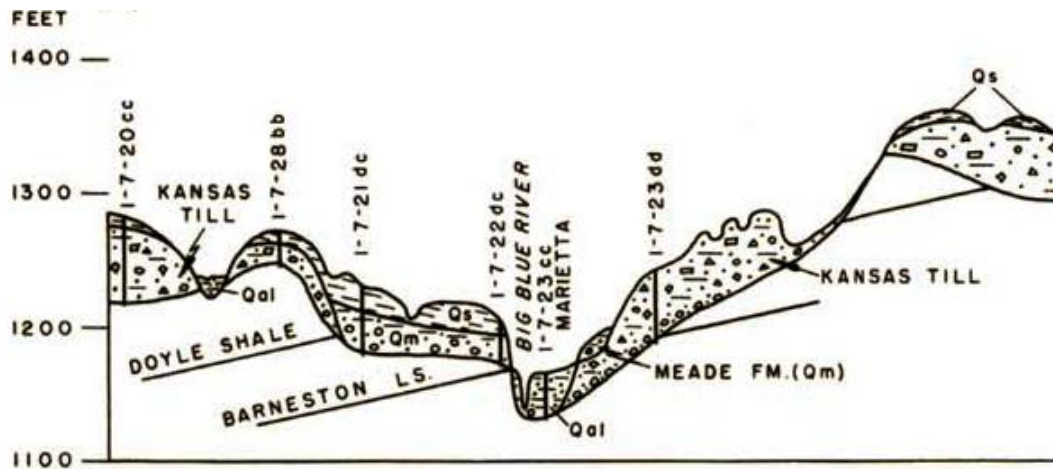


Figure 1.5 Geologic Cross Section Upstream of the Study Reach. Source: Walters 1954

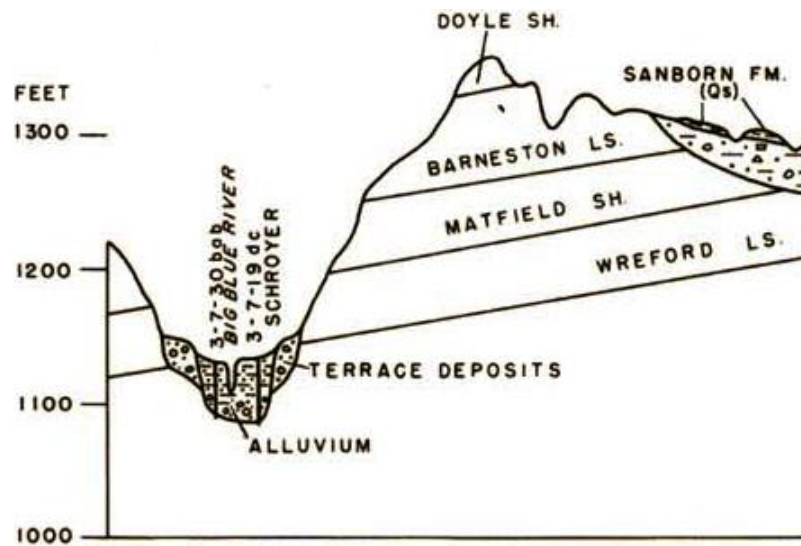


Figure 1.6 Geologic Cross Section Downstream of the Study Reach. Source: Walters 1954.

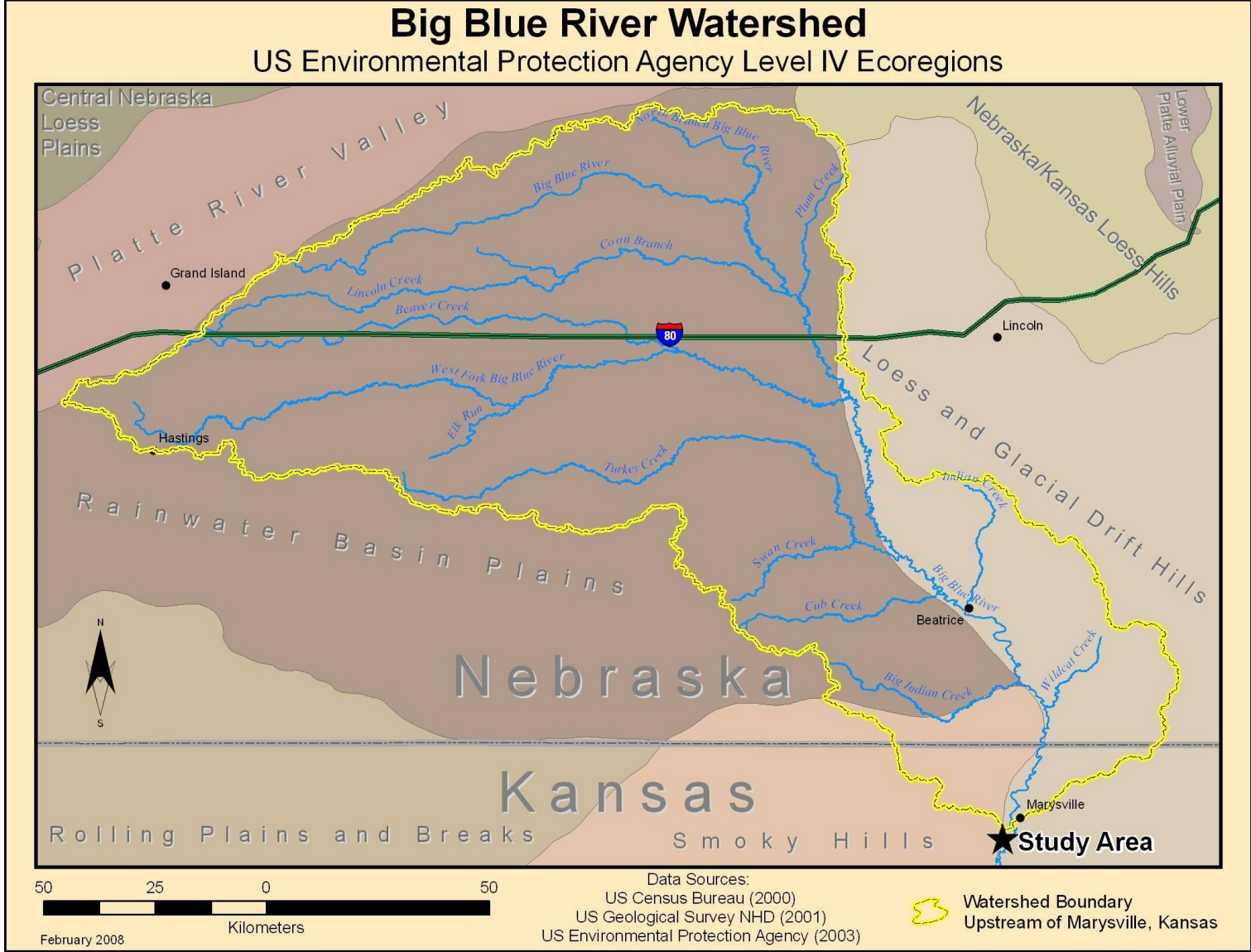


Figure 1.7 Map of Watershed Boundary and EPA Level IV Ecoregions

The Big Blue River forms the western edge for the maximum glacial extent in the region and serves as the boundary between two Environmental Protection Agency (EPA) ecoregions. The two level IV ecoregions divided by the Big Blue River in the study area are the Loess and Glacial Drift Hills on the east and the Smoky Hills on the west (Figure 1.7). The Loess and Glacial Drift Hills are characterized by rolling loess covered hills with areas of exposed glacial till and ranges in elevation from 300 to 500 meters above sea level and has local relief in the 30 to 90 meters range. Geologically the region has soils formed in loess and clay loam calcareous glacial till. The loess deposits are considered variable and generally have a greater thickness near rivers, with more exposed glacial till in the up lands. Soils are typically on the order of Mollisols and Entisols and belong to the Argiudolls and Udorthents great groups with the temperature and moisture regimes of Mesic and Udic. The underlying bedrock consists of Pennsylvanian shale, sandstone, and limestone, and Permian shale and limestone (Chapman et al. 2001).

Climatically the Loess and Glacial Drift Hills ecoregion has a mean annual precipitation in the range of 68 – 90 centimeters. Typically mean January temperatures range from a maximum of 1°C to a minimum of -10°C and mean July temperatures range from a maximum of 33°C to a minimum of 19°C for the region. The region experiences an average of 150 – 190 frost-free days per year with potential natural vegetation considered tallgrass prairie with floodplains consisting of cottonwood forests, and the hickory-oak forests on bluffs. Current land use in the area is typically cropland in the flatter loess hills with the main crops being wheat and corn, with some grain sorghum, soybean, and alfalfa. Pastureland is more typical for the upland glacial-till soils (Chapman et al. 2001).

Characterized by plains broken by undulating hills, with broad belts of low hills created from mature cretaceous rock layers, the Smoky Hills ecoregion has an elevation that range from 365 meters to 550 meters above sea level and local relief that ranges from 30 to 75 meters. Geologically the region has silty and loamy soils formed in loess deposits. Soils in the region are part of the Mollisol soils order, and belong to the Argiustolls, Haplustolls and Argiudolls great groups with a temperature and moisture regimes of Mesic, Ustic and Udic. A mix of sandstone, shale, loamy colluvium, and

chalky limestone layered over Cretaceous age sandstone form the bedrock in the region (Chapman et al. 2001).

Climatically the Smoky Hills ecoregion has a mean annual precipitation in the range of 60 – 70 centimeters. Typically mean January temperatures range from a maximum of 5.5°C to a minimum of -8°C and mean July temperatures range from a maximum of 35°C to a minimum of 20°C for the region. The region experiences a mean of 165 – 180 frost-free days per year with potential natural vegetation for the region considered transitional from tall grass prairie in the east to mixed grass prairie in the west, with some riparian forest. Cropland accounts for the majority of current land use within the region with the main crop being winter wheat, with some corn grown in irrigated areas (Chapman et al. 2001).

Watershed

The Big Blue River watershed upstream of the study area encompasses 12,372 square kilometers, located primarily in the Rainwater Basin Plains ecoregion, with the rest of the area being in the Loess and Glacial Drift Hills ecoregion and the Smoky Hills ecoregion (Figure 1.7). Historically characterized by flat to gently rolling loess covered hills with poor drainage creating natural wetlands, the Rainwater Basin Plains ecoregion now has had most of the wetlands drained in order to create agricultural land. Elevation ranges from 395 meters to 730 meters above sea level in the Rainwater Basin Plains ecoregion and local relief ranges from 1.5 to 30 meters. Geologically the region has soils formed in Quaternary loess, mixed loess and sandy alluvium. Soils in the region are on the order of Mollisols and Entisols, and belong to the Argiustolls, Argialbolls, Argiaquolls, Haplustolls, and Ustorthents great groups with a temperature and moisture regimes of Mesic, Ustic, Aquic, and Udic. Tertiary sandstone in the western part of the region and Cretaceous limestone and shale in the east comprise the bedrock in the region. The region also has wind-excavated depressions (Chapman et al. 2001).

Climatically the Rainwater Basin Plains ecoregion has a mean annual precipitation in the range of 55 – 72 centimeters. Typically mean January temperatures

that range from a maximum of 3°C to a minimum of -10°C and mean July temperatures that range from a maximum of 33°C to a minimum of 18°C for the region. The region experiences a mean of 150 – 170 frost free days per year with potential natural vegetation for the region considered to be transitional from tall grass prairie in the east to mixed grass prairie in the west, with the dominate grasses being big bluestem, little bluestem, and sideoats grama. Western wheatgrass, sedges, spike rushes, and slender bulrush dominate wetland grasslands. Extensive croplands makeup a majority of the current land use in the region with the main crops being sorghum and winter wheat in the dry areas and corn and alfalfa in the irrigated areas. The use of extensive irrigation in the region has lead to ground water contamination and significant depletion of ground water (Chapman et al. 2001).

CHAPTER 2 - Literature Review

The literature review is comprised of two sections organized by major research objectives in the study: first, to describe the spatial and temporal patterns of channel shifting, and second, to explain the patterns and process of channel shifting.

Description of the Spatial and Temporal Patterns of Channel Shifting

Use of Maps and Historical Aerial Photography in Geomorphology

Many studies in the field of geomorphology have used historical aerial photographs and documents in order to establish landform change over time. The use of aerial photography is probably the most common way in which different periods in time are established. This is most likely due to the availability of photographs, but other methods have been used, including historical documents, such as maps and surveys. For example, Graf (1988) also used various sources of historical data in order to establish a probability that Rillito Creek would be in any given cell of the study area, at any given time. Marston et al. (1995) used a combination of historical maps as well as aerial photographs to investigate complex changes on the Ain River in France. An article by Lane (2000) provides some examples of common problems encountered when using aerial photographs to analyze geomorphic changes in rivers. Juracek (2000) used successive aerial photography to assess pre- and post-dam channel stability. Juracek was also able to extract bankfull width from aerial photography based on channel characteristics, including breaks in slope, the tops of point bars and changes in vegetation. When Juracek brought the aerial photography into GIS software, he used twenty ground control points, including intersections of roads, railroads, and section lines for the rectification process. Marston et al. (2005) used two different periods in time to investigate the effects of the Jackson Lake Dam on the Snake River in northwest Wyoming. Graf (2006) used two photos from the same year, but different location to investigate geomorphic changes associated with very large dams throughout the country. Gautier et al. (2007) used the combination of aerial photography and satellite images to

investigate the temporal evolution of the Beni River. The images used were at low flow stages of the river to negate any bias caused by high flow events yielding precise information about the changes in the fluvial system.

Measurement of Meander Geometry and Movement

Leopold and Wolman (1960) identified certain parameters of meanders that are visible in planview. Leopold and Wolman identified L to represent meander wavelength, A to represent the amplitude of the wave, and radius of curvature represented by r_m . They also identified points of inflection, the axis of bend, convex bank and concave bank, and location of point bars (Figure 2.1). Leopold and Wolman specified that these meander patterns are typical of rivers with well-defined unconstrained flood plains. Leopold and Wolman also identify many similarities in meander geometry that are present independent of size. The most consistent correlations noted are meander wavelength, channel width, and radius of curvature. Two relationships between the aforementioned geometries are noted in the text.

$$L = 10.9w^{1.01} \text{ and } L = 4.7r_m^{0.98}$$

These relationships both contain wavelength as a parameter and can therefore be combined to create an idealized relationship between channel width and radius of curvature of 2.3. Leopold and Wolman determined that in a sample of 50 rivers, the median value for r_m/w was 2.7 and the mean was 3.1. They also ascertained that two-thirds of the meanders sampled fell between 1.5 and 4.3. A quarter of the values fell between 2.0 and 3.0.

Hickin (1974) used erosion pathways to quantify the effect of downvalley versus crossvalley movement of meander. Hickin used an axis that was oriented to tangent with the meander at the first initial time. He defined crossvalley movement as that which was normal to the axis and downvalley as that which was parallel with the axis. This approach can be used with any point along the meander as long as the points correspond between time intervals.

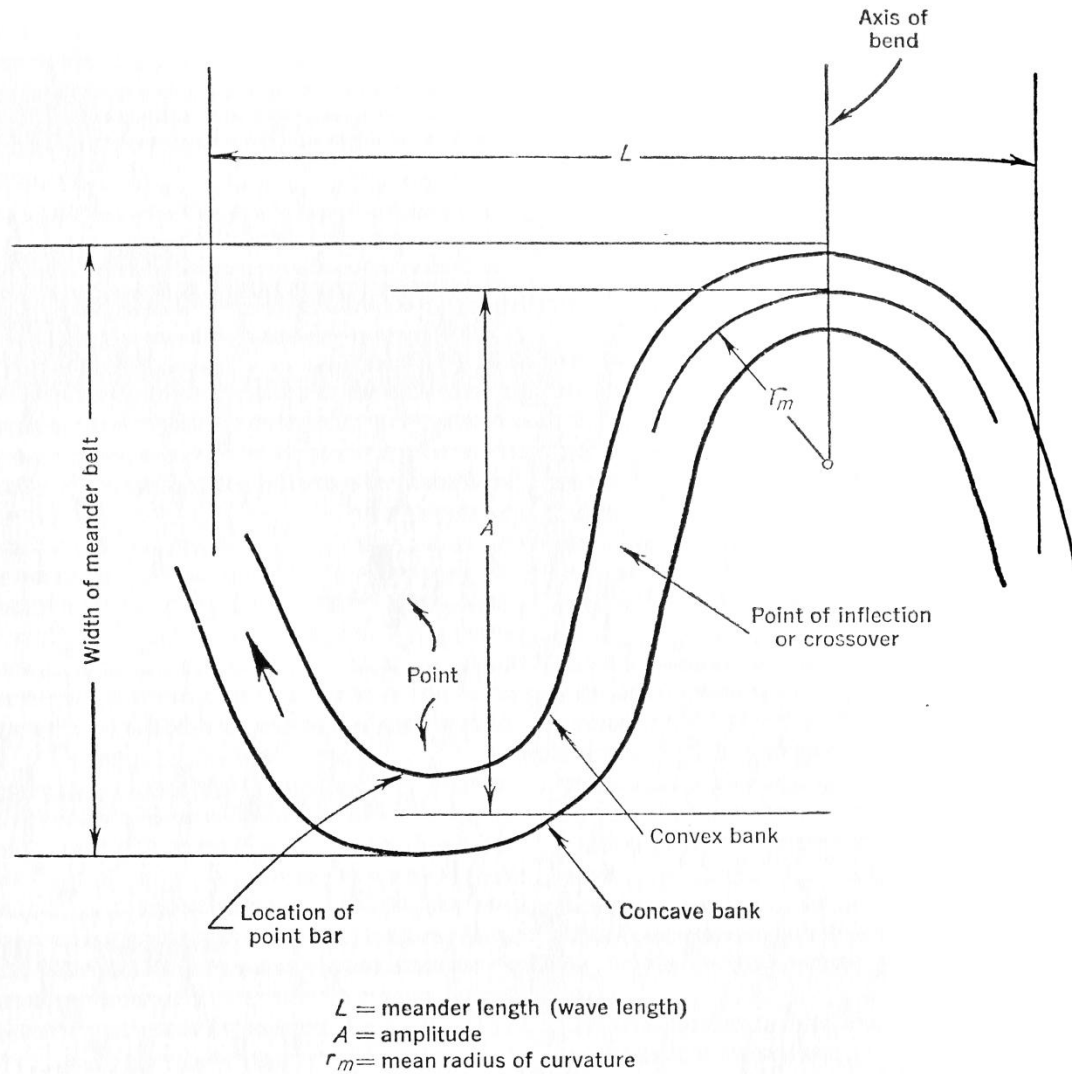


Figure 2.1 Meander Parameters. Source: Leopold and Wolman 1960

Hickin and Nanson (1975) discovered that the ratio of the radius of curvature to stream width, or bend curvature, could be related to how fast meanders migrate. Hickin and Nanson determined that mean bankfull width was the appropriate channel width to use when calculating bend curvature. Nanson and Hickin used dendrochronology to estimate the pace at which meanders migrate based on vegetation succession on the developing point bar. While this technique is innovative in studying meander migration, it is limited in being able only to measure the current channel width. This limitation forced Hickin and Nanson to use the bankfull width measurement at the time of the study for the width of all years of the meander migration. Hickin and Nanson observed that the

best way to measure radius of curvature is to use an average of the curvature of the apex with that of the less curved portions of the meander leading in and out of the apex.

Hooke (1984) identified five major approaches to meander analysis: bend parameters, curve fitting, spectral analysis, graphical analysis, and models of change. The five different approaches are not mutually exclusive and some overlap between the different approaches exists. Bend parameters involves the measurement of recognized meander geometry such as wavelength, amplitude, and radius of curvature. The combination of these three elements describes the size and shape of meanders. Hooke identifies four potentially problematic areas in this approach. The first is the possibility of subjectivity in the identification of bend parameters. The second is in the exact definition of parameters used when describing meanders. Hooke explained that often definitions are missing from the work published by other authors on the subject. The third potentially problematic area is in the use of statistical averages. The potential for error in the use of averages lies in that many natural phenomenon do not fall under normal distributions and therefore the average may not be the best representation of the phenomenon. The fourth major concern that Hooke noted was the measurement of bend parameters is the use of a single measurement to characterize meanders as a whole. Hooke suggests that several parameters are needed to characterize properly meanders and suggests three categories. These include scale or size, shape or sinuosity, and irregularity.

A second approach used in the study of river meanders is the idea of curve fitting. Hooke identifies two aspects to this technique. The first is how the curves are fit and the second is what curves are fit to the meander. One of two ways typically fits curves. First, visual techniques involving drawing circles, or second, a technique where a line is drawn mathematically to simulate the meander shape. Various mathematical formulas have been used in the description of meanders. These curves include sign curves, sign generated curves, parabolas, circles, and Fargue spirals.

A third general approach identified by Hooke is use of spectral analysis to classify and understand meanders. Spectral analysis is a type of curve fitting in that it relies on points digitized along the stream course. The use of spectral analysis accounts for the different shape of meanders by identifying different wavelength frequencies in the

meander shape. This is done by the use of a power spectrum graph whereas a single peak would indicate a regular meandering pattern and multiple peaks corresponding with different wavelengths would indicate an irregular meandering pattern.

A graphical comparison of courses is the fourth general approach that Hooke identifies. Graphical comparisons technique examines changes in meander form directly by the use of visual comparisons often simply by superimposing course at different times on top of one another. This technique has the advantage in that parameters such as the amount of bank erosion and area lost can easily be calculated. Therefore, the amount of change can be quantified. This technique can be combined with other techniques to create a vector plot of point movement.

Models and classification of change is the final general approach identified by Hooke. Case studies have provided the information needed to develop various models to study meander change. With the use of meander change models identification of different meander change patterns is possible, including expansion, rotation, and translation. Hooke combined six different simple modes of meander change based on movement of certain meander parameter such as inflection points and apexes (Figure 2.2) to create 70 complex types of meander movement. Reducing the 70 complex types of meander movement into eight categories of meander change (Figure 2.3) made classifying meander change less cumbersome.

Meanders migrate both laterally and downvalley. Meanders typically migrate in one of four ways, translation, extension, rotation, and lobing and compound growth (Knighton 1998), as shown in Figure 2.4. Translation is the movement of the meander in a downvalley direction without altering the shape of the meander. Extension is the process by which the meander moves in the lateral direction increasing the path length and amplitude. Rotation is a shift in the axis of orientation. Lobing and compound growth is the development of smaller meanders within the larger meander itself.

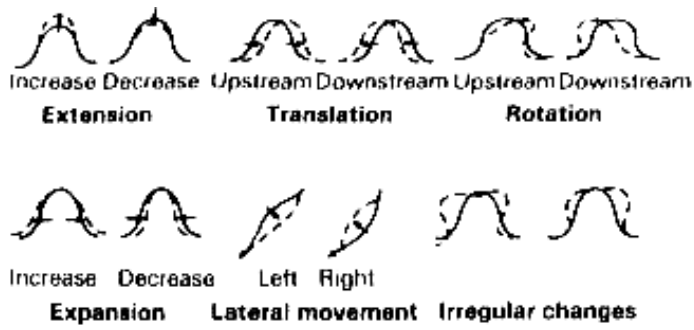


Figure 2.2 Simple Types of Meander Movement. Source: Hooke 1984.

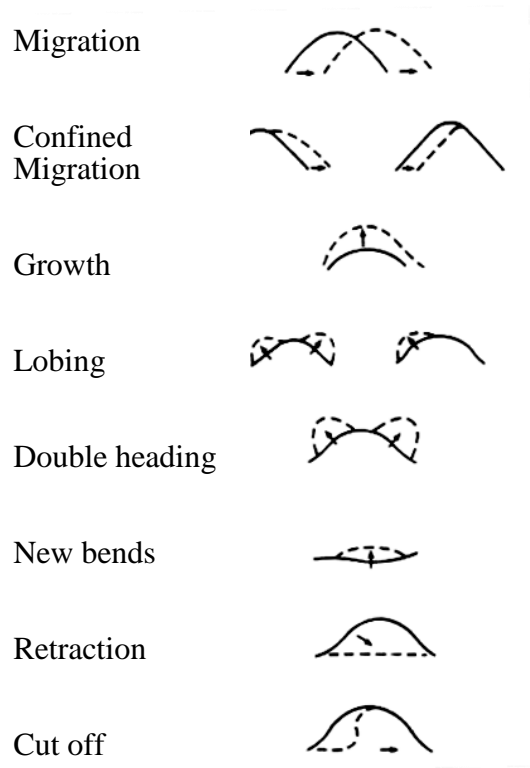


Figure 2.3 Categories of Meander Change. Source: Hooke 1984.

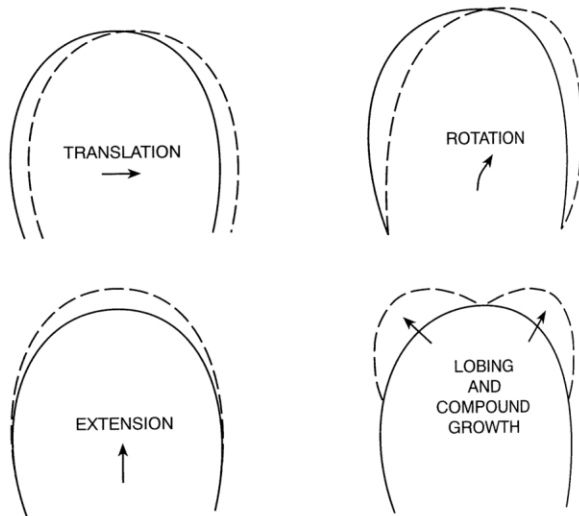


Figure 2.4 Types of Meander Migration. Source: Knighton 1998.

Methods for measuring channel geometry and meander parameters are not standardized, even to this day. When some of the well-known authors in geomorphology were asked about the measurement of translation versus extension various responses came back. Edward Hickin, Professor & Chair of the Department of Geography at Simon Fraser University, said in an e-mail on 26 March 2008 “I don't think that I can be of much help to you because I have never really thought much about your question.” Inci Gunalp, Assistant Professor in the Department of Geography at Texas A&M University, stated in an e-mail on 3 April 2008

“In my method, the movement (migration) of each point on the centerline is computed in an intrinsic coordinate system (i.e. the streamwise axis characterized by centerline). The planform migration series calculated this way gives the each point's lateral movement approximately orthogonal to the centerline at the point. Once the valley direction is determined, the components of each lateral movement can be determined in down valley–cross valley coordinate system (i.e. translation–extension).”

Janet Hooke, Professor of Geography at the University of Liverpool, said in an e-mail on 21 April 2008,

“amazingly little is standardized. I would divide translation and extension by the direction of maximum movement - in other words, translation is down valley and extension is across valley. So movement could be divided into these two orthogonal components. I know of no reference!”

When some of the well-known authors in geomorphology were asked about the measurement of channel width and again various responses came back. Jonathan Harbor, Vice President for Research at Purdue University stated in an e-mail on 2 April 2008

“In practice I have seen several different approaches used, and it boils down to data availability. So, often the analysis is air-photo based, so biased by Q [discharge] and user interpretation of the edge of the channel. Field based is typically bankfull based on survey data and field interpretation.”

Gerald Nanson, Professor in the School of Earth and Environmental Sciences at University of Wollongong, said in an e-mail on 3 April 2008 “From memory, and almost certainly, bankfull!” Gordon “Reds” Wolman, Professor of Geography and International Affairs at Johns Hopkins University said in an e-mail on 16 April 2008 “bankfull width makes the most sense but I believe some have used w at mean annual discharge and who knows what!”

Explanation of the Patterns and Process of Channel Shifting

Meanders occur in almost all types of flowing water and have remarkable similar characteristics. Despite decades of studies focusing on why rivers meander, a complete understanding still eludes researchers. What is understood about river meanders is that several important aspects exist to understand in meandering rivers. This section of the paper covers several aspects of river meanders that are not mutually exclusive, but is divided into sections based on theoretical perspectives of river meanders, flow characteristics of river meanders, processes and rates of meander migration, and resistance to meander migration.

Theories of River Meanders

Some of the earliest research investigating river meanders focused on the development of meanders. Starting in the 1950's and 60's relationships between different meander parameters were beginning to be explored. A previous section covered the relationships discovered between meander parameters by Leopold and Wolman (1960). Although simplistic, Leopold and Wolman revealed that meanders in rivers are largely explained by the velocity distribution within the meander, including helical flow. Leopold and Wolman state that if velocity distribution is all that is necessary to account for the asymmetrical cross section shape of meanders, the deposition and erosion pattern of meanders, and the progressive downvalley migration of meanders. Differential velocity distributions within meanders play important role in increasing the shear stress along the concave bank causing erosion.

Tanner (1960) examined river meanders that occurred on a glass plate. When water was flowing on a clean plate, it did not meander and followed the steepest path down. In contrast, when water was flowing on a dirty or dusty glass plate the water began to develop a meandering pattern. Tanner attributed this difference to the development of helical flow because of the resistance, created by the dust, causing turbulence. Tanner emphasizes that the meander development was not due to dust being entrained in the water but instead could be attributed to the development of helical flow.

Tanner hypothesized that the velocity of the flowing water could be explained by three terms. The first term is the velocity of the particle in downstream direction, the second is description of helical flow, and the third is the force of gravitational pull. Tanner showed that the balance of these three vector forces on stream particles explains the development of meanders in that when the helical flow begins to develop the stream begins to curve and will continue to curve until the gravitational force overcomes the helical force causing the stream to curve in the opposite direction. He determined that when the gravitational force surpassed the helical force the cross section became nearly symmetrical and shallow at which point the path becomes nearly straight and a new helix develops spiraling in the opposite direction of the previous helix. The development of helical flow within a meander increases the superelevation of water along the concave bank more than would be experienced by direction change alone, leading to greater shear stress and erosion.

Einstein and Shen (1964) demonstrated when looking at water flowing down a straight artificially created channel that the water started to develop a meandering pattern within the confines of the channel. Einstein and Shen attribute this meandering pattern to the development of secondary currents or helical flow noting that two opposing helical flows are present in the channel causing scour holes and corresponding bars to develop in an alternating pattern. Einstein and Shen observed four characteristics in the development of alternating scour holes. The first characteristic is that the alternating bars form in the presence of coarsely textured sloping bank materials. The second is that the alternating bars travel downstream. The third is that the highest elevation of the alternating bars is adjacent to the rough walls of the constructed channel. The fourth characteristic is that surface water flows in a meandering pattern from scour hole to scour hole around the alternating bars. The role of secondary currents is vital to the development and movement of meanders.

Yang (1971) introduced two laws of stream morphology. The first is the law of average stream fall and the second is the law of least time rate of energy expenditure. In order to follow the second law of stream morphology Yang hypothesized that a stream must meander. The conclusion that natural unbraided stable channels will lead to a smooth and sinuous meander is based on the idea that a meandering river maximizes the

energy loss along the course of flow and results in the minimum amount of work necessary for the river. Yang's theories indicate that meandering rivers form according to principles of energy dissipation and expenditure, and that a meandering river is not instable.

Gorycki (1973) observed river meanders on glass plates similar to the work of Tanner (1960) and emphasizes that meanders develop free of the influence of sediment. Gorycki made three important observations. The first is that dye injected in the water stream shows that even mostly straight channels have a meandering main flow. The second observation is that water depth along the meander mirrors that of natural streams (Figure 2.5). The final observation is that the relationship between wavelength, stream width, and radius of curvature closely match those of larger natural streams. The initiation of river meanders is dependent on the amount of water flowing and meeting a critical threshold. He interpreted that the pattern of the river varies with the amount of discharge. At low flow conditions, the channel will be straight, as flow increases a meandering pattern begins to develop. If flow increases beyond that, an unstable meandering pattern begins to develop with wild variation in wavelength and radius of curvature. The patterns observed by Gorycki indicate that discharge can alter the form of a river and the migration rates of meanders.

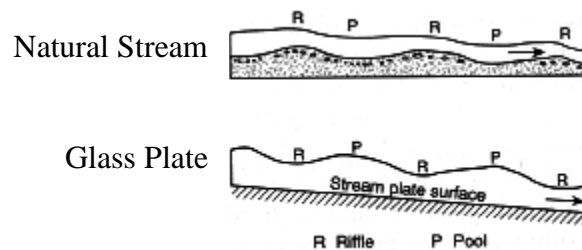


Figure 2.5 Pools and Riffles on a Glass Plate. Source Gorycki 1973

Callander (1978) postulated that the mechanism initiating river meanders is the periodic deformation of the river channel bed. Callander's ideas initiated the theory for the mechanism of river meanders formed by the deformation of the channel bed. The idea of bar theory suggests that riverbed deformation leads to the development of bars and scour holes, which then develop, into meanders. Rhoads and Welford (1991) argued

that the cornerstone of bar theory states that the dominant perturbation's wavelength will determine the meander wavelength. Nelson and Smith (1989) made further revisions to bar theory showing that migration of the perturbation decreases exponentially with wavelength leading to an expedient downvalley migration of the alternating bars with small wavelengths and a slow upvalley migration of alternating bars with long wavelengths. Nelson and Smith also demonstrated that bar theory explains meander development in gravel streams that have a high width to depth ratio better than other types of streams. Rhoads and Welford (1991) identify that, despite decades of refinement to bar theory, one fundamental shortcoming remains. Bar theory treats all river channels as though they have non-erodible channel walls and therefore the conversion from alternating bars to a truly meandering river is not possible. Bar theory demonstrates that meander wavelength affects migration.

Bend theory was developed in a response to the shortcomings of bar theory. Ikeda, Parker, and Sawai (1981) found that a model for predicting bend instability based on the momentum and continuity equations could be used to predict meandering behavior in rivers. They also illustrated that the predicted wavelength of bend instability corresponds to the predicted wavelength of unstable alternating bars in alluvial channels. This observation led to the hypothesis that unstable alternating bars, in combination with erodible banks, can lead to a truly meandering channel.

Many studies have combined the ideas of bar theory and bend theory to produce the unified bar-bend theory (Blondeaux and Seminara 1985, Parker and Johannesson 1989, and Seminara and Tubino 1989). All of the unifying theories hinge on the discovery of a previously unnoticed resonance phenomenon. Bar-bend theory states that small perturbations create disturbances that grow in amplitude. The fastest growing disturbance will create migrating alternating bars with a short wavelength. When the channel begins to develop a sinuous flow, the slower developing longer wavelength resonance disturbance forces the alternating bars to stabilize into point bars. This creates a meandering channel with the wavelength of the resonance wavelength. Resonance frequency can explain relationship between channel width and meander wavelength.

Thompson (1986) developed a model of meander development based on observations of secondary currents and the importance of a pool and riffle sequences in

the development of meanders (Figure 2.6). In Figure 2.6 black areas indicate scour pools, white areas indicate normal bed elevations, and textured areas indicate bars. Solid lines indicate near surface currents, dashed lines indicate near bed currents. Thompson remarked that the changes are driven by the flow of the water, which in turn is influenced by the meander curvature. In the first two stages of the Thomson meander evolution model the primary mode of development is that of a pool and riffle sequences that meander downvalley. In stage two a slight meandering channels begins to develop leading into stages three and four where channel curvature and circulation are increased leading to a period of growth in the meander shape. In the final two stages, five and six, the meander has reached a critical value of sinuosity and secondary currents begin to break down leading to the development of additional bed forms, which can lead to complex meander growth. Thompson's show that secondary currents influence the development of pool and riffle sequences and ultimately meander evolution.

Ideas of self-organizing processes and chaos theory have contributed to a series of thought looking at meandering river systems as a whole unit. Stølum (1996, 1998) investigated the idea that river systems are self-organizing. Stølum has proposed that river systems start to develop a meandering pattern and continue to increase in sinuosity until they reach a critical value. The river system starts to develop meander cutoffs, lowering the sinuosity at this critical value. The river system will then fluctuate around a desired sinuosity. Stølum exhibited through modeling river systems that in unconstrained channels, desired sinuosity is near the value of pi. Stølum 1998 provided an example of his theory using rivers in Brazil. Meandering rivers are dynamic systems where meander migration is to be expected.

Hooke (2007) tested the ideas of complexity and the ideas of self-organizing river systems on various rivers throughout the world. She revealed that self-organization could explain the behavior of some river systems. It failed to explain the organization of many other river systems. She discovered that a vast variety of meandering behaviors were evident. Many of which could be explained by simple linear processes. Despite many decades of research on river meanders, Hooke showed that one unifying theory that explains all river meanders does not yet exist.

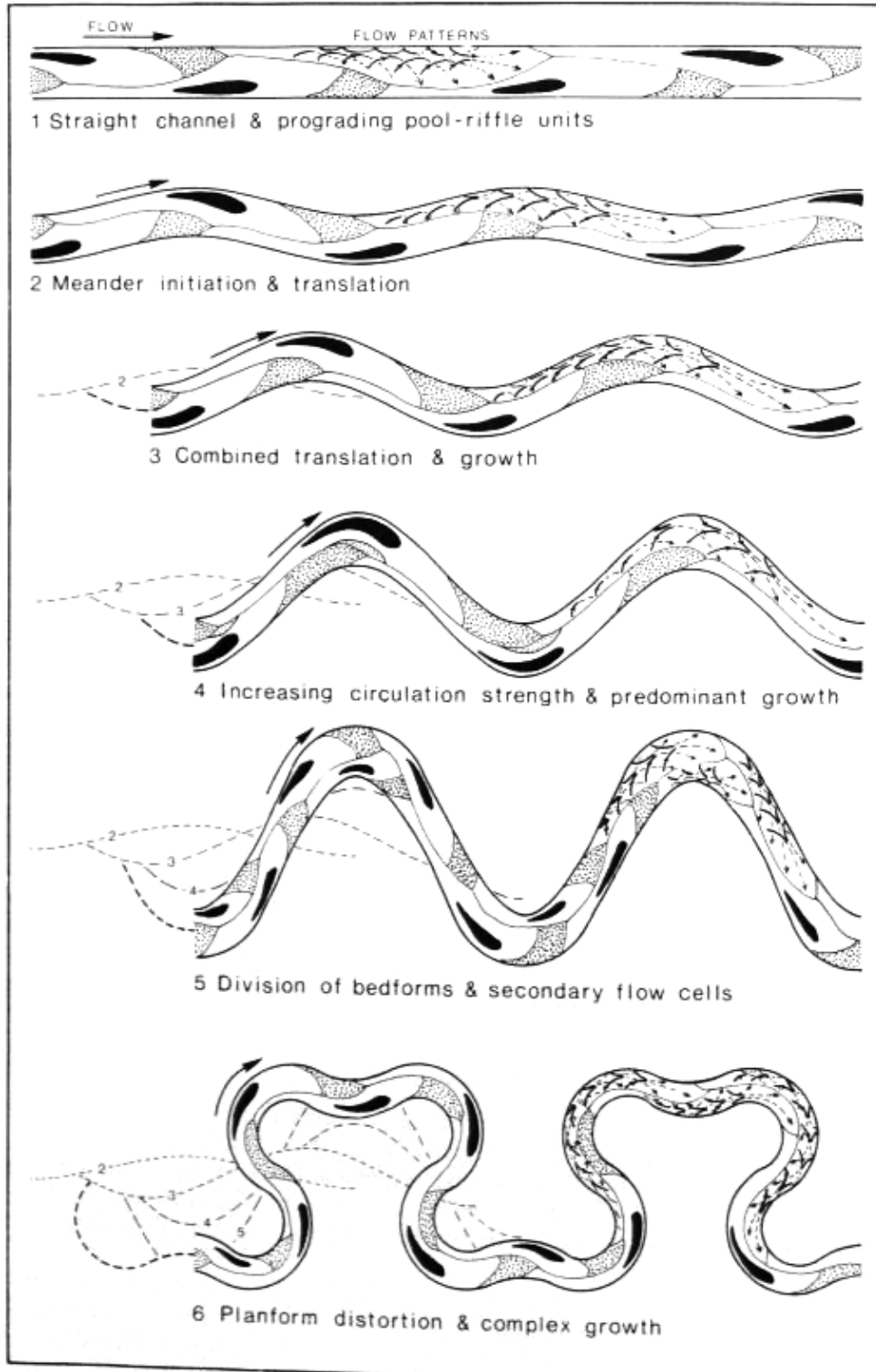


Figure 2.6 Meander Development. Source: Thompson 1986

Flow Characteristics of River Meanders

Leopold and Wolman (1960) established that in channel cross sections a cross-channel velocity component of the flow is directed towards the convex bank near the bed and toward the concave bank near the water surface. This in turn creates a helical flow with surface water moving downwards near the concave bank and an upwelling of water surfacing near the convex bank. They go on to note that water from one side of the channel does not cross completely to the other side of the channel. This causes material eroded from the concave bank on one side to deposit on the same side in the next meander downstream. Leopold and Wolman also note that the super elevation of water near the concave bank is a consequence of both the curved path of the flowing water and the corresponding helical motion. Leopold and Wolman observed that the velocity in meanders was not symmetrically distributed across the channel. The highest velocities are found near the concave bank on the outside of the bend from inflection point to inflection point. They also exhibited that the maximum velocity is just below the water surface. Leopold and Wolman note that despite the highest velocity being near the concave bank at no point does the velocity influence the bank but instead runs roughly parallel to the bank. This asymmetrical distribution of velocity mirrors the asymmetrical cross section shapes of river meanders.

Bagnold (1960) determined by looking at flow characteristics in pipes that a curve ratio between two and three creates the minimum resistance to channel flow. He discovered that when the curve ratio is below two that an eddy is created on the inside of the bend increasing resistance. Bagnold concluded that despite the flow resistance minimization being calculated for closed symmetrical pipes the importance of eddies being developed in tight bends is applicable to open-channel curved streams.

Roger Hooke (1975) interpreted that the helical motion in meander bends was not uniformly distributed (Figure 2.7). Hooke explained that at different flow rates that the helix strength was greatest in the meander upstream of the apex. One exception was that for a flow rate of 35 liters per second with a stabilized bed that the helix was not only stronger but the maximum intensity was downstream of the apex. Hooke also described that sediment movement within the meander was not uniformly distributed (Figure 2.8).

Hooke showed that the majority of the sediment is being moved from the portion of the meander that is downstream of the apex near the concave bank. In addition to helical strength and sediment movement Hooke also measured shear stress and illustrated it to be unevenly distributed throughout meander bends (Figure 2.9). Hooke explained that the maximum shear stress coincides with that of sediment movement and is located downstream of the apex along the concave bank. Hooke not only examined the shear stress along the bed of the channel but also along channel walls (Figure 2.10). Hooke observed that the maximum shear stress on the channel walls is at a point downstream of the meander apex. Hooke also remarked that the shear stress increases with discharge. Hooke also examines the shear stress along the outside bank of meander bends (Figure 2.11). He illustrated that the maximum shear stress occurs downstream of the meander apex and approximately halfway between the water surface and the channel bed. He commented that the shear stress distribution does not change with the flow rate. The only change is in the magnitude. He suggested that in meanders with small radius of curvature the downstream limb of the meander will grow faster than the upstream therefore increasing the radius of curvature. He also noted that on meanders with a large radius of curvature that the shear stress in the upstream limb prevents deposition and therefore the upstream limb will migrate downvalley at a faster rate than the downstream limb, reducing the radius of curvature.

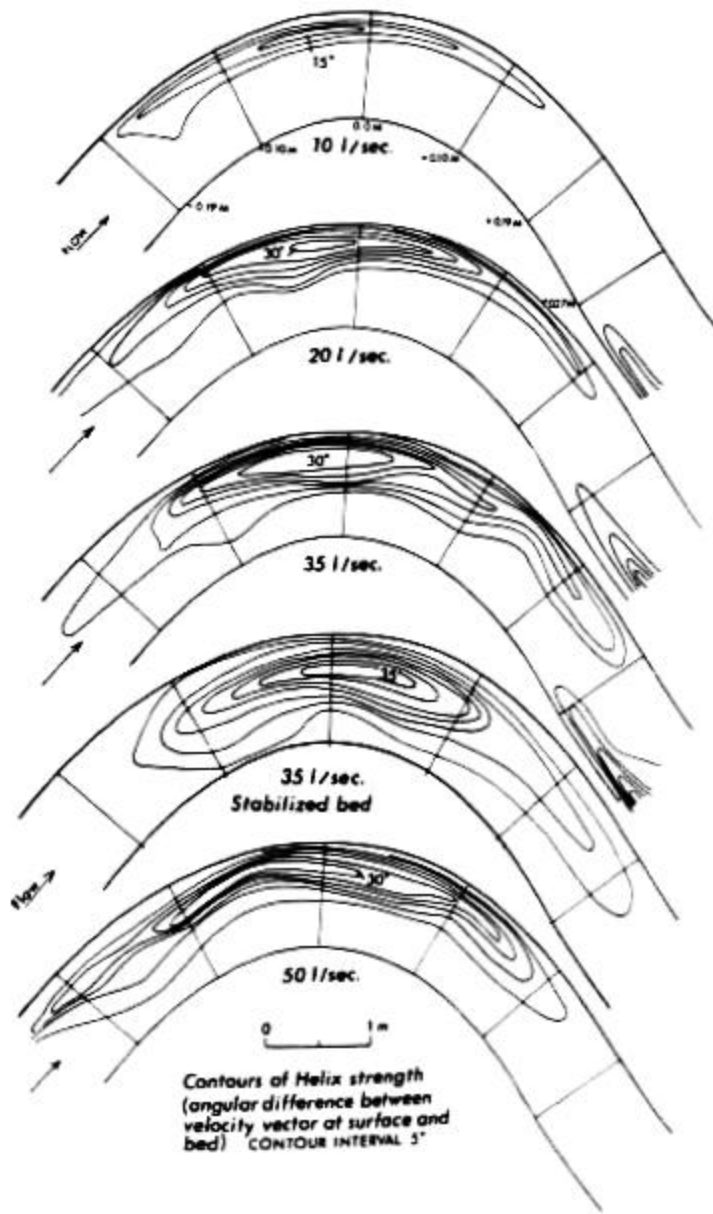


Figure 2.7 Helix Strength at Various Flow Rates. Source: Hooke 1975.

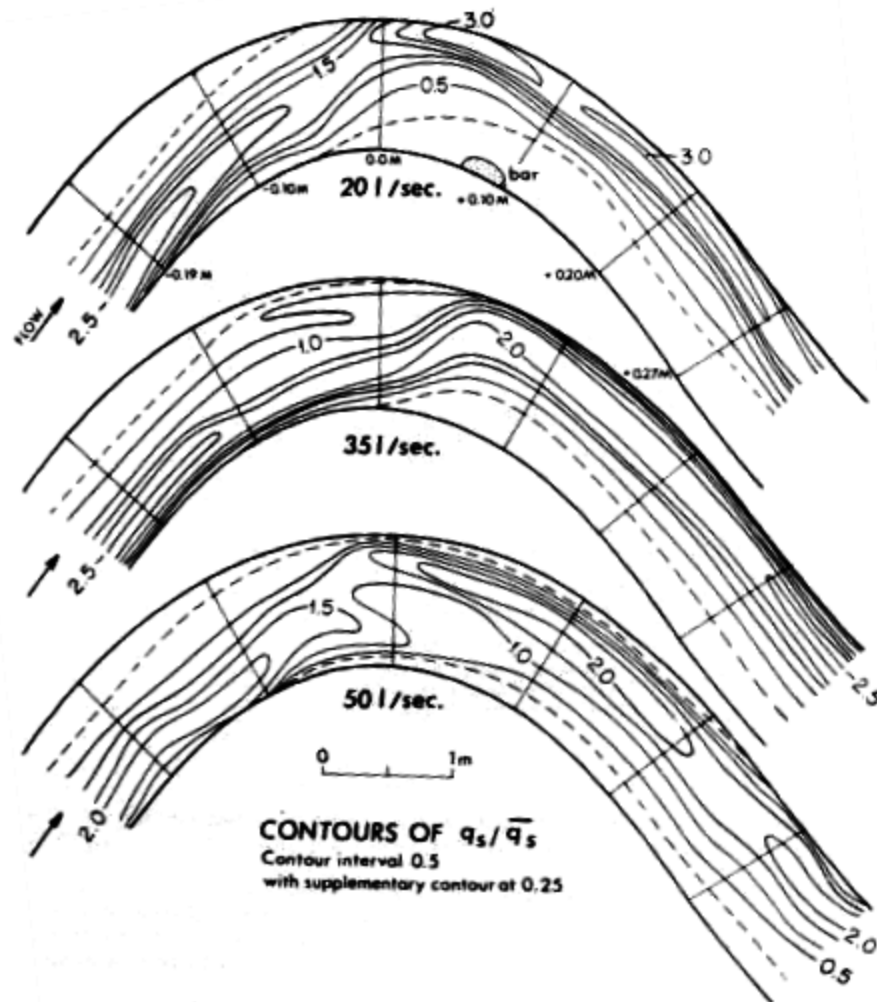


Figure 2.8 Map of Sediment Movement in Meander Bends. Source: Hooke 1975

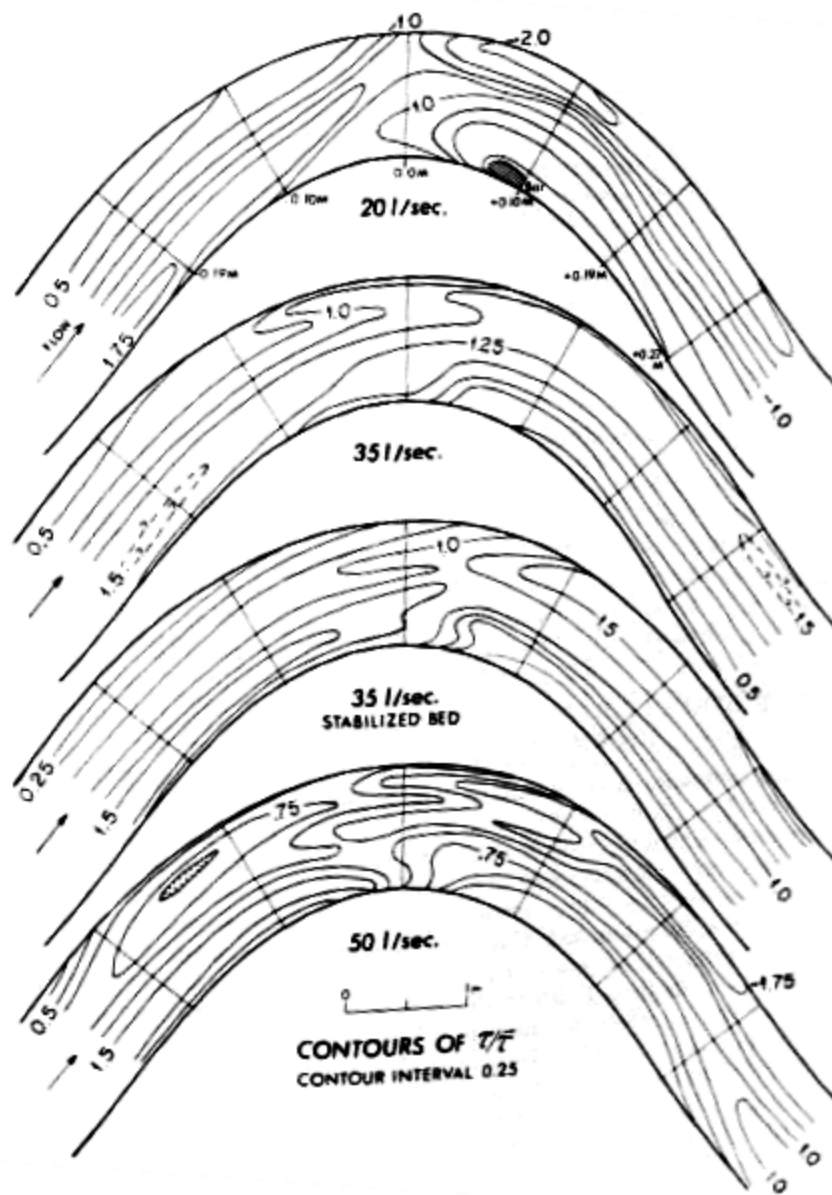


Figure 2.9 Meander Bed Shear Stress. Source: Hooke 1975.

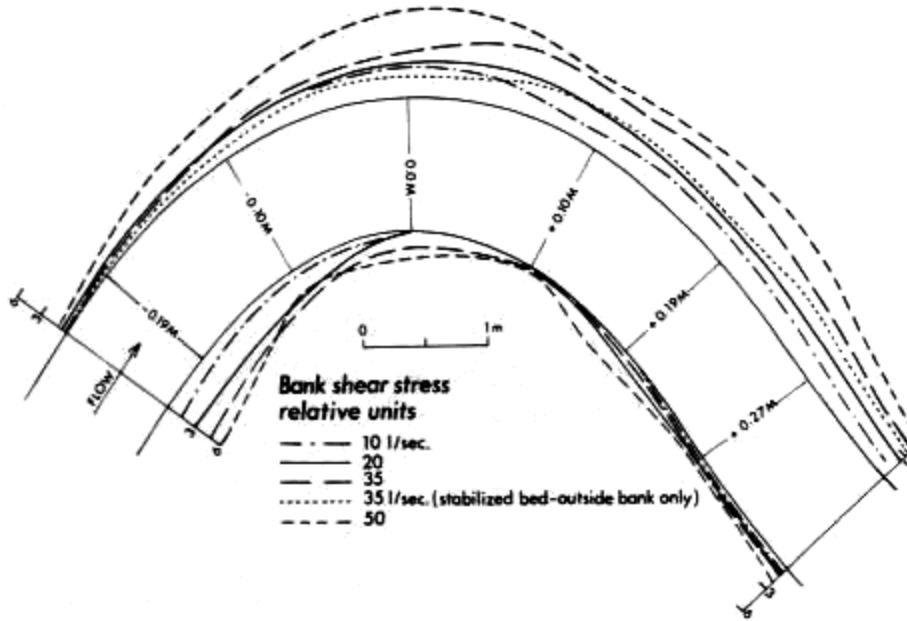


Figure 2.10 Plan View of Meander Shear Stress. Source: Hooke 1975

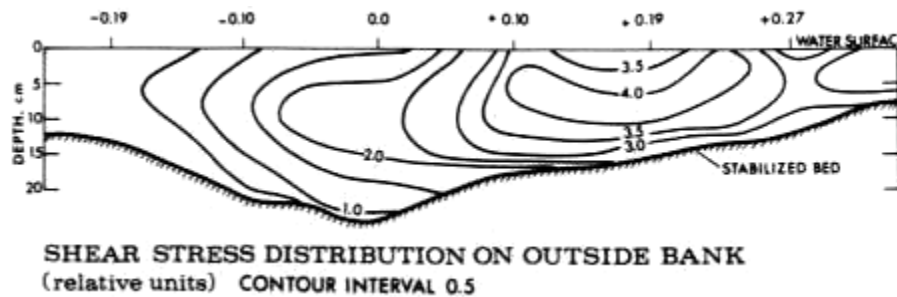


Figure 2.11 Concave Bank Shear Stress in a Meander Bend. Source: Hooke 1975

Einstein and Shen (1964) establish that two opposing helical flows develop in a straight channel with non-erodible walls. The helical flows being continuous throughout the channel contribute to the formation of a continuous meandering thalweg by one flow diminishing in size at the outside bend of the scour holes and being of equal sizes at inflection points (Figure 2.12, letter A). In Figure 2.12, black lines indicate surface currents, white lines indicate near bottom currents. Thompson (1986) made further revisions to the flow model developed by Einstein and Shen, and examined a straight channel with erodible walls. He showed that the meandering channel could be made of

overlapping sections based on pools, and riffles. He reported that bars began to develop immediately downstream of the scour holes and did not create a continuous helix or a continuous thalweg but instead create joined units of pools and riffles. Thompson illustrated that in pools units two opposing helical flows were present but in riffles four opposing helical flows begin to develop (Figure 2.12, letter B). Thompson generated a three-dimensional model showing flow structure in the meander bends. Thompson observed the importance of a relationship between the flow structure and channel bed elements such as bar head, bar tail, and riffle crest (Figure 2.13).

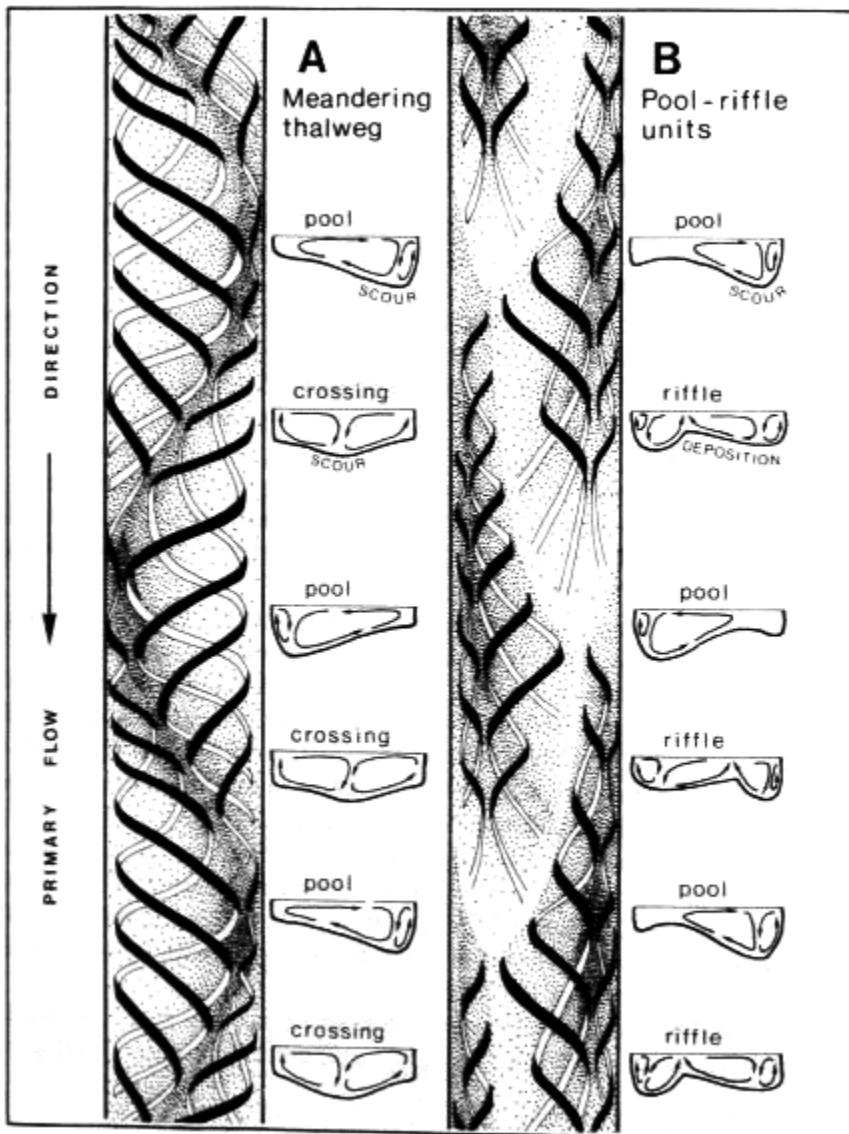


Figure 2.12 Meandering Flow in Straight Channels. Source: Thompson 1986.

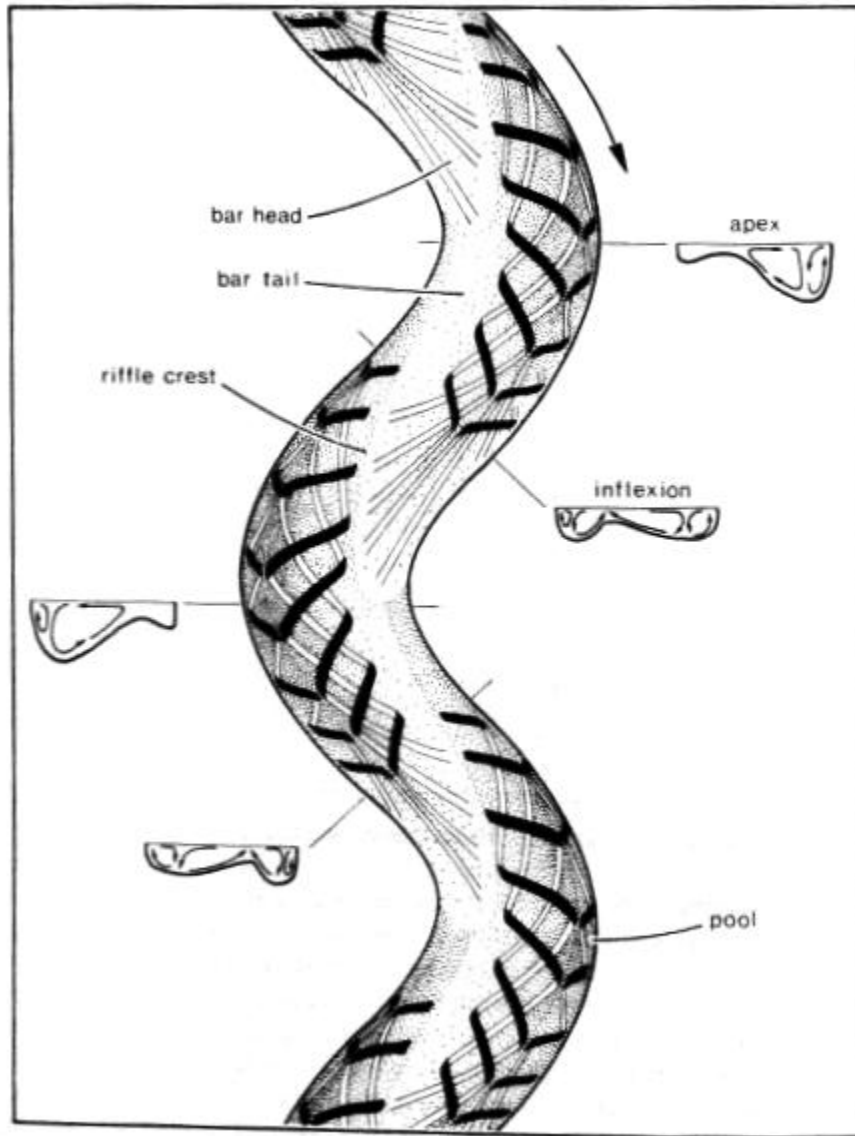


Figure 2.13 Flow in a Meandering Channel. Source: Thompson 1986.

Markham and Thorne (1992) reported that the cross section could be divided into three sections. They divided the cross section into a mid-channel region, outer bank region, and an inner bank region. They determined that the mid-channel region comprises about 80% of the flow in a meander bend and is characterized by a combination of radial forces, tangential, frictional, and centrifugal forces. They note that

the centrifugal force is the most important in that it accounts for the fast flowing surface water moving towards the outer bank. The fast flowing surface water piles up against the concave bank creating a phenomenon known as super elevation. The fast flowing water piling up against the concave bank also has the effect of lowering the water surface level along the convex bank. These forces lead to a tilting of the free surface therefore causing an inward-acting pressure gradient force. The balance between the centrifugal force and the cross-stream pressure gradient results in the water being driven outwards along the surface and inwards along the bed. This result creates a helical flow. Markham and Thorne disclosed that the outer bank region is dominated by an opposing circulation secondary flow. They established that this secondary flow increases with discharge and steepness of the outer bank. The inner bank region is dominated by an outward flowing centrifugal force. They note that this outward flowing force has the effect of causing the high velocity area to be pushed toward the outer bank, increasing the asymmetrical distribution of shear stress within the meander bend.

Processes and Rates of Meander Migration

Hickin and Nanson (1975) established that the rate of meander migration is greatest when the bend curvature was between two and three and note that this is likely due to the preservation of flow through the meander. They note that the curve ratio is important in changes to the stability of the separation zone at the convex bank. When the separation zone remains stable, the concave bank receives most of the force of the following water, therefore increasing the shear stress along the outer bank. When the separation zones begins to disintegrate large eddies are formed, similar to those described by Bagnold (1960), decreasing the amount of shear stress along the outer bank. When the shear stress is greatest, which will occur at a bend curvature just before separation begins to take place, the lateral migration rate will be greatest.

Begin (1981, 1986) used the momentum equation to model meander migration rates. The results of his studies agree with the finding of Hickin and Nanson (1975, 1984). The maximum rate of migration will occur with bend curvature between 2-3.

When the radius of curvature is below two the flow begins to separate from the inner bank.

Hooke (1980) ascertained when measuring the magnitude and distribution of meander migration that the drainage area size plays an important role in determining the migration rate. She established that the highest rates were associated with the rivers with the highest catchment area and that catchment area can be used to explain 53 % of the variation to the mean erosion rate.

Hickin and Nanson (1984) learned that when examining lateral migration rates for various size rivers that migration rates were still maximum with a bend curvature between 2-3 (Figure 2.14). They expressed that the size of the river was an important variable and attempted to normalize the distribution by dividing the migration rate by the channel width. They discovered that maximum migration rates for rivers could be as high as one tenth of the width of the river per year. They also realized that no movement occurred with bend curvature less than 1. They recognized that bank strength was a key predictor of erosion rate. Bank strength decreases as particle size increases when the mean particle size is smaller than fine sand. Bank strength is weakest when the particle size is fine sand. Bank strength increases as particle size increases when the mean particle size is greater than that of fine sand. The banks with the greatest strength are those composed of very small clays.

Hooke (1987) comprehended that lateral migration rates were best explained by the drainage area, which is specified as a crude measurement of discharge. She used a stepwise regression to explain the variance in lateral migration rates and acknowledged that drainage area was the best predictor followed by silt clay percentage and then followed by curvature.

Furbish (1991) showed that migration is related to both bend curvature and length. He remarked that meanders should be studied as an entire train as each meander influences neighboring meanders. He observed that large bends tend to grow at the expense of smaller bends and that intermediate bends tend not to grow.

Sun et al. (1996) established using computer models that meander migration could be influenced by amplitude. They discovered that rivers are more likely to migrate downvalley if they have low amplitude and are more likely to migrate laterally if they have high amplitudes.

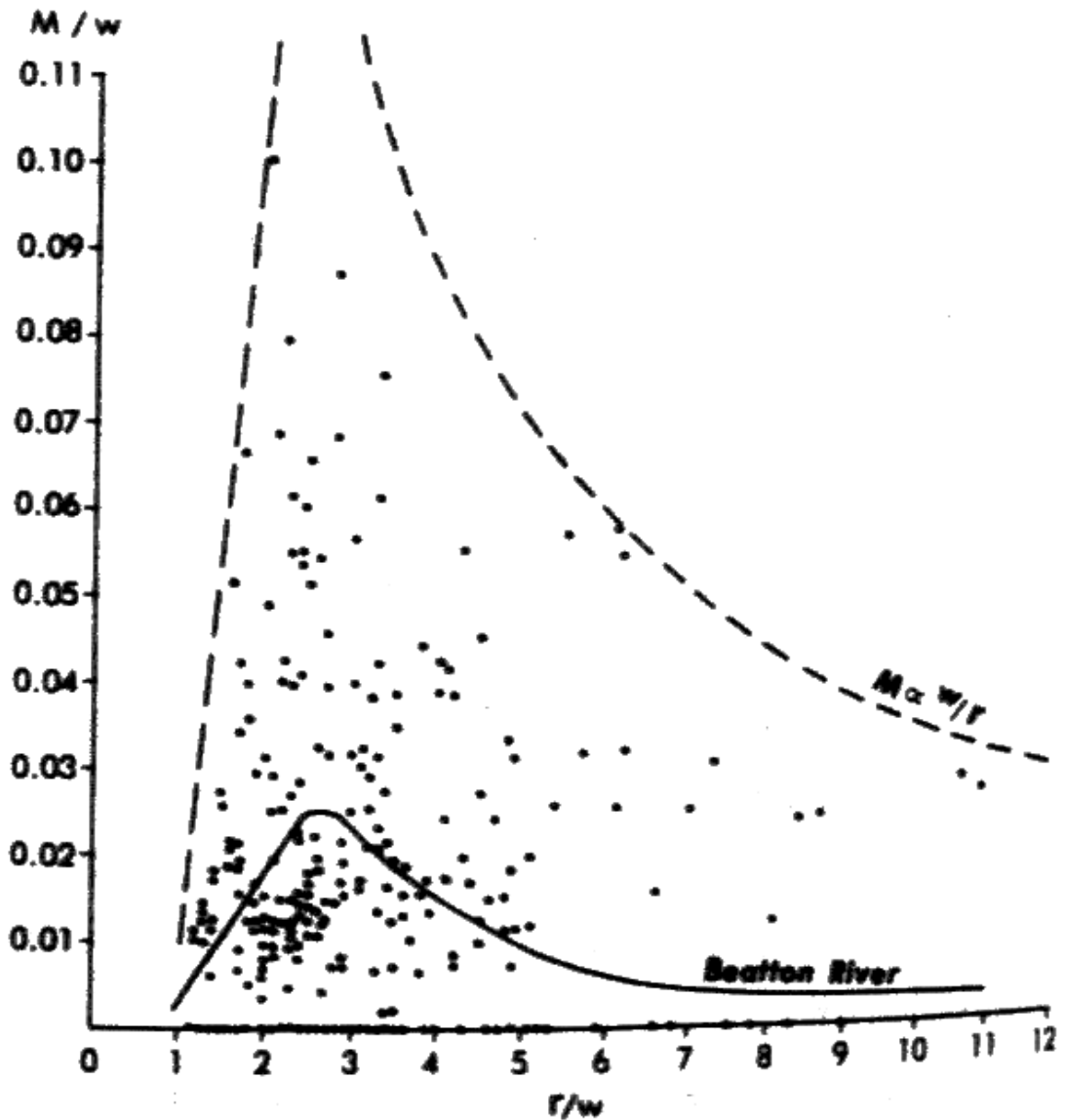


Figure 2.14 Bend Curvature and Relative Migration Rates. Source: Hickin and Nanson 1984.

Hudson and Kisel (2000) examined meander migration rates on the lower Mississippi River prior to major human modifications. The migration rates of the lower Mississippi ranged from one meter per year to 123 meters per year. The most significant division noted is between the alluvial valley and the deltaic plane, which is located near the Mississippi Louisiana border. Migration rates within the deltaic plane averaged 5.7 meters per year whereas migration rates in the alluvial plane averaged 45.2 meters per year. They conveyed that the maximum rate of meander movement occurred with bend curvature rating of approximately one, which is in contrast to studies by Nanson and Hickin 1986 and Hickin and Nanson 1975, 1984. The reason for the difference in both the peak value and shape of the meander migration rate and the bend curvature relationship is likely the complex flood plain of the lower Mississippi. The pioneering work done by Nanson and Hickin used a homogeneous floodplain. The lower Mississippi floodplain in contrast is more complex with the presence of clay plugs and areas of differential erosion.

Brooks (2003) realized that the Red River in Manitoba, Canada migrated at an average rate of .35 meters per year. He also discovered that the rate of migration has diminished since 8000 years before present. He ascertained that the current rate of meander migration is .04 meters per year. Brooks attributed the change in migration rates to a general lessening of post-glacial sediment supply.

Frothingham and Rhoads (2003) analyzed the three-dimensional flow characteristics in meanders. They gathered when looking at an elongated asymmetrical meander loop that the three-dimensional flow characteristics were similar to those in a symmetrical meander loop. They reported that the helix develops in pools and decays over riffles. They noticed that in the asymmetrical meander loop multiple pool and riffle sequences began to develop within a single meander loop. The different flow characteristics in each lobe of the asymmetrical loop meander in different directions. The upstream lobe migrated laterally and the downstream lobe migrated in a downvalley direction. This difference was attributed to where the maximum velocity encounters the bank. In the upstream lobe, the highest velocities were upstream of the apex. In the downstream lobe, the highest velocity was submerged near the base of the outer bank.

Richard, Julien, and Baird (2005) concluded that the lateral migration rates varied because of different sediment and water regimes in the Rio Grande of northern New Mexico. They used a multiple regression analysis to determine factors that could explain the lateral migration of the Rio Grande. They examined 13 independent variables including discharge, slope, total stream power, ratio of active channel width to total channel width, average median grain size for the bed material, and sinuosity. The multiple regression analysis revealed that lateral migration rates were most significantly associated with flow energy and the ratio of active channel width to total channel width.

Hooke (2007) discovered that rates of meander migration for the Dane River in northwest England averaged between .58 and .93 meters per year with a maximum of 1.3 meters per year. The middle part of the catchment proved to be the most unstable over a long period of time, which was attributed to moderately high stream power and highly erodible sediments.

Gautier et al. (2007) uncovered that migration rates on the Rio Beni had an average migration rate of 30 meters per year with a maximum of 120-140 meters per year. The river showed high spatial and temporal irregularities where the meandering took place. They observed that the watershed could be broken into three sections: the upper section, which represents most of the migration, a middle section that is near equilibrium, and a lower section that does not show much lateral migration.

Resistance to Meander Migration

Nanson and Hickin (1986) realized that vegetation did not significantly alter meander migration rates. They observed that meander migration occurs in an area of erosion that moves laterally from as deep as the thalweg and therefore undercuts most riparian vegetation. They noted that bank erosion was largely controlled by bed material transport, not the vegetation.

Abernethy and Rutherford (1998) revealed that riparian vegetation has differing impacts on a stream depending on its position in the drainage area. The influences of vegetation on stabilizing stream bank were divided into three effects. The first and

greatest influence was that of the transfer of bank sediment to the flow via fallen trees, which is most prevalent in the upper most part of the watershed. A second was in increase hydrologic resistance due to large woody debris and standing vegetation. This increased resistance can reduce the erosive effect of the flow and was most prevalent in the middle part of the drainage area. The third important aspect of riparian vegetation was protecting banks against mass failures by increasing the bank strength through the presence of deeply penetrating roots.

Micheli, Kirchner, and Larsen (2004) quantified the effect of removing riparian vegetation on rates of river channel migration. They pointed out that when studying the Sacramento River that migration rates through agriculturally lands were significantly higher on average than those of riparian forest. The 1949-1969 migration rates averaged 152% higher than their riparian forest counterparts. In the time-period between 1991-1997 the average migration rate for agriculturally lands was 11.2 meters per year while the average meander rate of areas covered by riparian forest were 5.9 meters per year which is an increase of 153%. Overall, they stated that the removal of riparian forest and the subsequent conversion to agricultural land resulted in an 80-150% increase in meander migration rates.

Stream banks are typically made up a material with at least some degree of cohesiveness, and because of this bond, some action needs to take place to break the bond. According to Brierley and Fryirs (2005) the three main ways in which a cohesive bank is weakened is through prewetting, desiccation, and freeze-thaw activity. Prewetting is the idea that soils are more susceptible to erosion when that are wet. Piping in the soil may also occur when the soils has been prewetted. Desiccation leads to increased bank erosion when small chips of the drier top soils fall to the toe slope, then entrained during high flow events, and act as an exfoliant to the surface of the bank. This exfoliation allows water in behind the larger soil peds and breaks them loose, leading to high rates of bank erosion. Freeze-thaw leads to increased bank erosion in that water seeps into the bank, freezes, thus expanding, forcing portions of the bank towards the river. Even if the ice does not directly force portions of the bank into the river, the space created by the ice can be filled with water during warmer high flow events, which leads to increased bank erosion. In agricultural streams, the change in land use and land cover

from native riparian vegetation to agriculture usually lowers the stabilization of riverbank by the loss of deep roots.

Brierley and Fryirs (2005) also identified the most common ways in which a bank might fail. The common processes involved are, hydraulic action and mass failure. Hydraulic action includes fluvial entrainment and undercutting, by the direct action of moving water. Mass failure includes slab failure, parallel slide, fall or sloughing, and rotational slip and slump.

Thorne (1999) divulged that banks erode in predictable slab failures creating first a simple slope and next a complex slope through progressive failures. The bank failure model predicts bank stability by the use of a stability number, which is the unit weight of the soil, multiplied by the height of the bank divided by the cohesion of the soil. The predicted stability number decreases exponentially as bank angle increases linearly. Different initial values of the stability number decrease as the friction angle decreases. This model has proven effective in the field at predicting bank erosion rates but does have some limitations. Some of the major limitations of the model are that it has no way of dealing with steep soils, undisturbed soils, and complex stratigraphy.

Bank erosion is controlled by the combination of two basic processes, stream bank characteristics, or the potential for erosion, and hydraulic and/or gravitational forces (Rosgen 2001). The Rosgen Bank Erosion Hazard Index (BEHI) and the Near Bank Stress (NBS) is part of the Rosgen system, which has also been adopted by the Environmental Protection Agency (EPA) for estimating stream bank erosion rates. The BEHI combines bank characteristics with the NBS of order to address the two basic processes involved in bank erosion. The NBS is calculated largely based on different streambed characteristics for the stream at or near the bank in question. In the Rosgen system seven variables are evaluated that can control a banks potential for erosion: bank height ratio (stream bank height/maximum bankfull depth), ratio of rooting depth/bank height, rooting density, percent surface area of bank protected, bank angle, number and location of various soil composition layers or lenses in the bank, and bank material composition (Rosgen 2001).

CHAPTER 3 - Methods

The methods chapter is comprised of two sections organized by major research objectives in the study: first, to describe the spatial and temporal patterns of channel shifting and second, to explain the patterns and process of channel shifting.

Description of the Spatial and Temporal Patterns of Channel Shifting

Three subsections comprise this section. The first section will focus on photographic analysis, the second, on measurement of area lost, and the third, on measurement of meander geometry.

Photographic Analysis

The location of the river at different time-periods needed to be known in order to describe the spatial and temporal pattern of the channel shifting between 1956 and 2006, and the associated impact on farmland erosion along the west bank of the Big Blue River. A series of topographic maps and aerial photographs were used to locate the channel at different times. A combination of the use of historical photographs and topographic maps has been well established in other research (Graf 1988, Marston 1995). A list of types and selected attributes for the time interval used is disclosed in Table 3.1.

To cover the 50 years of channel shifting required procuring a series of existing digital maps and aerial photographs then combining them with printed maps and aerial photographs. Digital maps and aerial photographs were found for the years 1983, 1991, 2002, and 2006. The year 1983 required using a Digital Raster Graphic (DRG), which is defined as a scanned and georeferenced image of a United States Geological Survey (USGS) topographic map. The process of creating a DRG started with the 24-bit full color scanning of the paper copy of the USGS topographic map using a 500 – 1000 DPI high-resolution scanner. The scanned file was then georeferenced using the known real world position of the 16 Universal Transverse Mercator (UTM) tick marks indicated on the scanned map, creating a digital map referenced using a UTM projection and the North

American Datum of 1983. The georeferenced map was then converted to a raster file with a grid size of 2.4 meters. The horizontal accuracy of the digital map was checked by comparing the latitude and longitude of the digital map with the listed book values for the location to assure that they are consistent (U.S. Geological Survey 1997b).

Table 3.1 Summary of select attributes for time interval data and sources

Year	Data Source	Spatial resolution (Meters)	Type
1956	USDA CSS	1	Black-and-white aerial photograph
1966	USGS	2.4	1:24:000 Scale Topographic Map
1969	USDA ASCS	3	Black-and-white aerial photograph
1977	USDA SCS	3	Black-and-white aerial photograph
1983	USGS	2.4	1:24:000 Scale Topographic Map
1986	FSA NAIP	1	Black-and-white aerial photograph
1988	FSA NAIP	2	True color aerial photograph
1991	USGS DOQQ	1	Black-and-white aerial photograph
1997	FSA NAIP	2	True color aerial photograph
2002	USGS DOQQ	1	Black-and-white aerial photograph
2006	FSA NAIP	1	True color aerial photograph

A mosaic of USGS Digital Orthophoto Quarter Quadrangles (DOQQ) was acquired for the years 1991 and 2002. DOQQ's are created by scanning black-and-white aerial photographic negatives using a precision image scanner at a resolution of 25 – 32 microns. The process produced an eight-bit black-and-white digital photograph with a ground resolution of one meter or less. The photographs were then georeferenced using nine control points, one at each corner, one at each center along the edge and one on the middle of the photograph. The digital image was then referenced using a UTM projection and the North American Datum of 1983. A Digital Elevation Model (DEM) for the area of the photographs, used in conjunction with the ground control points, was used to create an aerotriangulated image with a horizontal and vertical accuracy of 2.5 meters or greater (U.S. Geological Survey 1997a, 2002). DOQQ's do not cover a large

amount of area with each photograph, so to cover areas as large as a county, multiple DOQQ's are combined to make one mosaic. In this case, the mosaic of DOQQ's was compressed using an MrSID compression, a wavelet compression technique, in order to save space.

For the year 2006 a mosaic of United States Department of Agriculture (USDA) Farm Service Agency (FSA) National Agricultural Imagery Program (NAIP) aerial photographs was used. NAIP digital images were created to be a 24 bit true color image format with a ground resolution of one meter, and a horizontal and vertical accuracy of five meters or greater. The digital image was then referenced using a UTM projection and the North American Datum of 1983. The process of aerotriangulating the photographs can be done in lots of 200 – 1000 photographs at one time. With the use of a DEM for the area of the photographs, the output of the aerotriangulation process became a single georeferenced mosaic, compressed using a MrSID compression. The Kansas Geospatial Community Commons provided all of the existing digital files used in this and are freely available at www.kansasgis.org.

Printed maps and photographs were located for 1956, 1966, 1969, 1977, 1986, 1988, and 1997. Photographs not already existing in digital form were scanned at 600 dpi and imported into a Geographical Information System (GIS) software package known as Environmental Systems Research Institute (ESRI) ArcGIS, ArcINFO suite, version 9.2, and used in ArcMap. The geoprocessing toolbar included in the ESRI base software and license was used for the georeferencing process. The digital copies of the photographs were scanned into the GIS software in order to be georeferenced. Ten points were located that have not moved between the time in which the photograph used for the base image in the photo being rectified was taken, the points were primarily focused on the middle third of the image to reduce the amount of distortion. All of the photographs were rectified using the 2002 Digital Orthographic Quarter Quadrangles (DOQQ) as the base map. Common control points were used at road intersections and driveway entrances. Some error occurs when matching multiple points on photographs that are brought into the GIS software. This error, known as root mean square (RMS) error, can be calculated by taking the root mean of the difference from the user input point location and the location of the point after the equation used to transform the image has been run.

All of the images were transformed using a first order polynomial, meaning that the image was shifted, rotated and stretched, but not distorted in anyway. All photographs were projected using the Universal Transverse Mercator (UTM) Zone 14 North, using the North American Datum of 1983. The RMS values are in meters because the images are in the UTM system.

A set of three photographs was needed to cover the study area in the year 1956. The photographs are available in printed copy at Kansas State University's (KSU) Hale Library, and were flown for the Commodity Stabilization Service (CSS), a precursor to today's FSA. The images were scanned and georeferenced utilizing the previously detailed method creating an eight bit black-and-white photograph with a ground resolution of one meter. The RMS error associated with the 1956 photographs averaged 3.34 meters with the maximum being 3.58 meters.

A USGS topographic map was used for the year 1966. The topographic map used in this thesis can be acquired in printed copy at KSU's Hale Library. The topographic map was scanned using a method consistent with the one previously described above. Some of the control points used in the georeferencing were based on the corresponding points in the 1983 topographic map that was already in digital format because the 1966 image was a topographic map, not a photograph. The 1966 topographic map was scanned at full-color, creating a 1:24,000 scale 24-bit digital image. The RMS error associated with the 1966 topographic map was 2.26 meters.

A photo mosaic assembled by the USDA Agricultural Stability and Conservation Service (ASCS), a precursor to today's FSA, was used for the year 1969. Photographic mosaic composed by the USDA ASCS was in printed format before it was scanned. The mosaic can be acquired in printed format at KSU's Hale Library. The mosaic was scanned and georeferenced using the method described above, creating an eight-bit black-and-white photograph mosaic with a ground resolution of three meters. The RMS error associated with the 1969 photographic mosaic was 4.65 meters.

For the year 1977, the photo mosaic composed by the USDA Soil Conservation Service (SCS), a precursor to today's USDA Natural Resources Conservation Service (NRCS), was used. The photographic mosaic, produced by the USDA SCS was in printed format before converting to a digital file and is housed in printed format at KSU's

Hale Library. The mosaic was scanned and georeferenced using methods consistent with the one described above creating an eight bit black-and-white image with on the ground resolution of three meters. The 1977 USDA SCS image has an RMS error of 5.40 meters.

A USDA FSA NAIP was used for the year 1986 and the printed copy was acquired from the Marshall County Farm Service Agency. The NAIP photograph was scanned and georeferenced creating an eight bit black-and-white image with a ground resolution of two meters. The 1986 NAIP photograph has an RMS error of 5.21 meters. Two USDA FSA NAIP images were used for both the year 1988 and 1997. The printed copies were procured from the Marshall County Farm Service Agency. The photographs were scanned and georeferenced creating four 24 bit true color images, two for each year, with a ground resolution of two meters. The RMS error for the two 1988 images was 9.98 and 5.68 meters. The RMS error for the two 1997 images was 4.01 and 4.44 meters.

Sub-pixel accuracy may not seem like a feasible goal, given the RMS errors associated with the aerial photography. A study by Hughes, McDowell, and Marcus (2006) revealed that RMS error gives a global measure of lateral error but overestimates the amount of local lateral error associated with aerial photographs, particularly in cases of floodplains with control points on surrounding hillsides. Hughes, McDowell, and Marcus suggest that an independent measure looking at lateral displacement of features could be used to assess the accuracy of aerial photographic georeferencing. The use of a control point near the agricultural field that has experienced the loss of land was used in this study to assess the lateral accuracy of the aerial photographs in the area of concern. The lateral displacement of the control point was found to be less than the resolution of the largest pixel, therefore supporting the sub pixel accuracy desired when using aerial photography.

The thesis objectives were best met by the creation of GIS layers to facilitate geographic overlays and analysis. Once the photographs were imported into GIS software, the river, bars and islands, and riparian vegetation could be digitized using a technique known as “heads-up digitizing.” This process involved the user drawing polygons for each of the features of interest based on the on the screen image. The items in the photograph were identified using image interpretation guidelines set out in Howard and Mitchell (1985) as follows:

Shape: The configuration and general outline of objects.

Shadow: shadows can be used as a crude way of guessing height. Shadow angle and length vary a great deal with changing season, time of day and location on the earth. (Shadows are longest near the beginning or end of the day as well as near the winter solstice)

Tone and Color Contrast: Tone is the various shades of gray in black-and-white or monochromatic images. Darker locations of the images are areas where less light is received by the camera, for whatever reason. Color contrast is the equivalent in color images; however, multiple factors come into play such as value, hue, saturation, and chroma.

Texture: Texture is the product of tone, size, shape, pattern, shadow and reflective properties and can be seen as features too small to be discerned as individual objects.

Pattern: Pattern is the more broad arrangement of tones and textures and can be used to identify local landforms, topography, drainage networks, and other features.

The process of identifying the river, bars and islands, and riparian vegetation was repeated for each photograph. The location of the river was drawn around the current stage, or edge of water, for each time interval. Sand bars and islands are areas of sediment accumulation along the river with no vegetation. Riparian vegetation areas are areas of vegetation identified between cross sections one and three and in the immediate vicinity of the river. Further information about how the river, bars and islands, and riparian vegetation are defined and identified can be found in Table 3.2.

Measurement of Farmable Area

The maximum farmable area was mapped by combining the maximum extent of the farming between 1956 and 2006. The 2006 FSA NAIP image was used to define southern boundary of the farmable area. The western, northern and eastern boundaries are all based on the 1956 USDA CSS image. The maximum farmable area was crosschecked with the 1966 topographic map conforming that the area covers the entire flat field between the road and the river. This mix shows the clearing of trees from the southern edge on the field providing the maximum farmable area. Calculation of the lost farmable area requires removing the portion of the area eliminated by river erosion from the digital farmable area layer. This was accomplished by overlaying the river location with maximum farmable area and clipping, or removing, the overlapping portion to a distance of 10 meters from the river to account for impossibility of farming up to the river's edge. Further revisions to the northern boundary were done based on the extent of the field at the time the photograph was taken. The area of the field is calculated as function of having the field digitized into the GIS software. However, the area calculated is in square meters so a simple unit conversion is needed to convert square meters into hectares.

Table 3.2 Aerial photograph interpretation

	River	Bars	Islands	Riparian vegetation	Farmable area
Shape	An area of approximately uniform width winding through the photograph. Smooth boundaries.	Typically a crescent shaped area found often on the inside of river bends. The thickness varies, often thickest near the apex of the bend.	Irregular shape, typically longer in the downstream direction than the cross stream direction, surrounded on all sides by the river at the stage of the river when the photograph was taken.	Irregular borders. Often found in bands roughly parallel to the river.	Shape can vary. Have smooth borders and often maximizes available area, so borders are typically roads of rivers.
Shadow	Rivers are the typically the lowest features and therefore does not cast a shadow	Bars are low lying features and do not cast a shadow	Islands are low lying feature and do not cast a shadow	Areas of shadow can be seen where trees and other tall vegetation comes to an abrupt end, such as at water's edge.	Typically these areas have low profile crops that do not cast a shadow
Tone	Darker gray areas	Lighter areas	Lighter area	Can vary between gray and very dark grays.	Can vary between gray and very dark grays.
Color	Brown	Varies from light brown to a almost white	Varies from light brown to a almost white	Varies from brown to dark green	Varies from brown to dark green
Texture	Smooth	Smooth	Smooth	Typically very rough	Typically smooth
Pattern	Some areas of lighter tone in shallow water, and darker tone in deeper water. Patterns run roughly parallel to the banks	Some areas with banding of darker colored material.	Some areas with banding of darker colored material	No clear discernable pattern	Typically have parallel lines resulting from plowing and planting

Measurement of Meander Geometry

Measuring how the meander has moved, and changed shape over time summarizes the second important aspect of describing the spatial and temporal pattern of channel shifting. Meander geometry uses the various measurements, treating the meander as a waveform and can facilitate how the meander has changed shape over time in a quantifiable manor (Figure 3.1). L represents meander wavelength, measuring from two identical points on separate cycles, in this case inflection points, covering one cycle. Calculated from the apex of one meander to the apex of the next meander A represents amplitude. Quantified by fitting an arch to points at or near the meander apex R_c represents the radius of curvature. Determined at various points along the meander and averaged W represents the channel width. In this study, the key measurements of meander geometry are the radius of curvature and channel width, which can be used to show how the shape of the meander has changed over time. For the measurement of channel width, the active channel is used. The active channel is defined as the width of the channel that is clear vegetation. This definition was chosen because bankfull width is difficult to determine from aerial photographs. Since the channel that is clear of vegetation does not vary as much with discharge, and can be quantified, the active channel was used as a substitute for bankfull width.

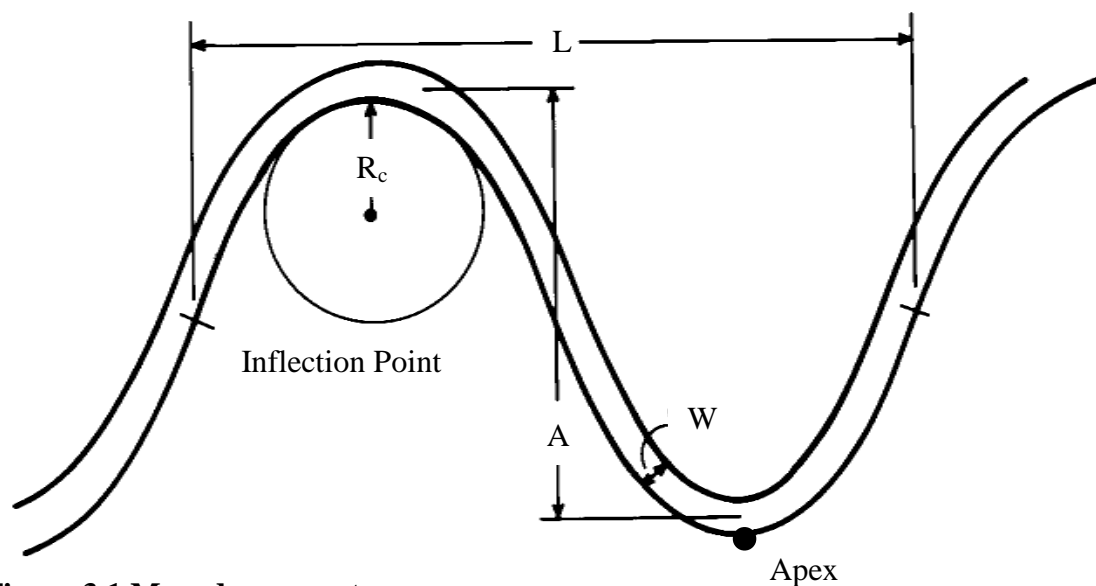


Figure 3.1 Meander geometry

Measuring how the meander has moved over time requires three measurements. The first being extension, the second being translation, and the third being rotation. The definition of each of the three terms was covered in the introduction. Total meander migration can be calculated by combining extension and translation by utilizing Pythagoreans' theory where the total migration is the hypotenuse using the following equation where M represents the total meander movement, E represents the extension, and T represents the translation.

$$M = \sqrt{(E^2 + T^2)}$$

Explanation of the Patterns and Process of Channel Shifting

The pattern and process of channel shifting, and farmland erosion result from the interaction of driving forces and resisting framework. Annual peak flows and meander geometry are the driving forces, while the Bank Erosion Hazard Index (BEHI) and percent riparian vegetation are the resisting framework.

The BEHI system was developed by Rosgen (2001) for estimating the predicted amount of bank erosion. The BEHI is based on the relationship between bankfull height and total bank height, the relationship of root depth to total bank height, percent root density of the bank, bank angle at bankfull height, and percent of surface protection. Each of the categories that the BEHI examines are qualitatively ranked from very low to extreme with intermediate ratings being low, moderate, high, and very high. Adjustments were made to the rankings based on bank material and stratification of the bank. Although, the BEHI can only be calculated for the current bank the assumption that over the past 50 years the bank material has not altered in composition can be made. Because only two data points are known for the BEHI, it will not be included in correlation regression analysis, but will instead be used as the qualitative measure.

Riparian vegetation was examined using polygons digitized around areas that show riparian vegetation in the aerial photographs. A polygon was digitized around the entire river valley between cross section one and cross section three yielding the total valley bottom area. The river valley was defined as the area adjacent to the river but between the edge of the farm fields on either side. The valley bottom was predominantly

covered by vegetation, so calculation of the area of riparian vegetation was accomplished by removing the area of the river and the area of the bars and islands from the total valley area. The bars and islands were digitized around area that did not have any vegetation. The river extent was digitized from the extent of the river at the time of the photograph.

Meander geometry, specifically bend curvature, will yield a number that has proved effective at predicting rates of meander migration (Hickin and Nanson 1975, 1984, Nanson and Hickin 1986). Bend curvature is calculated by taking the radius of curvature and dividing it by the channel width. The active channel width is the width of the non-vegetated channel. Another area of critical meander geometry includes the channel cross section. The cross section influences how the water flows thereby influencing where erosion takes place along the meander. The location of the greatest erosion will likely dictate whether extension or translation will be the dominate direction of meander movement.

Historical flood records for the Big Blue River were analyzed to establish a relationship between peak flows, bend curvature, and the amount of farmable area lost. The annual peak flows were noted for each year, 1985-2005 for the Big Blue River at Marysville (USGS gaging station 06882510). For the period 1929-1984, the annual peak flows for the gaging station at Marysville were estimated by correlating the 1985-2005 values for Marysville with those for an upstream gaging station on the Big Blue River at Barneston, Nebraska (USGS gaging station 06882000), for which stream flow records extend back to 1929. The r^2 for the gaging station correlation was 0.707 (Figure 3.2).

Estimations of peak flows were calculated for the Marysville gage by using the equation generated in the correlation (Figure 3.2). In this equation x represents the Marysville gage and y represents the Barneston gage. Entering in the actual amount of flow recorded at the Barneston gage into the equation for x the estimated amount of flow is calculated for the Marysville gage (Figure 3.3).

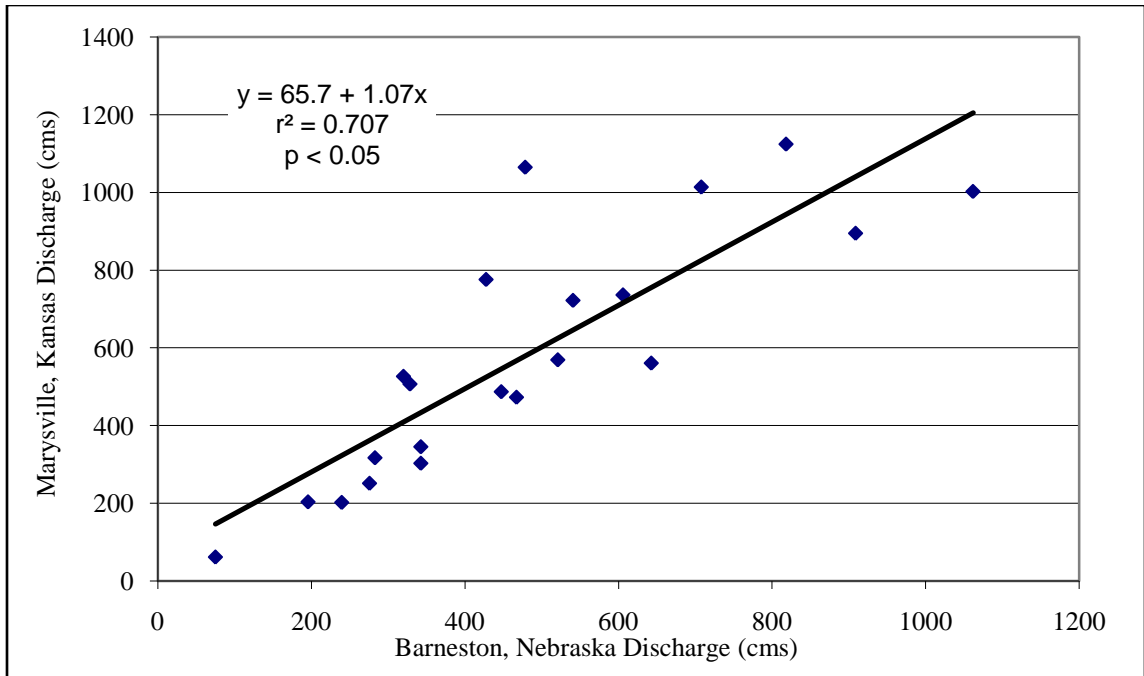


Figure 3.2 Regression between two Big Blue River gages

The annual peak flows show a low variability and relatively low flows for the late 1950's, 1960's, 1970's, and early 1980's. A large amount of variation in peak flows occurred in the mid 1980's through the mid 1990's, and interval that had several large flow events. Global Historical Climate Network (GHCN) data for Beatrice, Nebraska, located near the middle of the watershed, indicates that years of greater than average precipitation for the study period correspond with years of high peak annual peak flows (Figure 3.4). The same direct relationship can be observed for low annual peak flows and less than average precipitation.

A number of possibilities could explain the variation. First, poorly integrated streams in the Rainwater Basin plains ecoregion were artificially connected at some time in the past. This could increase the runoff-to-precipitation ratio for the watershed upstream of the study reach. The connection of the interior drainage networks to the larger watershed could lead to greater variability of peak flows downstream. Second, the distribution of precipitation throughout the year could have changed, again increasing the runoff-to-precipitation ratio. Third, the conversion of grassland to cropland could also increase the runoff-to-precipitation ratio.

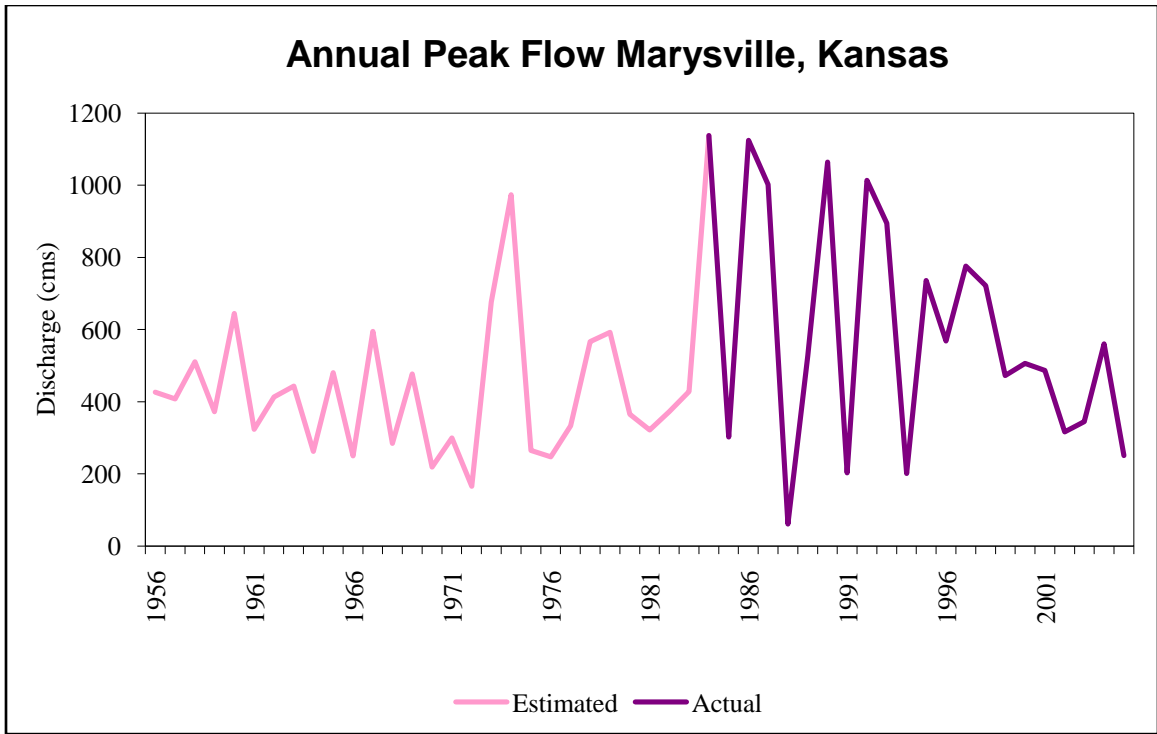


Figure 3.3 Annual Peak Flow at Marysville Gage

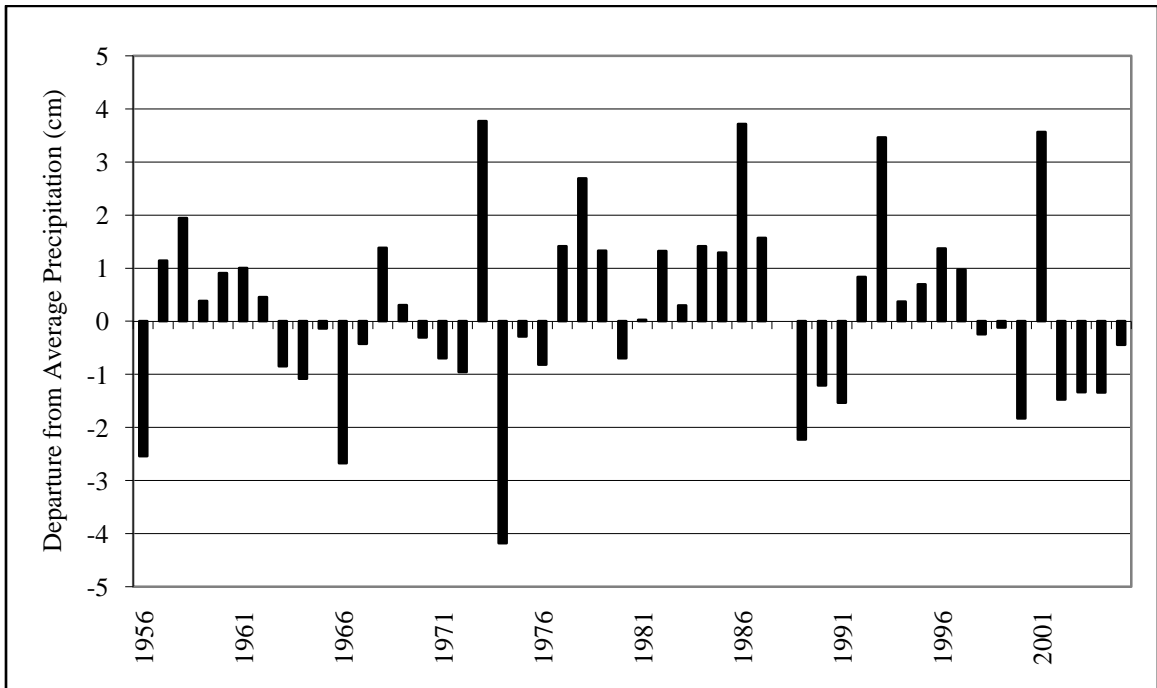


Figure 3.4 Departure from Average Precipitation at Beatrice, NE

The flood recurrence interval was calculated for each year, 1929-2006. Flood recurrence intervals calculate the probability of a given magnitude flood occurring in any given year. Recurrence interval can be calculated using the following equation:

$$RI = \frac{n+1}{N}$$

Where RI represents the recurrence interval, n represents the number of years in the record, and N represents the rank with one being the highest magnitude flow of the record. The average recurrence interval for each interval between successive aerial photographs could then be calculated. A complete list of annual peak flows at both gaging sites and the corresponding recurrence interval are found in Appendix A

Channel cross sections were surveyed using standard, accepted techniques in three locations on 11-12 August 2007 (Figure 1.2). The discharge was between 49.3 - 61.7 cubic meters per second (cms) on these dates as measured at the USGS gaging station on the Big Blue River at Marysville. A laser level was used in conjunction with a laser eye equipped rod to measure depth below the height of the laser. The three cross sections were monumented and locations marked with a GPS for future comparisons. Appendix B contains cross section survey data. The purpose of the cross section is twofold. The cross section data can be resurveyed to assess future impacts of dredging. In addition, steep sided cross sections provide another piece of evidence that the river is actively eroding.

Knowing the percent of riparian vegetation coverage, bend curvature, and peak flows allows the determination of the correlations between the amount of farmland lost to erosion and total meander migration. To test the existence of correlation between the variables the Pearson Correlation Analysis was run. The Pearson Correlation Analysis was chosen because the assumptions needed for the analysis are met by the data in this thesis, when certain data transformations are performed. The Pearson Correlation Analysis has underlying assumptions that must be met. The first assumes that the data be a random sample of paired variables. The second assumes that the variables have a linearly increasing or decreasing association. The third assumes that the variables are measured in an interval or ratio scale. The fourth and final assumption is that the

variables must have a bivariate normal distribution. The Pearson Correlation Analysis based on the following equation:

$$r = \frac{\sum XY - \left(\frac{(\sum X)(\sum Y)}{N}\right)}{\sqrt{\left(\sum X^2 - \left(\frac{(\sum X)^2}{N}\right)\right)} \sqrt{\left(\sum Y^2 - \left(\frac{(\sum Y)^2}{N}\right)\right)}}$$

Where r represents the Pearson correlation coefficient, X represents the value in the first data set, Y represents the value in the second data set, and N represents the number of paired data values. The Pearson Correlation value ranges from positive one for a perfect positive correlation to negative one for perfect negative correlation, with zero representing no correlation. Statistical significance of the Pearson correlation coefficient can be found with the following equation.

$$t = \frac{r\sqrt{n-2}}{\sqrt{1-r^2}}$$

Where t represents the t-score, r represents the Pearson correlation coefficient, and n represents the sample size.

Once the correlation between variables was known, a multiple regression was used to determine the amount of each dependent variable could be explained by each independent variable. A multiple regression was used to analyze three dependent variables. The first being annual farmable area lost, the second being a total annual migration and the third being the ratio of translation to extension. The independent variables were chosen based on the results of the correlation to avoid colinearity. It is worth noting that because of the small sample size both the correlation and the regression are used to explain the changes that have taken place and should not be used as a predictive measure.

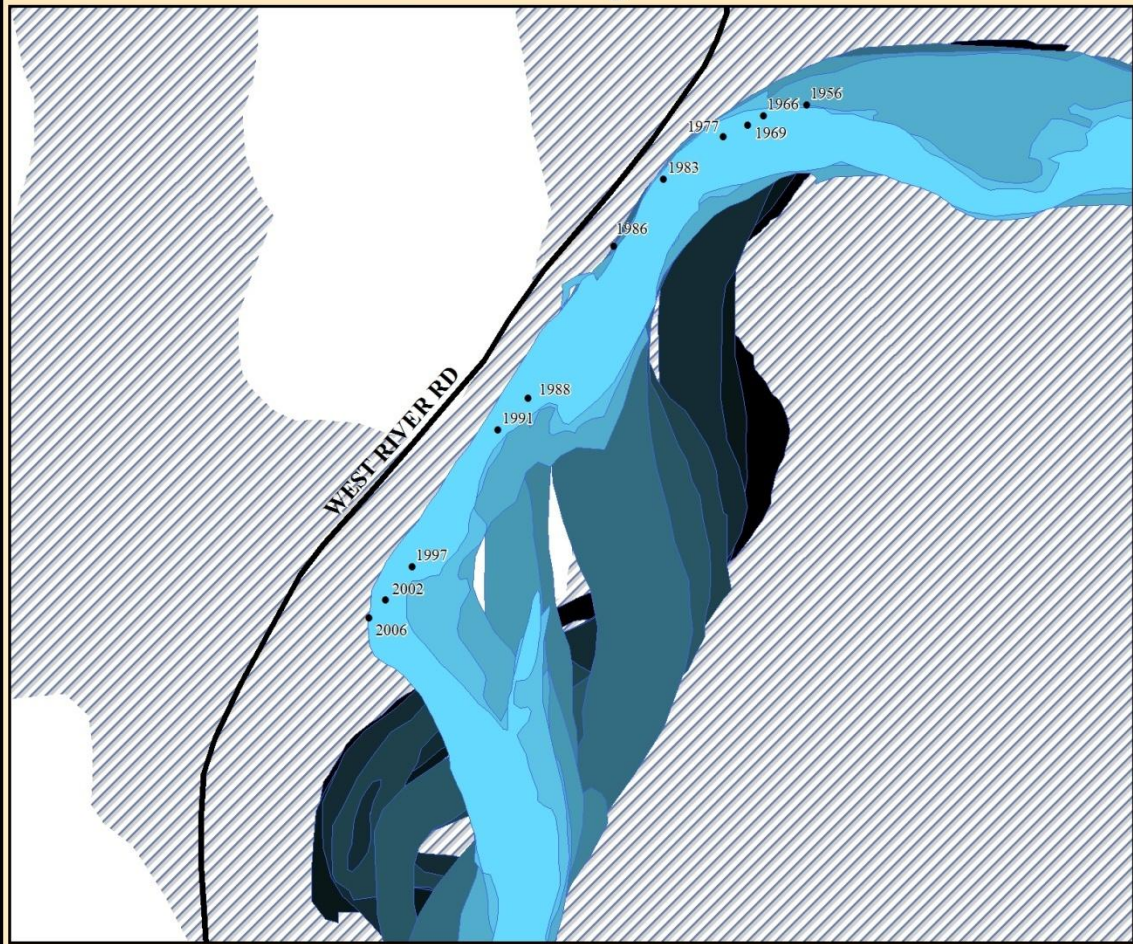
CHAPTER 4 - Results and Discussion

Three sections comprise the results and discussion chapter. First, describe the spatial and temporal patterns of channel shifting, second, explain the patterns and process of channel shifting, and third, discussion.

Description of the Spatial and Temporal Patterns of Channel Shifting

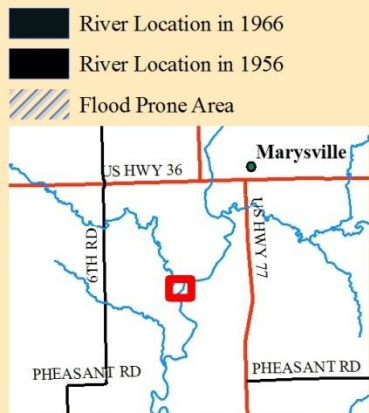
The results of the description of the spatial and temporal patterns of the channel shifting indicate that the Big Blue River has changed location over the past 50 years (Table 4.1, Table 4.2, Appendix C, and Appendix D). Appendix C (Figure C.1 through Figure C.9) contains maps showing the river location and change between successive years of known river location. The maps show that no farmland area was lost between 1956 and 1969 (Figure C.1) and that the maximum rates of erosion occurred for two intervals, between 1983 and 1986 and between 1986 and 1988 (Figure C.4 and Figure C.5). A diagram in the bottom left hand corner of each of the maps shows the amount of farmable area plotted against time, with a red section corresponding to the time of the map. Appendix D (Figure D.1 through Figure D.10) is comprised of maps that depict the meander movement between each successive year of known location. No evidence of the amount of movement prior to 1956 was found, so Figure D.1 shows the measure of the meander geometry for that year. Two diagrams are provided on the bottom of each map one showing the annual migration rate plotted against the year the other showing annual migration rate plotted against bend curvature. The diagrams show that the maximum migration rate occurred between 1986 and 1988, simultaneous when bend curvature was between two and three. Figure 4.1 shows a composite of river location for each time of known river location and corresponding meander apex.

50 Years of Channel Change: 1956 Through 2006



Data Source: 1956 river location based on USDA CSS photographs, 1966 river location based on USGS topographic map, 1969 river location based on USDA ASCS photographs, 1977 river location based on USDA SCS photographs, 1983 river location based on USGS photographically revised topographic map, 1988 river location based on FSA NAIP photographs, 1991 river location based on USGS DOQQ photographs, 1997 river location based on FSA NAIP photographs, 2002 river location based on USGS DOQQ photographs, 2006 river location based on FSA NAIP photographs. Flood Prone Area based on high water marks from the 1941 flood, compiled and mapped by the USGS. Projection: UTM Zone 14 North Datum: NAD 1983

- Meander Apex
- Light Blue: River Location in 2006
- Medium Light Blue: River Location in 2002
- Medium Blue: River Location in 1997
- Dark Blue: River Location in 1991
- Very Dark Blue: River Location in 1988
- Black: River Location in 1986
- Black: River Location in 1983
- Black: River Location in 1977
- Black: River Location in 1969



0 50 100 200 Meters April 2008

Figure 4.1 Overlay Map of Channel Change

Table 4.1 provides a list of variables measured, and the corresponding time. With the combination of the Figure C.1 through Figure C.9 and the data found in Table 4.1, it can be seen that only 20% of the previously farmable area remains as the river has changed course over the last 50 years. This study reports the reduction of the original 5.83 farmable hectares in 1956 to 1.18 farmable hectares in 2006, which is an average annual reduction of 0.093 hectares. Table 4.1 illustrates that the radius of curvature generally increases from 1956 to 1988 and then decreases rapidly after that. Bend curvature does not show as clear a pattern as the radius of curvature but still shows growth of the meander from 1956 to 1986 and contraction of the meander from 1988 to 2006.

Table 4.2 provides information about how the variables have changed over time. This table shows that the greatest rate of farmable area lost happened between 1986 and 1988 and closely followed by the interval between 1983 and 1986 with 0.32 hectares per year and 0.31 hectares per year respectively. The table also shows that the total annual migration was greatest during the same two intervals with an annual migration rate 70 meters per year between 1986 and 1988 and 22 meters per year between 1983 and 1986. The lowest rate of annual hectares lost was between 1956 and 1969 when of farmable area was lost. 1969 to 1977 represents the time interval for which the least of meander movement took place with a total annual migration rate of only 2.75 meters per year. It can also be noted that translation that far exceeded extension for all years and makes up a majority of the total migration. Extension makes a negligible portion of the movement between 1983 to 1986 and 1986 to 1988, and extension and translation were nearly balanced between 2002 to 2006. Average flood magnitude shows a similar pattern to that of annual hectares lost and total migration that it increased to a maximum the interval from 1986 to 1988 with a value of 19.5 and decreases after that a low value of 1.97 for the interval from 2002 to 2006.

Table 4.1 Measured Variables

Year	Farmable Area (Ha)	Riparian Vegetation Area (Ha)	River Area (Ha)	Bars and Islands Area (Ha)	Radius of Curvature (M)	Active Channel Width (M)	Bend Curvature	Extension (M)	Translation (M)	Total Movement (M)	Rotation (Degrees)
1956	5.28	4.54	3.88	1.33	250.12	61.00	4.10	-	-	-	-
1969	5.28	5.88	4.19	0.87	228.19	69.00	3.31	15.62	47.44	50.45	0.82
1977	4.86	7.06	3.19	1.90	241.68	66.00	3.66	6.13	21.15	22.02	3.61
1983	4.37	4.33	4.00	2.96	254.72	74.00	3.44	8.79	57.70	58.37	3.01
1986	3.43	5.50	6.09	0.34	309.74	72.00	4.30	0.25	66.98	66.98	9.95
1988	2.79	6.26	2.99	4.34	241.16	89.00	2.71	1.28	140.18	140.19	7.43
1991	2.29	6.88	3.93	3.19	212.74	94.00	2.26	20.35	30.97	37.06	10.72
1997	1.59	7.05	6.41	1.72	104.13	131.00	0.79	39.45	124.01	130.13	3.60
2002	1.28	7.23	4.46	3.43	61.84	125.00	0.49	19.36	26.57	32.88	12.12
2006	1.10	3.86	9.59	2.26	56.54	52.00	1.09	13.51	14.55	19.86	2.45

Table 4.2 Observed Changes

Interval	Annual Hectares Lost	Annual Total Migration (M/Y)	Translation/Extension	Annual Extension (M/Y)	Annual Translation (M/Y)	Average Recurrence Interval	Percent Riparian Vegetation	Percent River	Percent Bar	Bend Curvature	Rotation (Degrees)
1956 thru 1969	0.00	3.84	3.04	1.20	3.65	2.42	46.56	39.8	13.6	4.10	0.82
1969 thru 1977	0.05	2.75	3.45	0.77	2.64	3.11	53.78	38.3	7.9	3.31	3.61
1977 thru 1983	0.08	9.73	6.56	1.47	9.62	2.41	58.12	26.3	15.6	3.66	3.01
1983 thru 1986	0.31	22.33	267.92	0.08	22.33	14.24	38.33	35.4	26.2	3.44	9.95
1986 thru 1988	0.32	70.09	109.52	0.64	70.09	19.50	46.08	51.1	2.8	4.30	7.43
1988 thru 1991	0.17	12.35	1.52	6.78	10.32	7.88	46.09	22.0	31.9	2.71	10.72
1991 thru 1997	0.12	21.69	3.14	6.58	20.67	6.40	49.13	28.0	22.8	2.26	3.60
1997 thru 2002	0.06	6.58	1.37	3.87	5.31	4.64	46.43	42.2	11.3	0.79	12.12
2002 thru 2006	0.05	4.96	1.08	3.38	3.64	1.97	47.79	29.5	22.7	0.49	2.45
Skewness	1.0117	2.3804	2.3404	0.7833	2.3945	1.4035	0.2701	0.3845	0.0430	-0.8289	0.3944
Kurtosis	-0.3354	6.1322	5.3566	-0.9443	6.1672	1.0958	1.3586	-0.3676	-0.8562	-0.5669	-1.6654

Explanation of the Patterns and Process of Channel Shifting

The three cross sections that were surveyed are shown, as viewed looking upstream, in Figure 4.2. The steep west banks of the Big Blue River are clearly shown on all three cross sections. These cross sections are a typical shape for cross sections in river meanders, showing the asymmetrical shape. These steep, nearly vertical Westside (left) banks are composed of highly erodible silty soils. The steep west bank is a future indication that the river is actively eroding the field on the west side of the river.

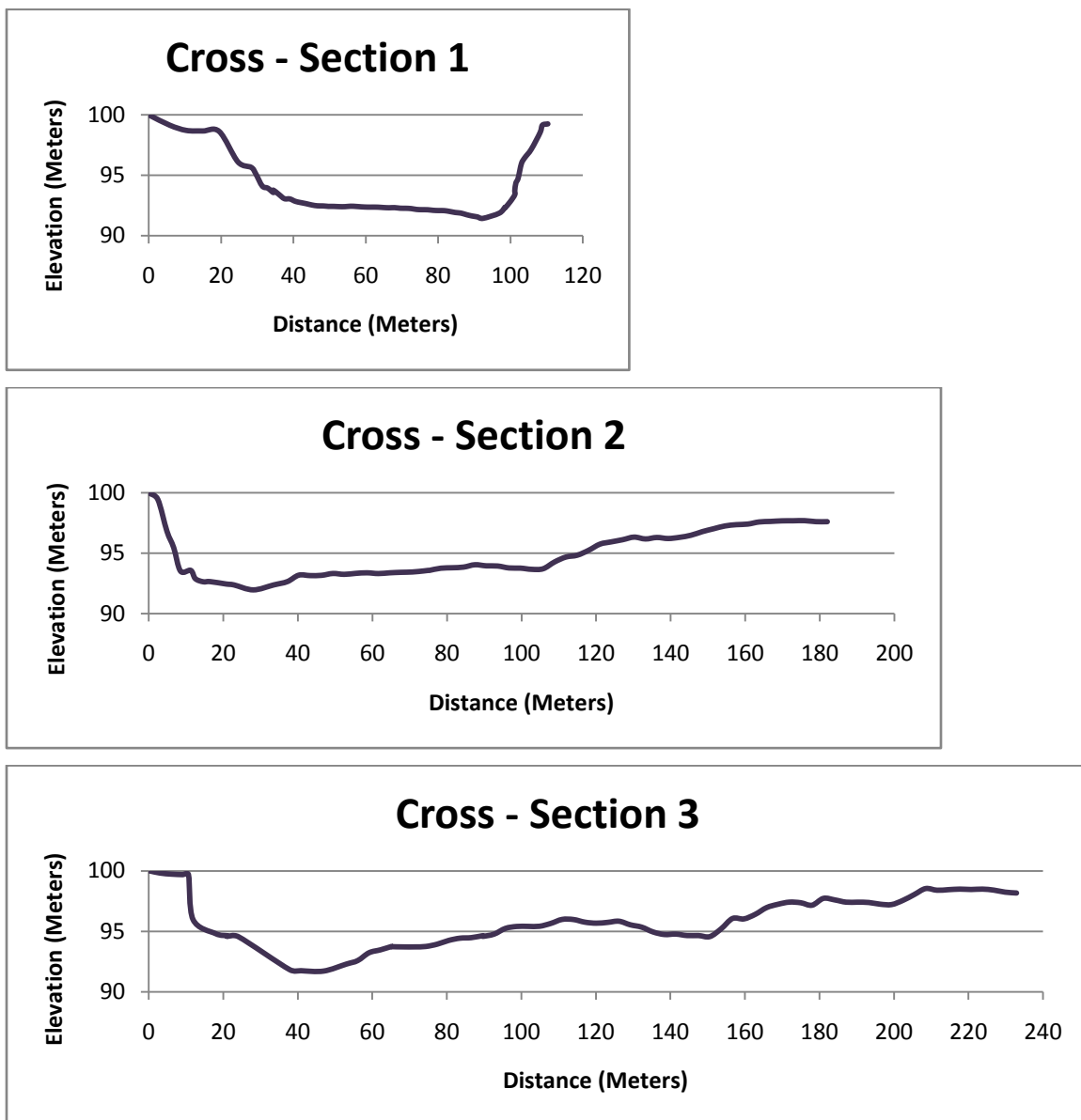


Figure 4.2 Cross sections Viewed Looking Upstream.

Because both Pearson correlation and linear regression have an underlying assumption that the data are normally distributed some data transformations need to take place in order to perform these tests. Table 4.3 provides an example of eight levels of transformation as detailed in Helsel and Hirsch (2002). These levels of transformation include two for positive skewness, five for negative skewness, and one for non-transformed data. The two transformation for positively skewed data are that a cube and a square transformation. The five transformations for negatively skewed data are square root, cube root, logarithmic, reciprocal root, and reciprocal. For each variable and transformation was chosen that would allow both the skewness and kurtosis to be as near zero as possible.

Table 4.3 Data Transformations

	Equation	Name of Transformation
For (-) Skewness	X^3	Cube
	X^2	Square
	X	Non-Transformed
For (+) Skewness	$X^{1/2}$	Square Root
	$X^{1/3}$	Cube Root
	$\ln X$	Logarithmic
	$1 / X^{1/2}$	Reciprocal Root
	$1 / X$	Reciprocal

Table 4.4 provides the observed changes for each time interval with the transformation noted in parentheses the following the name of the variable. When the values of skewness and kurtosis are compared with that of the original data found Table 4.2 it is clear is see that both skewness and kurtosis have greatly been reduced by the transformations.

Table 4.5 provides the results of Pearson correlation in the form of a matrix. Table 4.6 Provides the probability associated with a Pearson correlation. The underlined values in both tables indicate significant correlations at the 95th percentile. Some significant correlations worthy of note are that of the annual hectares lost correlated with

average recurrence interval, annual total migration correlated with average recurrence interval, and translation / extension correlated with bend curvature. Total annual migration is highly correlated with annual translation, which may be a false positive since the majority of the migration is translation. An unexpected correlation is that with average recurrence interval showing a strong correlation with rotation.

Table 4.4 Transformed Observed Changes

Interval	Annual Hectares Lost (Square Root Transformation)	Annual Total Migration (M/Y) (Reciprocal Root Transformation)	Translation/Extension (Reciprocal Root Transformation)	Annual Extension (M/Y) (Cube Root Transformation)	Annual Translation (M/Y) (Reciprocal Root Transformation)	Average Recurrence Interval (Reciprocal Root Transformation)	Percent Riparian Vegetation (Cube Root Transformation)	Percent River (Cube Root Transformation)	Percent Bar	Bend Curvature (Squared Transformation)	Rotation (Degrees) (Square Root Transformation)
1956 thru 1969	0.00	-0.51	-0.57	1.06	-0.52	-0.64	3.60	3.42	13.6	16.81	0.91
1969 thru 1977	0.23	-0.60	-0.54	0.92	-0.62	-0.57	3.98	3.37	7.9	10.94	1.90
1977 thru 1983	0.28	-0.32	-0.39	1.14	-0.32	-0.64	4.06	2.97	15.6	13.41	1.73
1983 thru 1986	0.56	-0.21	-0.06	0.44	-0.21	-0.27	3.65	3.28	26.2	11.85	3.15
1986 thru 1988	0.57	-0.12	-0.10	0.86	-0.12	-0.23	3.83	3.71	2.8	18.51	2.73
1988 thru 1991	0.41	-0.28	-0.81	1.89	-0.31	-0.36	3.83	2.80	31.9	7.34	3.27
1991 thru 1997	0.34	-0.21	-0.56	1.87	-0.22	-0.40	3.89	3.04	22.8	5.12	1.90
1997 thru 2002	0.22	-0.39	-0.85	1.57	-0.43	-0.46	3.84	3.48	11.3	0.63	3.48
2002 thru 2006	0.21	-0.45	-0.96	1.50	-0.52	-0.71	3.87	3.09	22.7	0.24	1.57
Skewness	-0.0780	-0.2797	0.3638	-0.1143	-0.0858	0.0847	-0.3508	0.0657	0.0430	-0.1770	-0.0015
Kurtosis	-0.0875	-0.7980	-0.8652	-0.8782	-1.3023	-1.5450	-0.0185	-0.6781	-0.8562	-1.1944	-1.3593

Table 4.5 Pearson Correlation Matrix

	Annual Hectares Lost (Square Root Transformation)	Annual Total Migration (M/Y) (Reciprocal Root Transformation)	Translation/Extension (Reciprocal Root Transformation)	Annual Extension (M/Y) (Cube Root Transformation)	Annual Translation (M/Y) (Reciprocal Root Transformation)	Average Recurrence Interval (Reciprocal Root Transformation)	Percent Riparian Vegetation (Cube Root Transformation)	Percent River (Cube Root Transformation)	Percent Bar	Bend Curvature (Squared Transformation)	Rotation (Degrees) (Square Root Transformation)
Annual Hectares Lost (Square Root Transformation)	1.000	<u>.828</u>	.608	-.254	<u>.827</u>	<u>-.861</u>	.024	.059	.143	.165	<u>.689</u>
Annual Total Migration (M/Y) (Reciprocal Root Transformation)		1.000	.533	.003	<u>.990</u>	<u>.784</u>	.088	0.015	.190	.185	.499
Translation/Extension (Reciprocal Root Transformation)			1.000	<u>.777</u>	.620	.570	.175	.408	0.287	<u>.772</u>	.109
Annual Extension (M/Y) (Cube Root Transformation)				1.000	.073	.167	.290	.561	.397	.656	.048
Annual Translation (M/Y) (Reciprocal Root Transformation)					1.000	<u>.803</u>	.087	.013	.144	.288	.467
Average Recurrence Interval (Reciprocal Root Transformation)						1.000	.274	.248	.067	.239	<u>.733</u>
Percent Riparian Vegetation (Cube Root Transformation)							1.000	.321	.193	.220	.066
Percent River (Cube Root Transformation)								1.000	<u>.820</u>	.387	.070
Percent Bar									1.000	.425	.184
Bend Curvature (Squared Transformation)										1.000	.238
Rotation (Square Root Transformation)											1.000

Table 4.6 Pearson Probability Matrix

	Annual Hectares Lost (Square Root Transformation)	Annual Total Migration (M/Y) (Reciprocal Root Transformation)	Translation/Extension (Reciprocal Root Transformation)	Annual Extension (M/Y) (Cube Root Transformation)	Annual Translation (M/Y) (Reciprocal Root Transformation)	Average Recurrence Interval (Reciprocal Root Transformation)	Percent Riparian Vegetation (Cube Root Transformation)	Percent River (Cube Root Transformation)	Percent Bar	Bend Curvature (Squared Transformation)	Rotation (Square Root Transformation)
Annual Hectares Lost (Square Root Transformation)	-	<u>0.006</u>	0.083	0.510	<u>0.006</u>	<u>0.003</u>	0.951	0.880	0.713	0.671	<u>0.040</u>
Annual Total Migration (M/Y) (Reciprocal Root Transformation)		-	0.140	0.994	<u>0.000</u>	<u>0.012</u>	0.822	0.970	0.625	0.634	0.171
Translation/Extension (Reciprocal Root Transformation)			-	<u>0.014</u>	0.075	0.109	0.652	0.276	0.455	<u>0.015</u>	0.780
Annual Extension (M/Y) (Cube Root Transformation)				-	0.852	0.668	0.450	0.116	0.290	0.055	0.903
Annual Translation (M/Y) (Reciprocal Root Transformation)					-	<u>0.009</u>	0.823	0.974	0.712	0.452	0.205
Average Recurrence Interval (Reciprocal Root Transformation)						-	0.475	0.520	0.865	0.537	<u>0.025</u>
Percent Riparian Vegetation (Cube Root Transformation)							-	0.400	0.619	0.570	0.865
Percent River (Cube Root Transformation)								-	<u>0.007</u>	0.303	0.858
Percent Bar									-	0.254	0.635
Bend Curvature (Squared Transformation)										-	0.538
Rotation (Square Root Transformation)											-

The results of the correlation analysis indicated that colinearity exist between three independent variables. Annual translation shows a strong correlation with average recurrence interval, percent river shows a strong correlation with percent bar, and average recurrence interval shows strong correlation with rotation. Because of the strong correlation that exists between the three sets of paired variables, only one of each variable can be used in a multiple regression. For the multiple regressions, the same three independent variables are used in all three tests. The average recurrence interval, the percent riparian vegetation, and bend curvature are the three independent variables used.

Table 4.7 shows the results of the first multiple regression, explaining the annual farmable area lost. The model proves to be significant at the $p < 0.05$ level and explains 70.3% of the variance. The one of the independent variables proves to be significant in that is the average recurrence interval. The other two variables, percent riparian vegetation, and bend curvature are not significant but do contribute to the overall ability of the model to explain the variation in annual hectares lost.

Table 4.8 shows the results of the second multiple regression, explaining that the total annual migration. This model shows that 41.2% of events can be explained by the independent variables; however, this model does not prove to be statistically significant overall but does have one statistically significant independent variable, in the average recurrence interval.

Table 4.9 shows the results of the third and final multiple regression explaining the ratio of translation to extension. The model shows that 62.0% of the variation can be explained by the independent variables and that the model is significant overall at the $p < 0.05$ level. In addition to the modeling significant one independent variable, bend curvature proves to be statistically significant in explaining the variation. Again, since the model is statistically significant the other two of variables should not be completely ignored since they hope to create an overall significant model but do not show significant on their own.

Table 4.7 Annual Hectares Lost Explained

Summary Output – Annual Hectares Lost (Square Root Transformation)					
<i>Regression Statistics</i>					
Multiple R	0.902				
R Square	0.814				
Adjusted R Square	0.703				
Standard Error	0.098				
Observations	9				
ANOVA					
	df	SS	MS	F	Significance F
Regression	3	0.209	0.070	7.301	0.028
Residual	5	0.048	0.010		
Total	8	0.256			
	Coefficients	Standard Error	t Stat	P-value	
Intercept	-0.558	0.949	-0.588	0.582	
Average Recurrence Interval (Reciprocal Root Transformation)	0.951	0.207	4.590	0.006	
Percent Riparian Vegetation (Cube Root Transformation)	0.345	0.249	1.387	0.224	
Bend Curvature (Squared Transformation)	0.000	0.005	0.016	0.987	

Table 4.8 Annual Total Migration Explained

Summary Output – Annual Total Migration (M/Y) (Reciprocal Root Transformation)					
<i>Regression Statistics</i>					
Multiple R	0.795				
R Square	0.632				
Adjusted R Square	0.412				
Standard Error	0.120				
Observations	9				
ANOVA					
	df	SS	MS	F	Significance F
Regression	3	0.124	0.041	2.865	0.143
Residual	5	0.072	0.014		
Total	8	0.196			
	Coefficients	Standard Error	t Stat	P-value	
Intercept	0.586	1.169	0.501	0.638	
Average Recurrence Interval (Reciprocal Root Transformation)	-0.726	0.255	-2.846	0.036	
Percent Riparian Vegetation (Cube Root Transformation)	-0.151	0.307	-0.494	0.642	
Bend Curvature (Squared Transformation)	0.000	0.007	-0.073	0.945	

Table 4.9 Translation/Extension Explained

Summary Output - Translation/Extension (Reciprocal Root Transformation)					
Regression Statistics					
Multiple R	0.873				
R Square	0.763				
Adjusted R Square	0.620				
Standard Error	0.195				
Observations	9				
ANOVA					
	df	SS	MS	F	Significance F
Regression	3	0.612	0.204	5.360	0.051
Residual	5	0.190	0.038		
Total	8	0.802			
	Coefficients	Standard Error	t Stat	P-value	
Intercept	-1.273	1.897	-0.671	0.532	
Average Recurrence Interval (Reciprocal Root Transformation)	0.775	0.414	1.871	0.120	
Percent Riparian Vegetation (Cube Root Transformation)	0.206	0.498	0.413	0.697	
Bend Curvature (Squared Transformation)	0.033	0.011	3.036	0.029	

The field measurements of variables pertaining to BEHI on 30 April 2008 show contrasting potential for bank erosion at two sites. The two locations to assess potential for bank erosion were selected near cross sections two and three (Figure 1.2). For the location near cross section three, it was found that the bank height was 7.6 meters and the bankfull height was 4.3 meters. The rooting depth was .1 meters, with a density of 50%. The bank angle was 90°. No adjustments were made for bank material or stratification. These numbers yield a predicted bank erosion of very high, almost extreme. For the location near cross section two, it was found that the bank height was 9.4 meters and the bankfull height was 4.3 meters. The rooting depth was 3.3 meters, with a density of 15%. The bank angle was 85°. No adjustments were made for bank material or stratification. These numbers yield a predicated bank erosion of high.

Discussion

The findings of this study have shown that a significant spatial and temporal pattern exists to both the amount of farmable area lost and the total meander migration. Both the amount of farmable area lost and the total meander migration are largely explained by the average recurrence interval of annual peak flows. The maximum rates for both the farmable area lost and the total meander migration occurred in the same two intervals, between 1983 and 1986, and between 1986 and 1981. The same two intervals correspond with the time of the greatest magnitude flow events, further emphasizing the importance of high flow events for meander migration. This finding is consistent with Hooke (1987) where she demonstrated that drainage area was the largest predictor of meander migration. She specified that drainage area was a crude substitution for flow rate, and in this case the recurrence interval analogous to the drainage area used by Hooke in that it is a measure of discharge.

Bend curvature in this study did not end up being the major predictor of migration rates, which is in contrast to that much of the work on meander migration (Hickin 1974, Hickin and Nanson 1975 and 1984, and Nanson and Hickin 1986). The difference between the findings of this report and that of previous studies can be explained partly as a difference in measuring technique. Many past studies of meander migration have used the lateral migration rate. Lateral migration is the maximum displacement normal to the channel (Hickin 1974). For this study, meander movement oriented to the axis of the meander of the first year of the interval, where extension is moving in the direction of the axis and translation is movement normal to the axis. In this study, extension is the closest match to that of lateral migration.

A second explanation for the difference between this study and the findings of previous studies is that of local controls. In this area, an exposed outcropping of limestone is visible along the west side of the river. In the years in which meander migration was greatest, 1983 to 1988, the apex of the meander is moving along the now exposed outcropping of limestone. For the time interval from 1983 to 1988, the meander extension was negligible. The significance of the limestone outcropping is unknown but

could very easily be affecting the meander migration, which in turn could explain why extension was negligible for the intervals of greatest movement.

Bend curvature may not have predicted total meander migration, but did prove useful in explaining the direction that the meander moved. This study has shown that a positive correlation between bend curvature and the ratio of translation to extension exists. This means that for tight bends, that extension will be the dominant process and for larger bends, translation will be the dominant process. The works of Bagnold (1960), Hooke (1975), and Markhan and Throne (1992) showing that in meanders that have a tight radius of curvature that the flow begins to break away from the convex bank leading to a greater shear stress on the concave bank near the apex than can be explained by the curvature it's self support this observation. The increase in shear stress leads to greater erosion and to greater extension.

Rates of meander migration on the Big Blue River are difficult to compare with that of other studies because the measurement is not a pure lateral migration. The migration rates shown in this study are greater than the rates established by Hickin and Nanson on the Beaton River, but again that these rates are lateral migration rate on a relatively small stream. Migration rates found in this study are less than those reported by Hudson and Kesel (2000) on the much larger lower Mississippi River. With a maximum annual rate of 87% of the channel width, the relative rates of total meander migration demonstrated on the Big Blue River exceed the maximum relative lateral meander found by Hickin and Nanson (1984), with a maximum annual rate of 11% of the channel width (Table 4.10). The maximum annual extension relative rate of meander movement does match the maximum relative lateral meander described by Hickin and Nanson (1984), which is logical, since extension closely matches the measurements of lateral migration.

Table 4.10 Relative Rates of Meander Migration

Interval	Average Active Channel Width	Annual Total Migration / Average Active Channel Width	Annual Translation / Average Active Channel Width	Annual Extension / Average Active Channel Width
1956 thru 1969	65.0	0.06	0.06	0.02
1969 thru 1977	67.5	0.04	0.04	0.01
1977 thru 1983	70.0	0.14	0.14	0.02
1983 thru 1986	73.0	0.31	0.31	0.00
1986 thru 1988	80.5	0.87	0.87	0.01
1988 thru 1991	91.5	0.14	0.11	0.07
1991 thru 1997	112.5	0.19	0.18	0.06
1997 thru 2002	128.0	0.05	0.04	0.03
2002 thru 2006	125.0	0.04	0.03	0.03

Riparian vegetation did not prove to be an explaining factor in rates of meander migration. Given the extremely tall unstable bank of the study reach, this is not a surprise. Nanson and Hickin (1986) support this view, noting that the process of undercutting can undermine even dense vegetation. The fact that riparian vegetation did not prove to be explanatory does not rule out the possibility that the conversion from riparian forest to agricultural land on the reach has not contributed to an overall rapid rates of migration. The statistics revealed that the variation in amount of riparian vegetation did not match the variation in erosion, not that land cover had any effect on the rates of erosion. If changes in erosion, due to land cover change, were uniform throughout the study, than the statistics would not show land cover change as an explanatory measure.

CHAPTER 5 - Conclusions

The purpose of this study was to evaluate channel change and the associated loss of farmland between 1956 and 2006 along the west side of a short reach of the Big Blue River, downstream of Marysville, Kansas. Two objectives were pursued. The first was to describe the spatial and temporal patterns of channel shifting and the associated impact on farmland erosion. The second was to explain the patterns and process of channel shifting, farmland erosion, and direction of meander movement in terms of potential bank erosion, riparian vegetation, meander geometry, and peak flows.

The channel shifting varied from 2.75 – 70.1 meters per year during the 50 years of the study, attaining maximum rates from 1983-1988. It follows that farmable area lost varied from 0.00 – 0.32 hectares per year for the time of the study, and the interval of maximum change corresponds to the interval of maximum change with annual migration. The meander movement was dominated by translation especially in years of high movement. This movement resulted in the apex of the meander moving in a southwesterly direction.

The channel shifting or total migration was controlled primarily by annual peak flows. The rate of farmable area lost during specific intervals could almost entirely be attributed to the annual peak flows during those same periods. Riparian vegetation and meander geometry were not shown to have a direct impact on the farmable area lost or total migration. The largest contributor to both total meander movement and area lost is annual peak flows. Many past studies of meanders have concluded that meander geometry or removal of riparian vegetation is the key factor in meander movement. Differences between this study and other studies can be attributed to site condition. Potential bank erosion was found to be very high for the vertical bank that borders the farmland to the point where vegetation was not a stabilizing factor. The presence of bedrock along the west side of the river likely limits the ability of the meander to migrate by extension.

Meander geometry was shown to have the greatest influence on the direction of meander migration. Meanders are more likely to move by translation when the radius of

curvature is large and by extension more when the radius is small. Although not a common area of focus in research of river meanders, the finding that the curvature of the channel influences the direction of movement supports what others have found. In meanders with a large radius of curvature the zone of maximum shear stress shifts further downstream from the apex, leading to greater translation. Conversely, in meanders with a small radius of curvature, the maximum shear stress strikes the outside of the meander bend closer to the apex, leading to greater extension.

This study has identified several avenues for potential future research on river meanders. Standards should be adopted for measuring stream width in studies of meander geometry. This study examined one meander, in a valley containing an outcropping of bedrock along the concave bank, within a relatively short time interval. A study mapping the shear stress along meanders could prove invaluable in understanding which direction a meander is like to move. The lack of influence of riparian vegetation is probably similar for highly incised rivers with erodible banks, such as those found throughout the Temperate Prairies, Ozark, Ouachita-Appalachian Forests, and Southeastern USA Plains level II ecoregion. Potential exists for the comparison of the extension verses translation found in this study with studies of confined meanders and of unconfined meanders to understand further the influence bedrock control has on translation verses extension. More studies are recommended on the factors that affect the relative migration by translation and extension, which would yield greater insights into the complex nature of meandering rivers.

References

- Abernethy, B. and I.D. Rutherford. 1998. Where along a river's length will vegetation most effectively stabilise stream banks? *Geomorphology* 23:55-75.
- Bagnold, R. A. 1960. Some aspects of the shape of river meanders. *U.S. Geological Survey Professional Paper 282E*: 135-44
- Begin, Z. B. 1981. Stream curvature and bank erosion: a model based on the momentum equation. *Journal of Geology* 89:497-504.
- _____. 1986. Curvature Ratio and the rate of river bend migration - update. *Journal of Hydraulic Engineering* 112:904-908.
- Blondeaux, P and G. Seminara. 1985. A unified bar-bend theory of river meanders. *Journal of Fluid Mechanics* 157:449-470.
- Brierley, G.J. and K. A. Fryirs. 2005. *Geomorphology and river management: applications of the river style framework* Oxford, UK: Blackwell.
- Brooks, G.R. 2003. Holocene lateral channel migration and incision of the Red River, Manitoba, Canada. *Geomorphology* 54:197-215.
- Callander, R. A. 1978. River Meandering. *Annual Review of Fluid Mechanics* 10:129-158.
- Chapman, S. S., J. M. Omernik, J. A. Freeouf, D. G. Huggins, J. R. McCauley, C. C. Freeman, G. Steinauer, R. T. Angelo, and R. L. Schlepp. 2001. *Ecoregions of Nebraska and Kansas* U.S. Geological Survey, Reston, Va.

- Einstein, H. A. and H. W. Shen. 1964. A study of meandering in straight alluvial channels. *Journal of Geophysical Research* 69:5239-47.
- Frothingham, K. M. and B.L. Rhoads. 2003. Three dimensional flow structure and channel change in an asymmetrical compound meander loop, Embarras River, Illinois. *Earth Surface Processes and Landform* 28:625-644.
- Furbish, D. J. 1988. River-bend curvature and migration: how are they related? *Geology* 16:752-755.
- _____. 1991. Spatial autoregressive structure an meander evolution. *Bulletin of the Geological Society of America* 103:1576-1589.
- Gautiere, E., D. Brunstein, P. Vauchel, M. Roulet, O. Fuertes, J.L. Guyot, J. Darozzes and L. Bourrel. 2007. Temporal relations between meander deformation, water discharge and sediment fluxes in the floodplain of the Rio Beni (Bolivian Amazonia). *Earth Surface Processes and Landforms* 32:230-248.
- Gorycki, M. A. 1973. Hydraulic drag: a meander initiating mechanism. *Bulletin of the Geological Society of America* 84:175-186.
- Graf, W. L. 1988. *Fluvial processes in dryland rivers*. New York: Springer.
- _____. 2006. Downstream hydrologic and geomorphic effects of large dams on American rivers. *Geomorphology* 79: 336–360.
- Helsel, D. R. and R. M. Hirsch. 2002. Statistical Methods in Water Resources. In *Techniques of Water-Resources Investigations Book 4* 1-524. U.S. Geological Survey: Denver, CO

- Hickin, E.J. 1974. The development of meanders in natural river-channels. *American Journal of Science* 274:414-442.
- _____. and G. C. Nanson. 1975. The character of channel migration on the Beaton River, north-east British Columbia, Canada. *Bulletin of the Geological Society of America* 86:487-794.
- _____. and G. C. Nanson. 1984. Lateral migration rates of river bends. *Journal of Hydraulic Engineering* 110:1557-1567.
- Hooke, R. L. B. 1975. Distribution of sediment transport and shear stress in a meander bend. *Journal of Geology* 83:543-566.
- Hooke, J.M. 1980. Magnitude and distribution of rates of river bank erosion. *Earth Surface Processes* 5:143-157.
- _____. 1984. Changes in river meanders: a review of techniques and results of analyses. *Progress in Physical Geography* 8:473-508.
- _____. 1987. Lateral migration rates of river bends. *Journal of Hydrolic Engineering* 113:915-918.
- _____. 2007. Complexity, self-organization and variation in behavior in meandering rivers. *Geomorphology* 91:236-258.
- Howard, A.D. and A.T. Hemberger. 1991. Multivariate characterization of meandering. *Geomorphology* 4:161-186.
- Howard, J.A. and C.W. Mitchell. 1985. *Phytogeomorphology*. New York: John Wiley and Sons.

- Hudson, P. F. and R. H. Kesel. 2000. Channel migration and meander-bend curvature in the lower Mississippi River prior to major human modification. *Geology* 28:531-534.
- Hughes, M. L., P. F. McDowell, and W. A. Marcus. 2006. Accuracy assessment of georectified aerial photographs: Implications for measuring lateral channel movement in a GIS. *Geomorphology* 74:1-16.
- Ikeda, S., G. Parker, and K. Sawai. 1981. Bend theory of river meanders, part 1: Linear development. *Journal of Fluid Mechanics* 112:363-377
- Juracek, K.E. 2000. Channel stability downstream from a dam assessed using aerial photographs and stream-gage information. *Journal of the American Water Resources Association* 36: 633-645.
- Knighton, A. D. 1998. *Fluvial forms and processes*. New York: Oxford University Press.
- Lane, S. A. 2000. The measurement of river channel morphology using digital photogrammetry. *Photogrammetric Record* 16(96):937-961.
- Leopold, L. B. and M. G. Wolman. 1960. River meanders. *Geological Society of America Bulletin* 71(6):769-793.
- Markhan, A. J. and C. R. Thorne. 1992. Geomorphology of gravel-bed rivers bends. In *Dynamics of Gravelbed Rivers* ed. Billi, P., R. D. Hey, C. R. Thorne, and P. Tacconi. 433-450: Chichester: Wiley.
- Marston, R. A., J. Girel, G. Pautou, H. Piegay, J. Bravard and C. Arneson. 1995. Channel metamorphosis, floodplain disturbance, and vegetation development: Ain River, France. *Geomorphology* 13: 121-131.

- _____. J. D. Mill, D. R. Wrazienc, B. Bassettd, D. K. Splintere. 2005. Effects of Jackson Lake Dam on the Snake River and its Floodplain, Grand Teton National Park, Wyoming, USA. *Geomorphology* 71:79-98.
- Micheli, E.R., J.W. Kirchner and E.W. Larsen. 2004. Quantifying the effect of riparian forest versus agricultural vegetation on river meander migration rates, Central Sacramento River, California, USA. *River Research and Applications* 20:537-548
- Nanson, G. C. and E. J. Hickin. 1986. A statistical analysis of bank erosion and channel migration in western Canada. *Bulletin of the Geological Society of America* 97:497-504.
- Nelson, J. M. and J. D. Smith. 1989. Evolution and stability of erodible channel beds. In *River meandering*. ed. Ikeda, S. and G. Parker. Water Research Monograph 12:321-377: American Geophysical Union.
- Parker, G. and H. Johannesson. 1989. Observations on several recent theories of resonance and overdeepening in meandering channels. In *River meandering*. ed. Ikeda, S. and G. Parker. Water Research Monograph 12:379-415 American Geophysical Union.
- Rhoads, B. L. and M. R. Welford. 1991. Initiation of river meandering. *Progress in Physical Geography* 15:127-156.
- Richard, G.A., P.Y. Julien and D.C. Baird. 2005. Statistical analysis of lateral migration of the Rio Grande, New Mexico. *Geomorphology* 71:139-155.
- Rosgen, D L., 2001. A practical method of computing streambank erosion rate. In *The Seventh Federal Interagency Sedimentation Conference*, Vol. 2, 9-15, Reno, Nevada.

- Seminara, G. and M. Tubino. 1989. Alternating bars and meandering: free, forced and mixed interactions. In *River meandering*. ed. Ikeda, S. and G. Parker. Water Research Monograph 12:267-320: American Geophysical Union.
- Stølum, H.H. 1996. River meandering as a self-organization process. *Science* 271:1710-1713.
- _____. 1998. Planform geometry and dynamics of meandering rivers. *Bulletin of the Geological Society of America* 110:1485-1498.
- Sun, T., P. Meakin, T. Jossang, and K. Schwarz. 1996. A simulation model for meandering rivers. *Water Resources Research* 23: 2937-2954.
- Tanner, W. F. 1960. Helicoidal flow, a possible cause of meandering. *Journal of Geophysical Research* 65: 993-995.
- Thompson, A. 1986. Secondary flows and the pool-riffle unit: a case study of the processes of meander development. *Earth Surface Processes and Landforms* 11:631-641.
- Thorne, C. R. 1991. Bank processes and channel evolution in the incised rivers of north-central Mississippi. In *Incised river channels: processes, forms, engineering and management*, ed. S. E. Darby and A. Simon, 97-121: Wiley, New York, NY.
- U.S. Department of Agriculture. 2001. *Soil survey geographic (SSURGO) database for Marshall County, Kansas*. U.S. Department of Agriculture, Natural Resources Conservation Service. Fort Worth, TX: U.S. Department of Agriculture, Natural Resources Conservation Service.

_____. 2006. *FSA National Agriculture Imagery Program (NAIP) 2006*. USDA-FSA Aerial Photography Field Office. Salt Lake City, UT: USDA FSA Aerial Photography Field Office.

U.S. Geological Survey. 1997a. *Digital Orthophoto Quarter Quadrangles (DOQQ) 1991*. U.S. Geological Survey. Reston, VA: U.S. Geological Survey.

_____. 1997b. *Digital Raster Graphics (DRG) UTM NAD 83 Clipped*. U.S. Geological Survey. Reston, VA: U.S. Geological Survey.

_____. 2002. *Digital Orthophoto Quarter Quadrangles (DOQQ) 2002*. U.S. Geological Survey. Reston, VA: U.S. Geological Survey.

Walters, K.L. 1954. *Geology and ground-water resources of Marshall County, Kansas*: Kansas Geological Survey, Bulletin 106, 116 p.

Yang, T.C. 1971. Potential energy and stream morphology. *Water Resources Research* 7:311-322.

Appendix A - Gage and Recurrence Interval Data

Year	Annual Peak Flow Barneston, NE Gage (cms)	Annual Peak Flow Marysville, KS Gage (Estimated) (cms)	Annual Peak Flow Marysville, KS Gage (Actual) (cms)	Rank of Marysville Gage Discharge	Recurrence Interval (Marysville Gage)
1929	334.14	316.84	-	53	1.49
1930	322.81	309.37	-	54	1.46
1931	370.95	341.10	-	46	1.72
1932	288.83	286.98	-	57	1.39
1933	157.16	200.21	-	71	1.11
1934	59.47	135.83	-	77	1.03
1935	368.12	339.23	-	47	1.68
1936	351.13	328.03	-	49	1.61
1937	91.75	157.10	-	74	1.07
1938	213.79	237.53	-	66	1.20
1939	279.77	281.01	-	59	1.34
1940	113.27	171.28	-	72	1.10
1941	1633.88	1173.37	-	1	79.00
1942	444.57	389.61	-	41	1.93
1943	668.28	537.03	-	24	3.29
1944	461.56	400.81	-	40	1.98
1945	761.72	598.62	-	16	4.94
1946	248.34	260.29	-	62	1.27
1947	974.10	738.57	-	10	7.90
1948	487.05	417.61	-	36	2.19
1949	761.72	598.62	-	16	4.94
1950	603.15	494.11	-	28	2.82
1951	736.24	581.82	-	20	3.95
1952	484.22	415.74	-	37	2.14
1953	62.58	137.88	-	76	1.04
1954	801.37	624.74	-	15	5.27
1955	174.71	211.78	-	68	1.16
1956	501.21	426.94	-	35	2.26
1957	472.89	408.28	-	39	2.03
1958	628.63	510.91	-	26	3.04
1959	419.09	372.82	-	42	1.88
1960	832.52	645.27	-	14	5.64
1961	345.47	324.30	-	50	1.58
1962	481.39	413.87	-	38	2.08
1963	526.69	443.73	-	33	2.39
1964	252.02	262.72	-	61	1.30
1965	583.33	481.05	-	30	2.63
1966	232.76	250.03	-	64	1.23
1967	756.06	594.88	-	18	4.39
1968	286.00	285.11	-	58	1.36
1969	577.66	477.32	-	31	2.55

1970	185.48	218.87	-	67	1.18
1971	308.65	300.04	-	56	1.41
1972	105.34	166.06	-	73	1.08
1973	880.65	676.99	-	13	6.08
1974	1330.89	973.70	-	7	11.29
1975	255.70	265.15	-	60	1.32
1976	229.65	247.98	-	65	1.22
1977	359.62	333.63	-	48	1.65
1978	713.58	566.89	-	22	3.59
1979	753.23	593.02	-	19	4.16
1980	407.76	365.36	-	44	1.80
1981	342.63	322.44	-	51	1.55
1982	419.09	372.82	-	42	1.88
1983	504.04	428.80	-	34	2.32
1984	1580.08	1137.91	1137.91	2	39.50
1985	342.63	-	302.99	55	1.44
1986	818.36	-	1124.18	3	26.33
1987	1061.88	-	1002.42	6	13.17
1988	75.04	-	61.73	78	1.01
1989	319.98	-	526.69	25	3.16
1990	478.55	-	1064.71	4	19.75
1991	195.67	-	203.60	69	1.14
1992	707.92	-	1013.74	5	15.80
1993	908.97	-	894.81	8	9.88
1994	239.56	-	202.18	70	1.13
1995	605.98	-	736.24	11	7.18
1996	521.03	-	569.17	21	3.76
1997	427.58	-	775.88	9	8.78
1998	540.85	-	722.08	12	6.58
1999	467.23	-	472.89	32	2.47
2000	328.48	-	506.87	27	2.93
2001	447.41	-	487.05	29	2.72
2002	282.89	-	317.15	52	1.52
2003	342.63	-	345.47	45	1.76
2004	642.79	-	560.67	23	3.43
2005	275.81	-	251.45	63	1.25
2006	150.36	-	149.23	75	1.05

Appendix B - Cross Section Data

Cross - Section 1		Cross - Section 2		Cross - Section 3	
Elevation (m)	Distance (m)	Elevation (m)	Distance (m)	Elevation (m)	Distance (m)
100.00	0.00	100.00	0.00	100.00	0.00
99.15	5.79	99.45	2.44	99.81	3.05
98.71	10.36	96.82	4.88	99.72	6.10
98.66	14.94	95.45	6.71	99.68	9.14
98.62	19.51	93.50	8.53	99.68	10.67
96.10	24.69	93.57	11.28	95.97	11.89
95.65	28.35	92.88	12.50	94.80	17.98
95.14	29.57	92.62	14.63	94.63	21.03
94.11	31.39	92.64	16.46	94.57	21.03
93.93	32.92	92.44	20.73	94.54	24.08
93.57	34.44	92.36	22.86	91.82	37.80
93.77	34.44	91.95	28.04	91.73	40.84
93.42	35.97	92.36	33.53	91.70	46.94
93.07	37.49	92.64	37.19	92.28	53.04
93.04	39.01	93.17	40.23	92.57	56.08
92.84	40.54	93.13	43.28	93.22	59.13
92.74	42.06	93.16	46.33	93.46	62.18
92.65	43.59	93.31	49.38	93.74	65.23
92.54	45.11	93.24	52.43	93.72	65.23
92.47	46.63	93.32	55.47	93.70	68.28
92.47	48.16	93.37	58.52	93.70	71.32
92.43	49.68	93.30	61.57	93.74	74.37
92.43	49.68	93.37	64.62	93.93	77.42
92.43	51.21	93.41	67.67	94.23	80.47
92.40	52.73	93.43	70.71	94.42	83.52
92.40	54.25	93.52	73.76	94.47	86.56
92.44	55.78	93.57	74.98	94.63	89.61
92.42	57.30	93.57	75.29	94.57	89.61
92.39	58.83	93.75	78.33	94.76	92.66
92.37	60.35	93.78	81.38	95.23	95.71
92.37	61.87	93.84	84.43	95.39	98.76
92.36	63.40	94.03	87.48	95.40	101.80
92.33	64.92	93.94	90.53	95.41	104.85
92.31	66.45	93.93	93.57	95.64	107.90
92.32	67.97	93.77	96.62	95.97	110.95
92.28	69.49	93.75	99.67	95.97	114.00

92.27	71.02	93.65	102.72	95.75	117.04
92.25	72.54	93.70	105.77	95.66	120.09
92.17	74.07	94.26	108.81	95.73	123.14
92.15	75.59	94.67	111.86	95.83	126.19
92.15	77.11	94.82	114.91	95.53	129.24
92.10	78.64	95.23	117.96	95.34	132.28
92.08	80.16	95.74	121.01	94.94	135.33
92.08	81.69	95.93	124.05	94.72	138.38
92.01	83.21	96.11	127.10	94.76	141.43
91.92	84.73	96.32	130.15	94.64	144.48
91.87	86.26	96.17	133.20	94.64	147.52
91.75	87.78	96.29	136.25	94.55	150.57
91.64	89.31	96.21	139.29	95.20	153.62
91.56	90.83	96.30	142.34	96.05	156.67
91.43	92.35	96.48	145.39	96.02	159.72
91.87	96.93	96.77	148.44	96.40	162.76
92.35	98.45	97.01	151.49	96.95	165.81
92.29	98.45	97.25	154.53	97.23	168.86
92.83	99.97	97.35	157.58	97.40	171.91
93.39	101.19	97.40	160.63	97.35	174.96
93.75	101.19	97.58	163.68	97.15	178.00
94.36	101.50	97.62	166.73	97.71	181.05
94.74	102.11	97.67	169.77	97.59	184.10
95.96	103.02	97.68	172.82	97.40	187.15
96.44	103.94	97.69	175.87	97.40	190.20
97.16	105.77	97.60	178.92	97.37	193.24
98.54	108.20	97.60	181.97	97.23	196.29
99.14	108.81			97.20	199.34
99.25	110.34			97.55	202.39
				98.03	205.44
				98.53	208.48
				98.39	211.53
				98.43	214.58
				98.48	217.63
				98.45	220.68
				98.48	223.72
				98.40	226.77
				98.23	229.82
				98.16	232.87

Appendix C - Farmable Area Lost

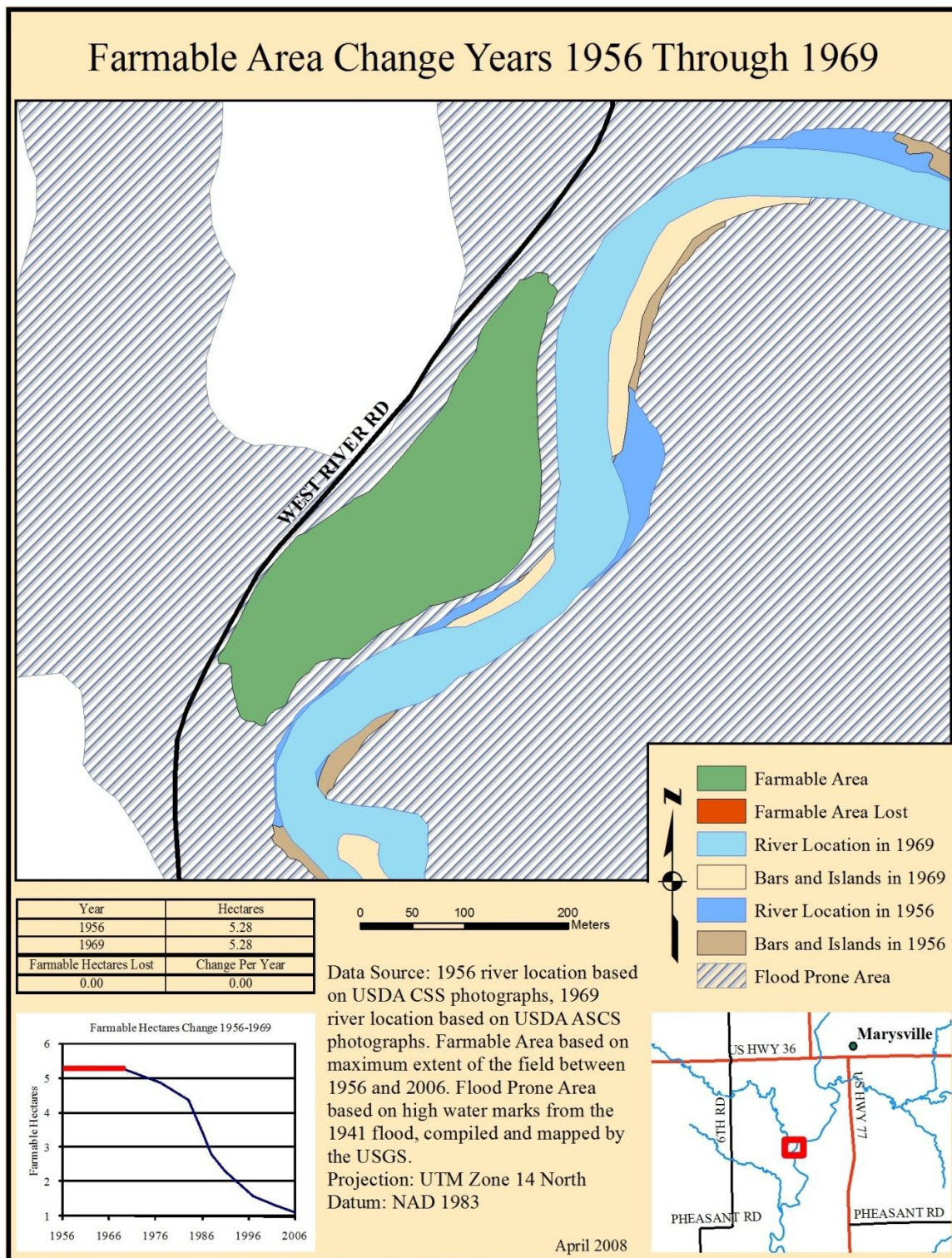


Figure C.1 Farmable Area Change 1956-1969

Farmable Area Change Years 1969 Through 1977

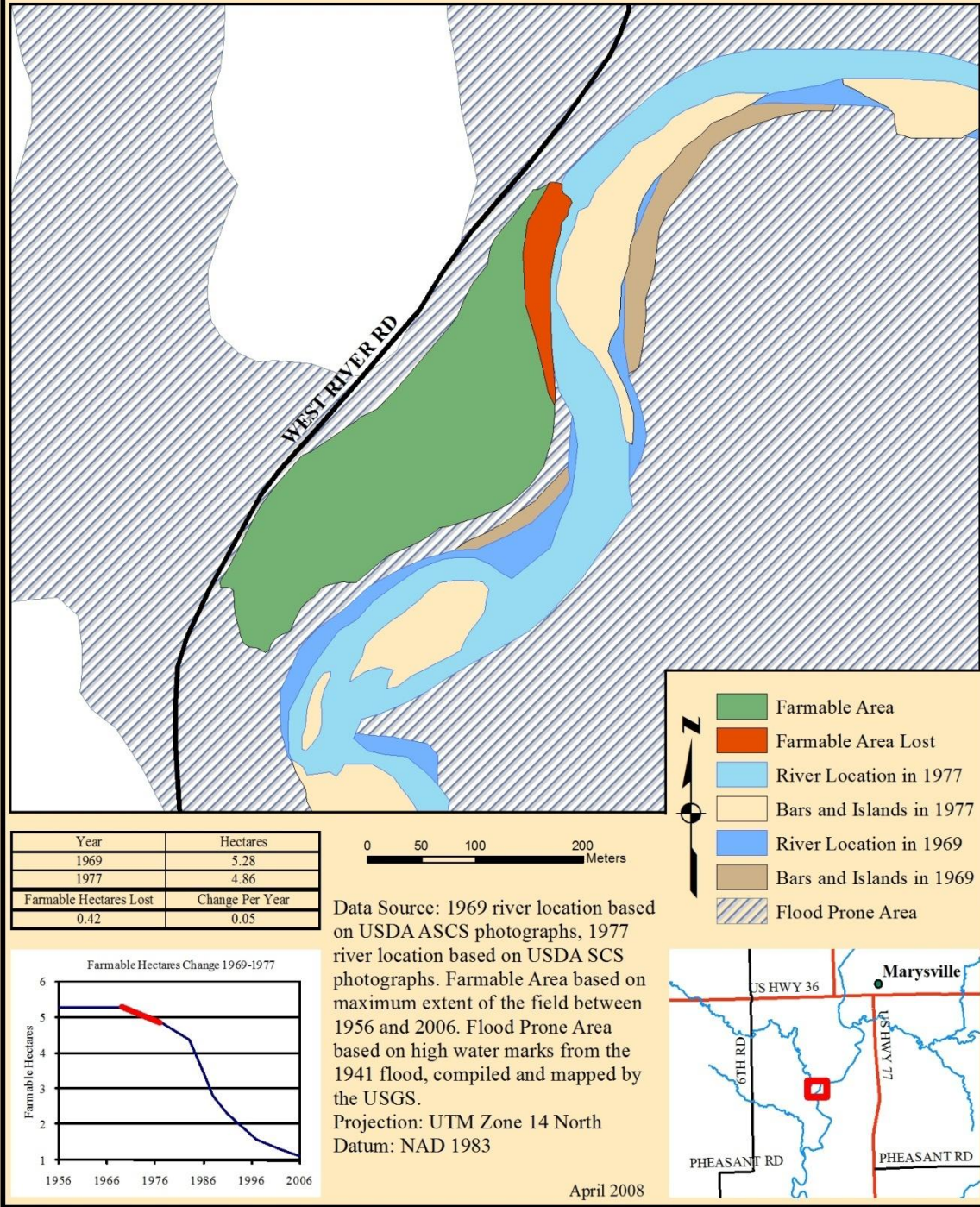


Figure C.2 Farmable Area Change 1969-1977

Farmable Area Change Years 1977 Through 1983

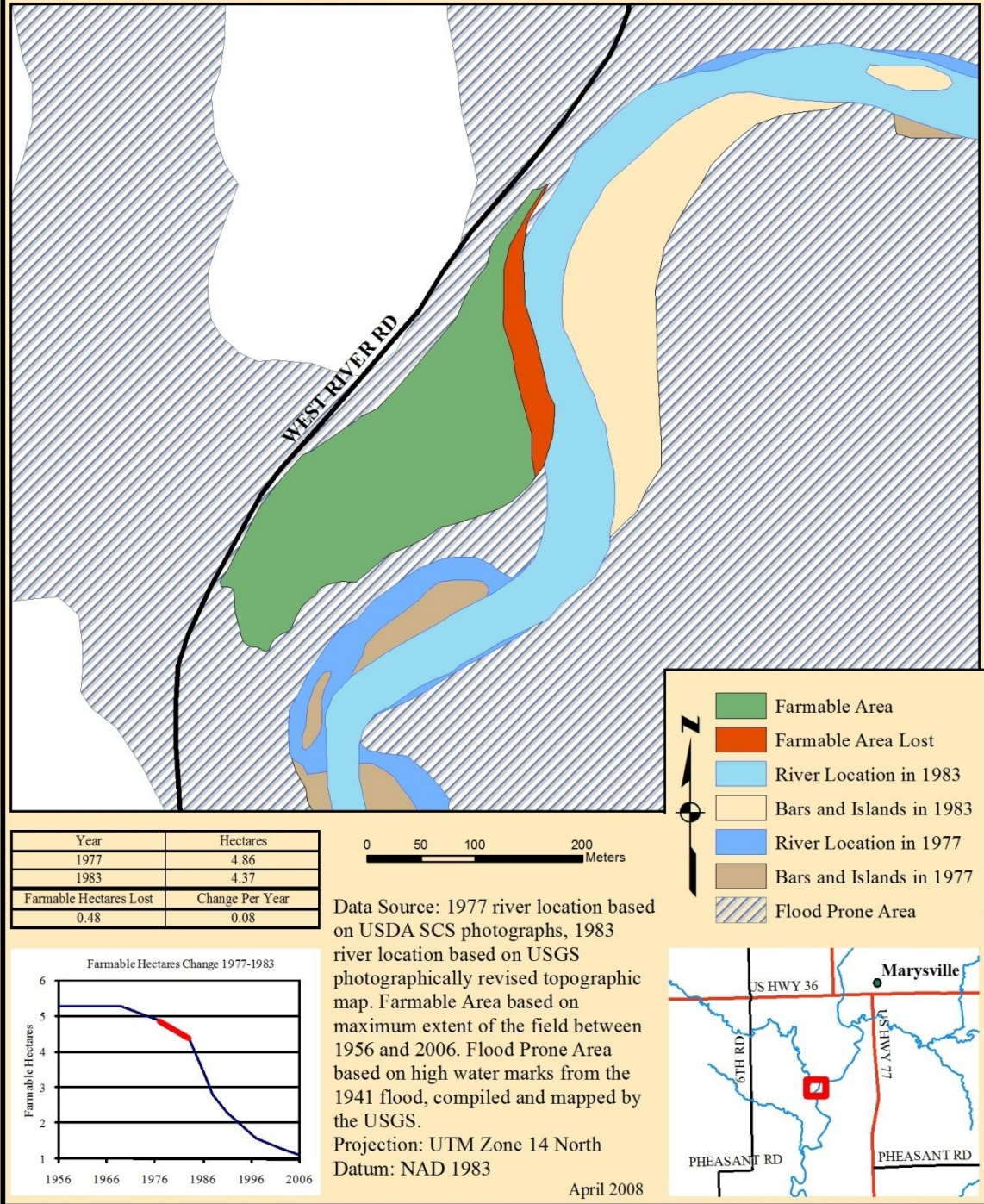


Figure C.3 Farmable Area Change 1977-1983

Farmable Area Change Years 1983 Through 1986

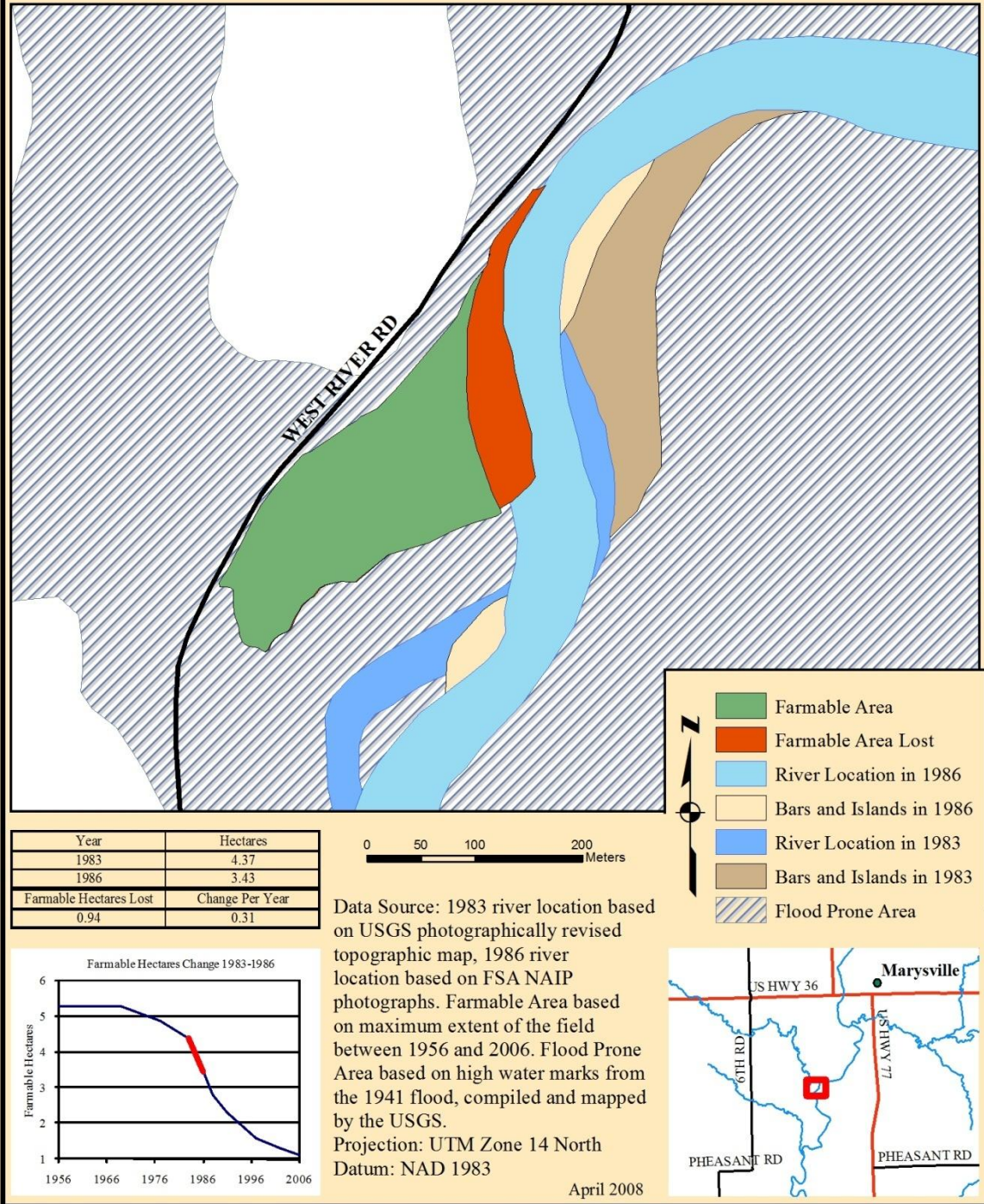


Figure C.4 Farmable Area Change 1983-1986

Farmable Area Change Years 1986 Through 1988

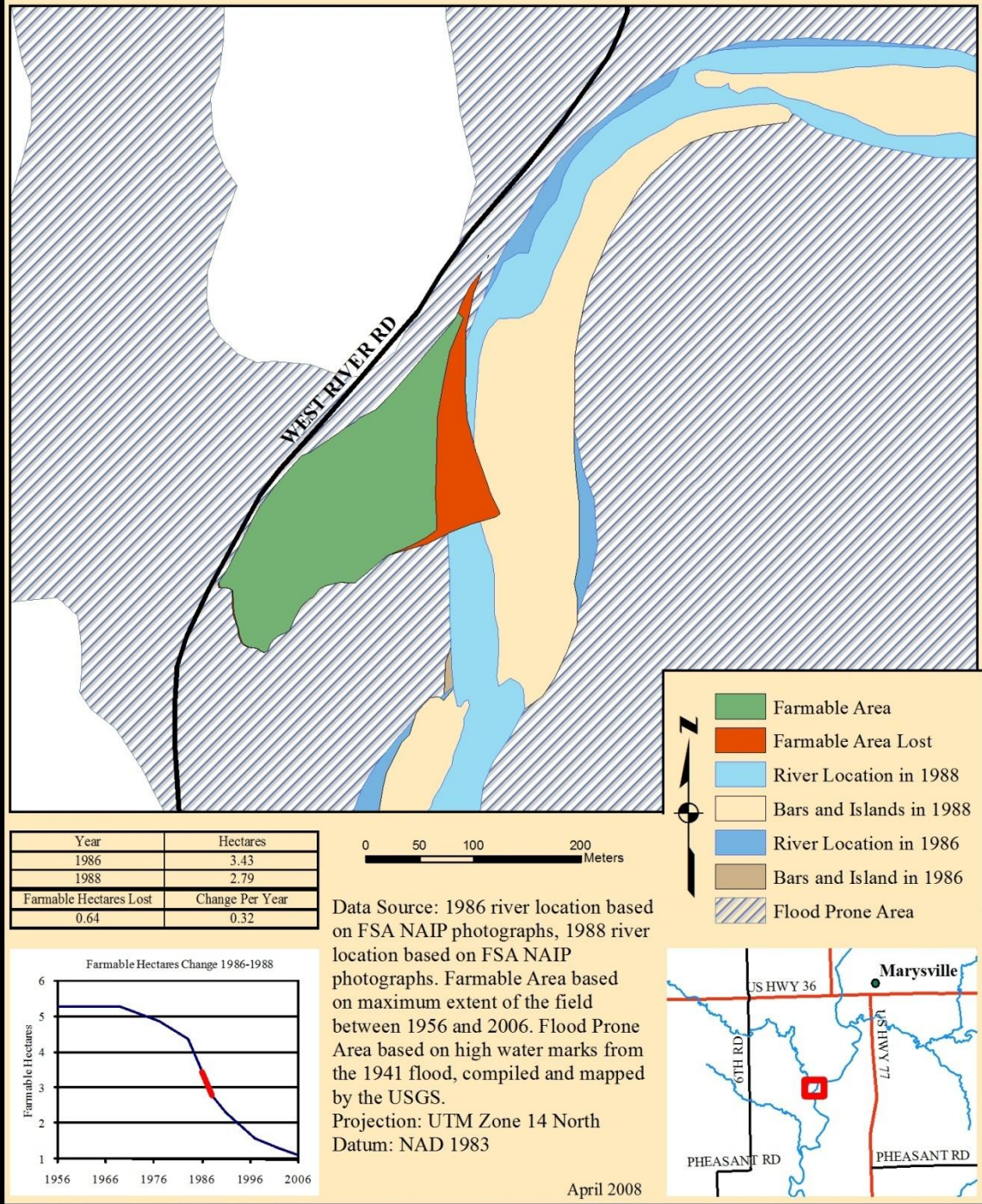


Figure C.5 Farmable Area Change 1986-1988

Farmable Area Change Years 1988 Through 1991

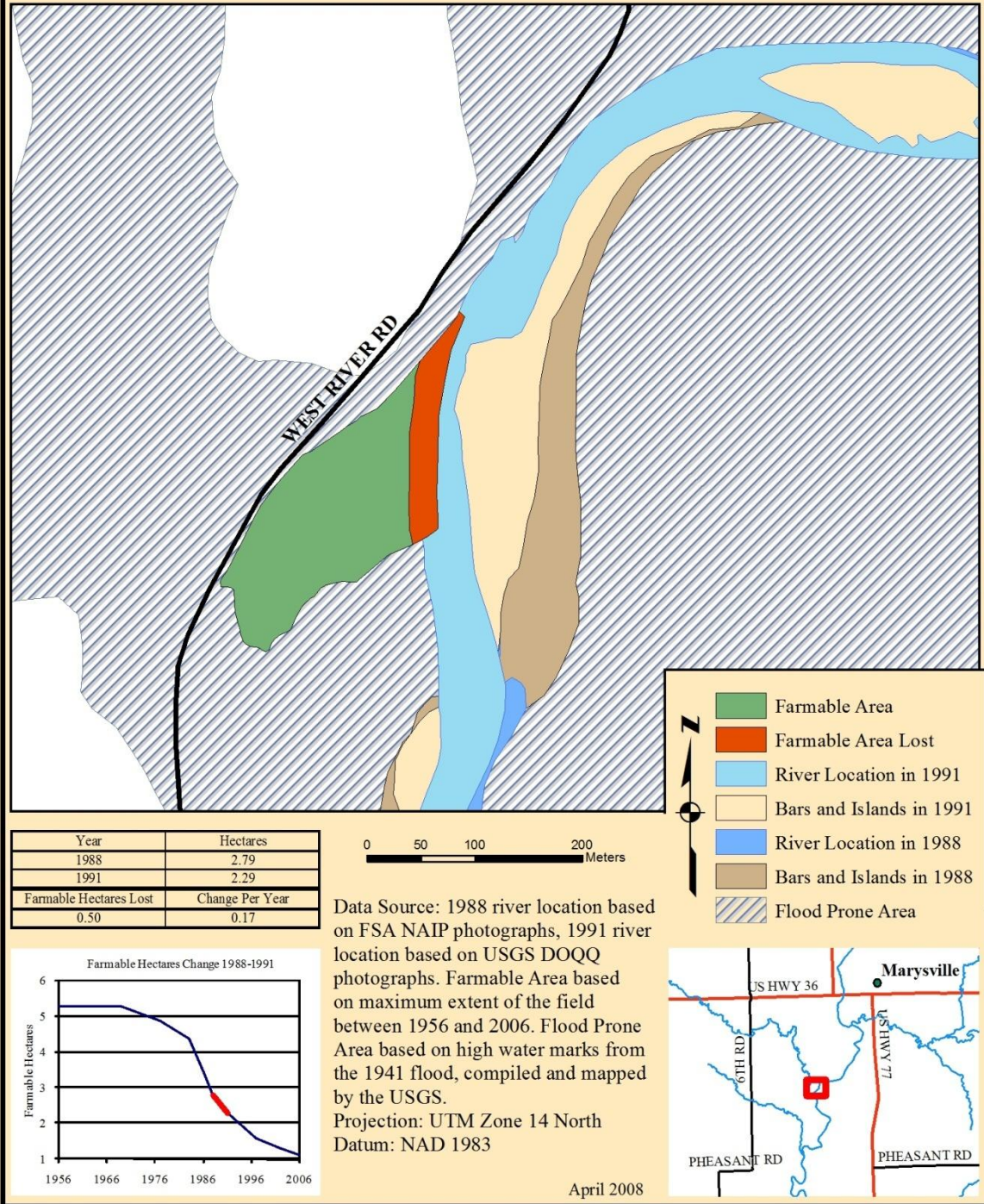


Figure C.6 Farmable Area Change 1988-1991

Farmable Area Change Years 1991 Through 1997

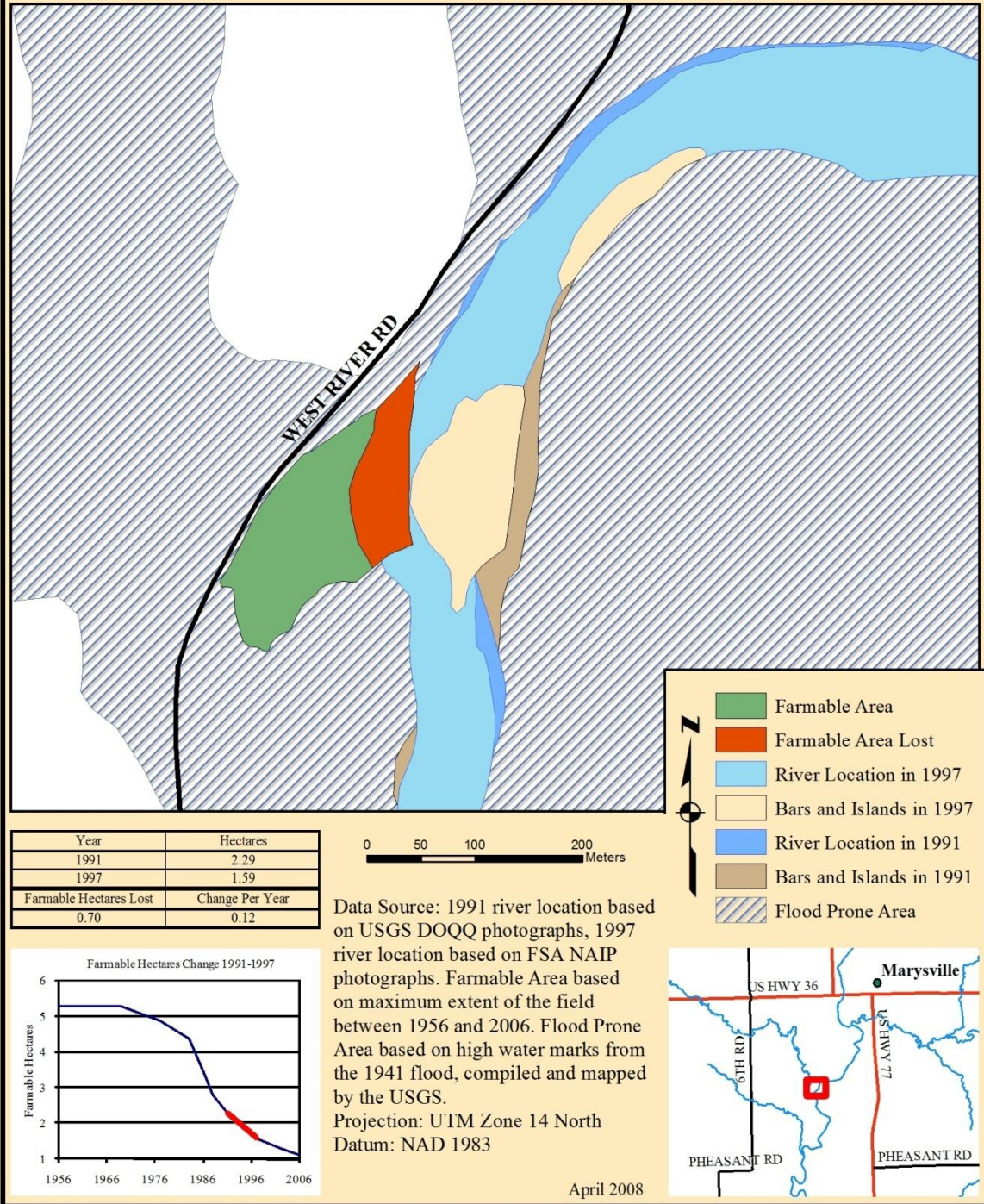
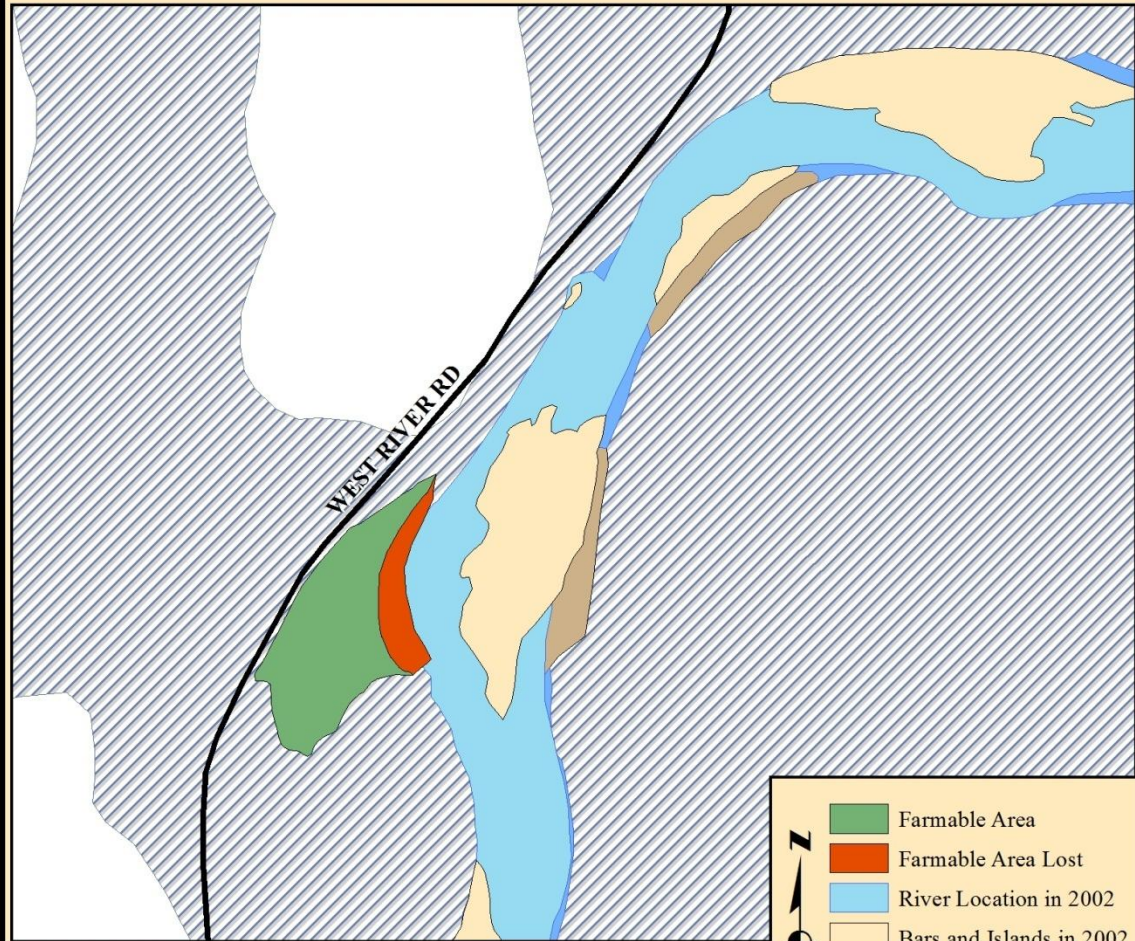


Figure C.7 Farmable Area Change 1991-1997

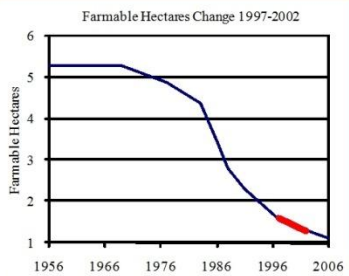
Farmable Area Change Years 1997 Through 2002



Year	Hectares
1997	1.59
2002	1.28
Farmable Hectares Lost	Change Per Year
0.30	0.06



- Farmable Area
- Farmable Area Lost
- River Location in 2002
- Bars and Islands in 2002
- River Location in 1997
- Bars and Islands in 1997
- Flood Prone Area



Data Source: 1997 river location based on FSA NAIP photographs, 2002 river location based on USGS DOQQ photographs. Farmable Area based on maximum extent of the field between 1956 and 2006. Flood Prone Area based on high water marks from the 1941 flood, compiled and mapped by the USGS. Projection: UTM Zone 14 North Datum: NAD 1983



April 2008

Figure C.8 Farmable Area Change 1997-2002

Farmable Area Change Years 2002 Through 2006

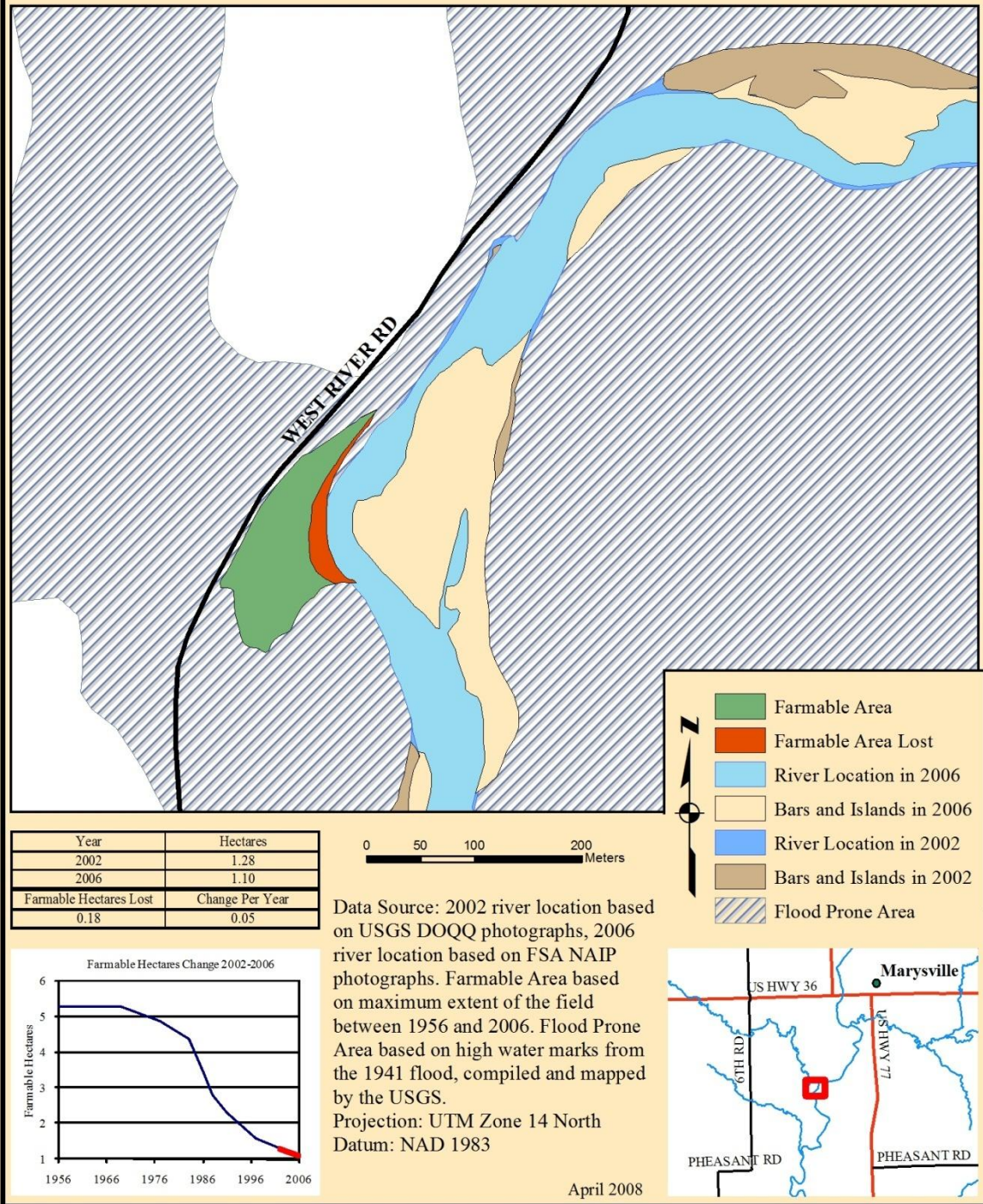


Figure C.9 Farmable Area Change 2002-2006

Appendix D - Meander Movement

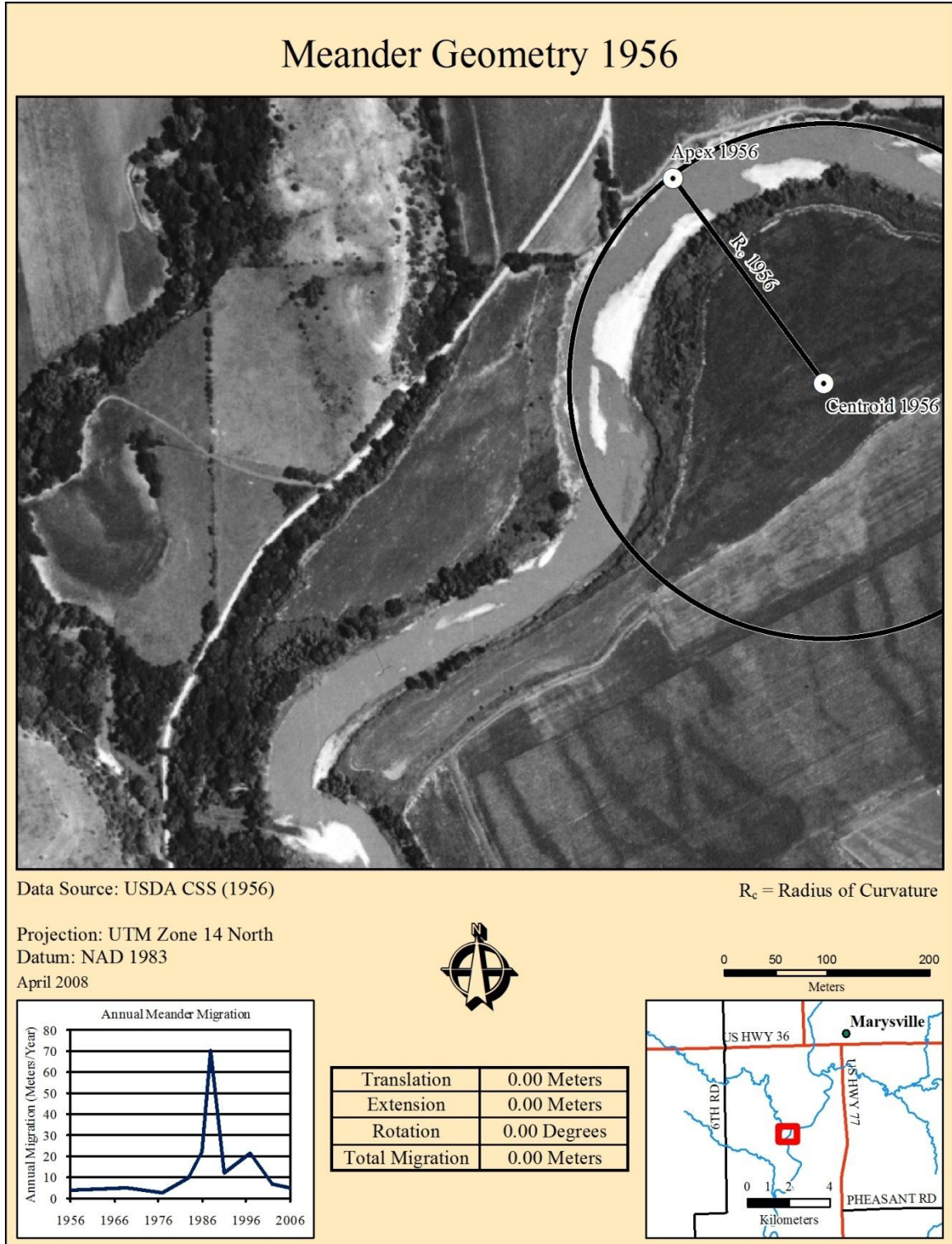


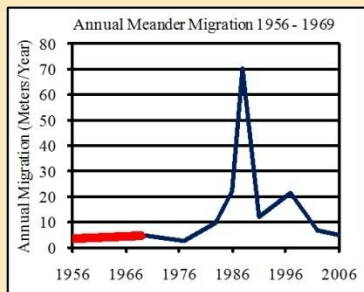
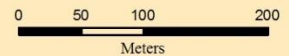
Figure D.1 Meander Geometry 1956

Meander Migration 1956 - 1969



Data Source: USDA CSS (1956),
 USDA ASCS (1969)
 Projection: UTM Zone 14 North
 Datum: NAD 1983
 April 2008

T = Translation, E = Extension,
 M = Total Migration, θ = Rotation,
 and R_c = Radius of Curvature

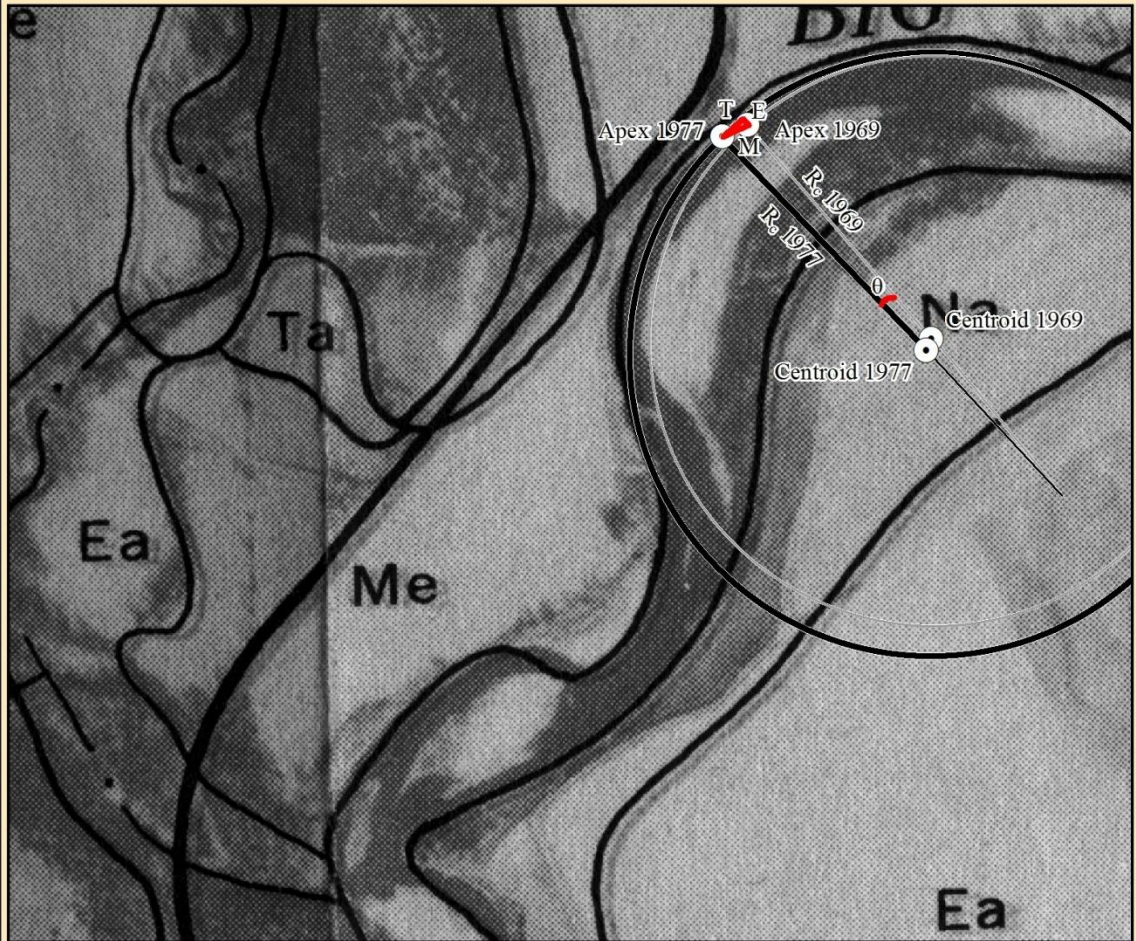


Translation	47.44 Meters
Extension	15.62 Meters
Rotation	0.82 Degrees
Total Migration	49.95 Meters



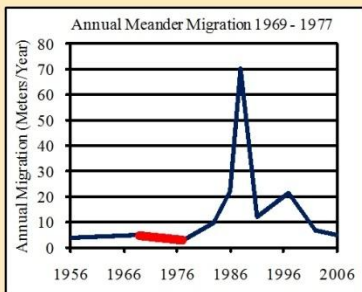
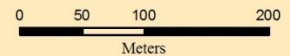
Figure D.2 Meander Migration 1956 - 1969

Meander Migration 1969 - 1977



Data Source: USDA ASCS (1969),
 USDA SCS (1977)
 Projection: UTM Zone 14 North
 Datum: NAD 1983
 April 2008

T = Translation, E = Extension,
 M = Total Migration, θ = Rotation,
 and R_c = Radius of Curvature

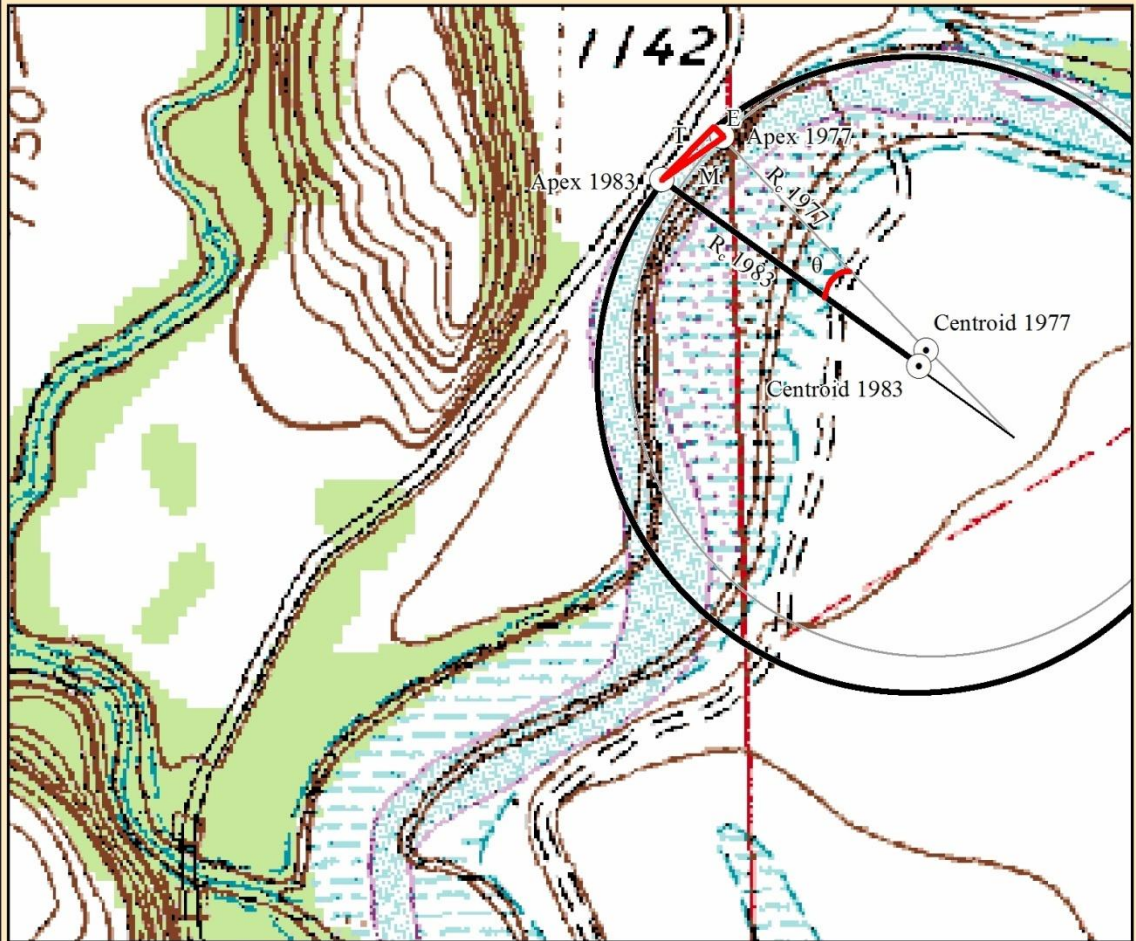


Translation	21.15 Meters
Extension	6.13 Meters
Rotation	3.61 Degrees
Total Migration	22.02 Meters



Figure D.3 Meander Migration 1969 - 1977

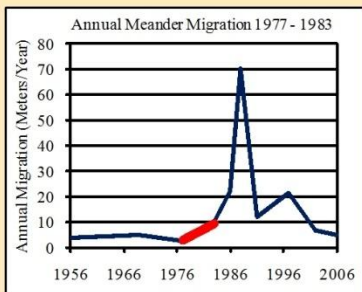
Meander Migration 1977 - 1983



Data Source: USGS SCS (1977),
USGS DRG (1983)
Projection: UTM Zone 14 North
Datum: NAD 1983
April 2008

T = Translation, E = Extension,
M = Total Migration, θ = Rotation,
and R_c = Radius of Curvature

0 50 100 200
Meters

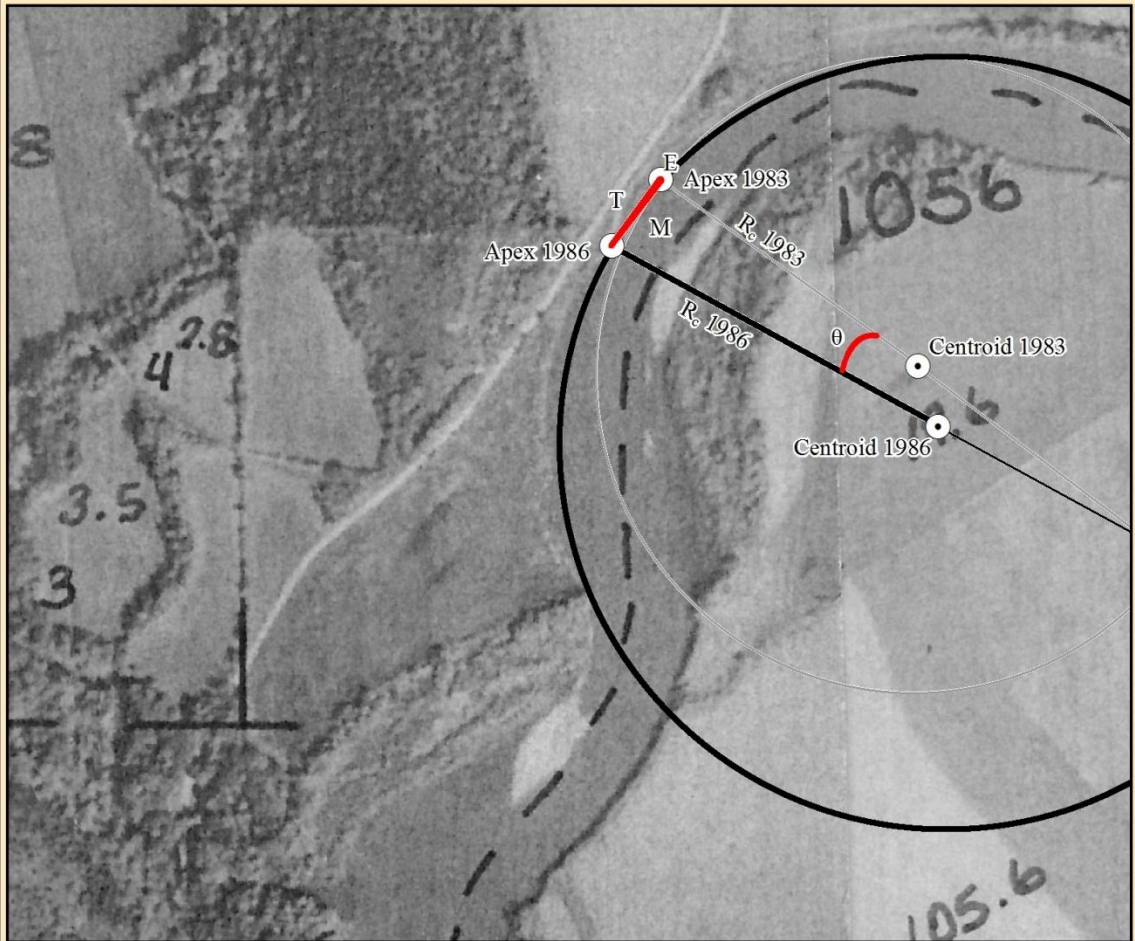


Translation	57.70 Meters
Extension	8.79 Meters
Rotation	3.01 Degrees
Total Migration	58.37 Meters



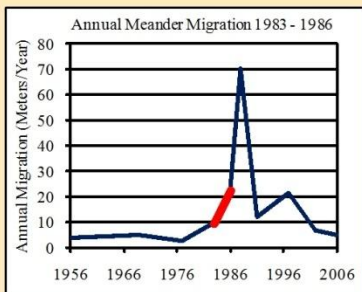
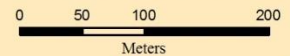
Figure D.4 Meander Migration 1977 - 1983

Meander Migration 1983 - 1986



Data Source: USGS DRG (1983),
 FSA NAIP (1986)
 Projection: UTM Zone 14 North
 Datum: NAD 1983
 April 2008

T = Translation, E = Extension,
 M = Total Migration, θ = Rotation,
 and R_c = Radius of Curvature

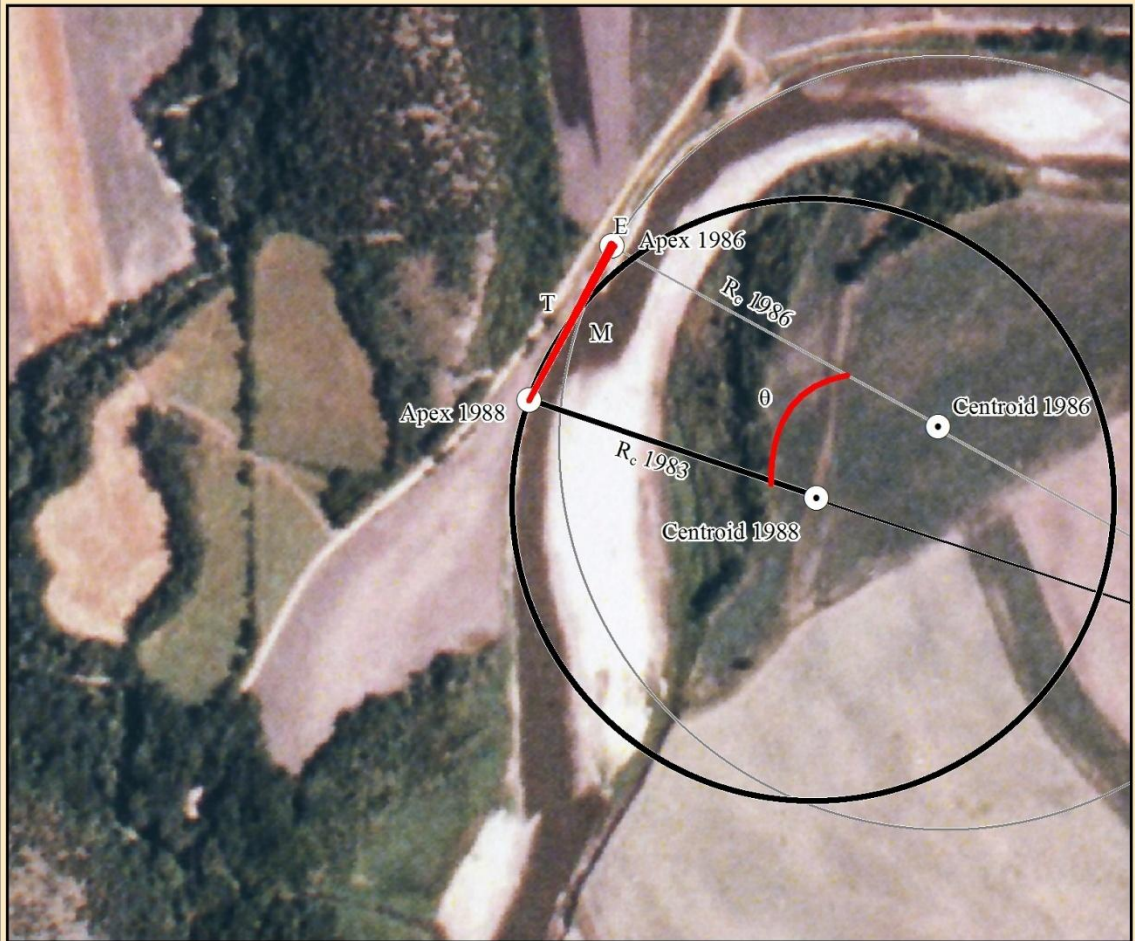


Translation	66.98 Meters
Extension	0.25 Meters
Rotation	9.95 Degrees
Total Migration	66.98 Meters



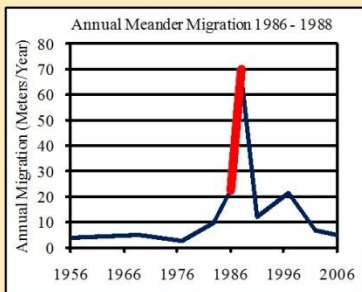
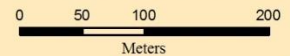
Figure D.5 Meander Migration 1983 - 1986

Meander Migration 1986 - 1988



Data Source: FSA NAIP (1986),
 FSA NAIP (1988)
 Projection: UTM Zone 14 North
 Datum: NAD 1983
 April 2008

T = Translation, E = Extension,
 M = Total Migration, θ = Rotation,
 and R_c = Radius of Curvature



Translation	140.18 Meters
Extension	1.28 Meters
Rotation	7.43 Degrees
Total Migration	140.19 Meters



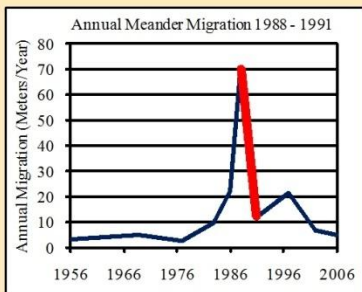
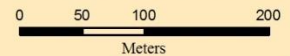
Figure D.6 Meander Migration 1986 - 1988

Meander Migration 1988 - 1991



Data Source: FSA NAIP (1988),
USGS DOQQ (1991)
Projection: UTM Zone 14 North
Datum: NAD 1983
April 2008

T = Translation, E = Extension,
M = Total Migration, θ = Rotation,
and R_c = Radius of Curvature

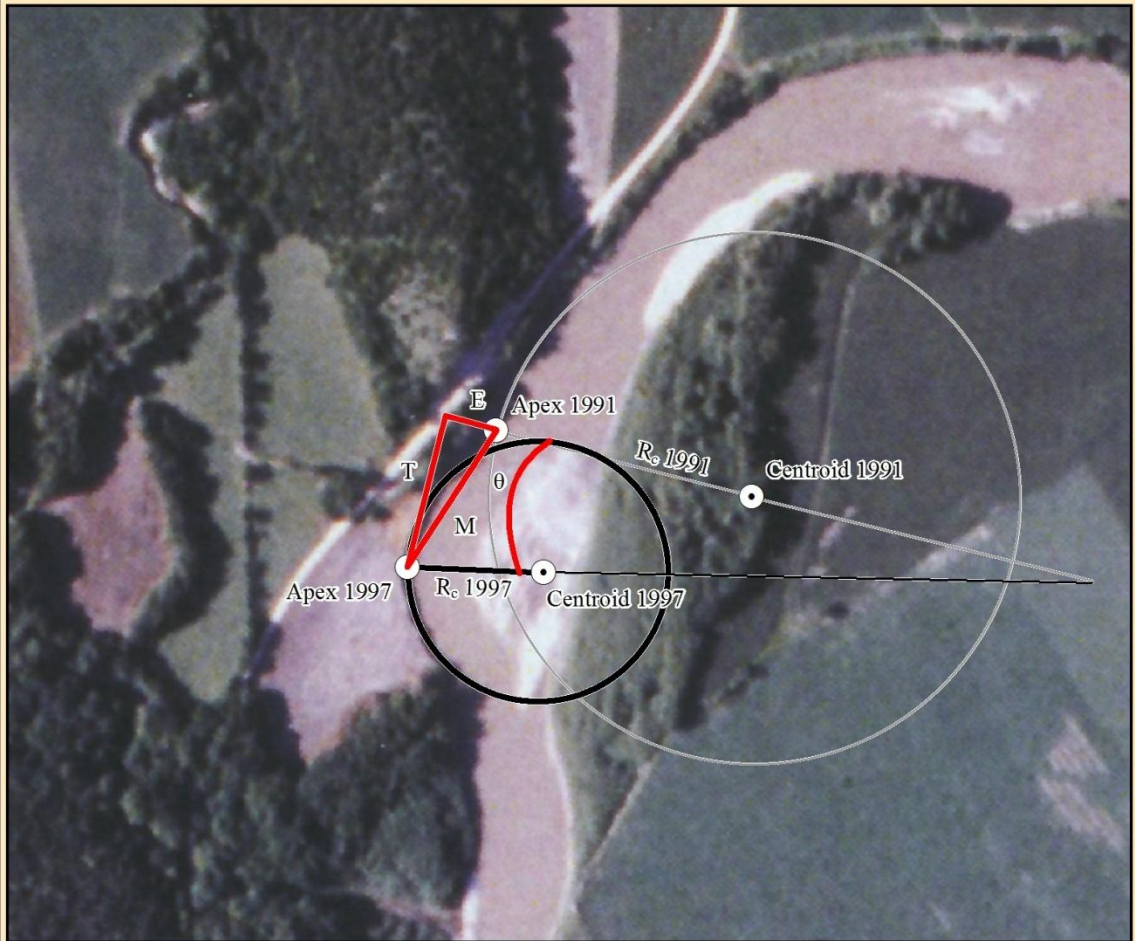


Translation	30.97 Meters
Extension	20.35 Meters
Rotation	10.72 Degrees
Total Migration	37.06 Meters



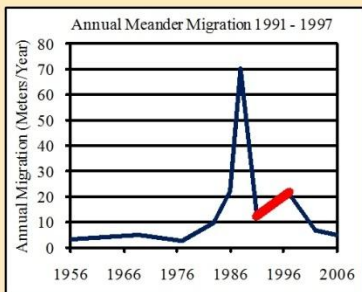
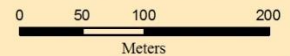
Figure D.7 Meander Migration 1988 - 1991

Meander Migration 1991 - 1997



Data Source: USGS DOQQ (1991),
 FSA NAIP (1997)
 Projection: UTM Zone 14 North
 Datum: NAD 1983
 April 2008

T = Translation, E = Extension,
 M = Total Migration, θ = Rotation,
 and R_c = Radius of Curvature



Translation	124.01 Meters
Extension	39.45 Meters
Rotation	3.60 Degrees
Total Migration	130.13 Meters



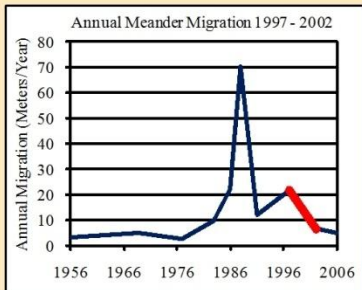
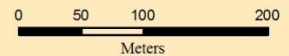
Figure D.8 Meander Migration 1991 - 1997

Meander Migration 1997 - 2002



Data Source: FSA NAIP (1997),
USGS DOQQ (2002)
Projection: UTM Zone 14 North
Datum: NAD 1983
April 2008

T = Translation, E = Extension,
M = Total Migration, θ = Rotation,
and R_c = Radius of Curvature

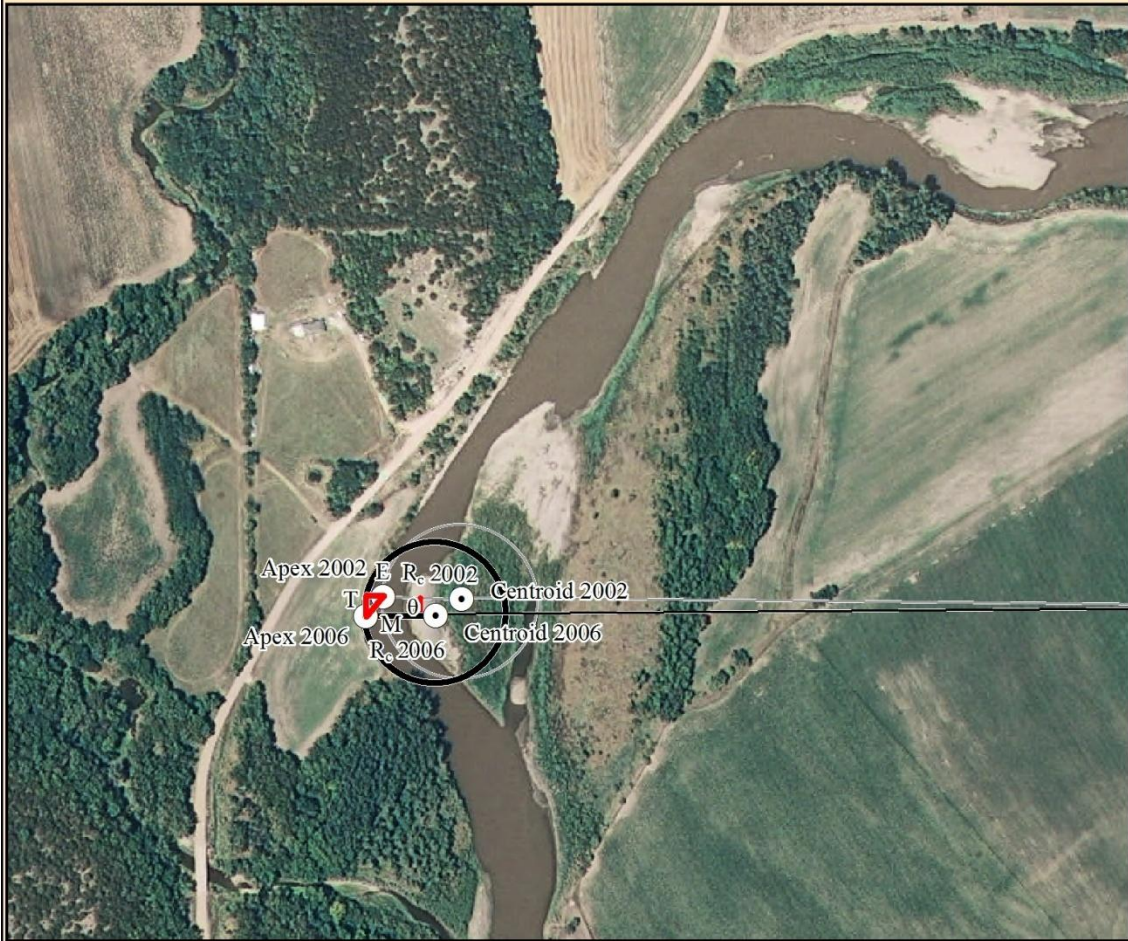


Translation	26.57 Meters
Extension	19.36 Meters
Rotation	12.12 Degrees
Total Migration	32.88 Meters



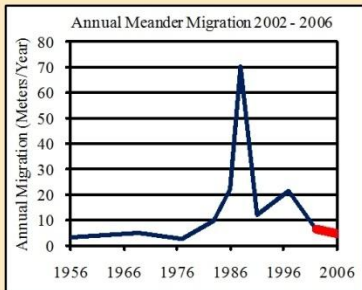
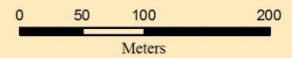
Figure D.9 Meander Migration 1997 - 2002

Meander Migration 2002 - 2006



Data Source: USGS DOQQ (2002),
 FSA NAIP (2006)
 Projection: UTM Zone 14 North
 Datum: NAD 1983
 April 2008

T = Translation, E = Extension,
 M = Total Migration, θ = Rotation,
 and R_c = Radius of Curvature



Translation	14.55 Meters
Extension	13.51 Meters
Rotation	2.45 Degrees
Total Migration	19.86 Meters



Figure D.10 Meander Migration 2002 - 2006